Radiation protection calculations related to the decommissioning of the European Spallation Source

PhD Dissertation

by

Zsófia Kókai
Master in Engineering Physics
Centre for Energy Research, Budapest
European Spallation Source ERIC, Lund

submitted to the

Environmental Physics PhD Program (Imre M. Jánosi, DsC, Professor)
Doctoral School of Environmental Sciences (Imre M. Jánosi, DsC, Professor)
Faculty of Science
Eötvös Loránd University, Budapest

Advisors:

Szabina Török, DsC
Head of Environmental Physics Department
Centre for Energy Research, Budapest

Péter Zagyvai, PhD
Senior research fellow
Centre for Energy Research, Budapest
Associate professor
Budapest University of Technology, Budapest

Luca Zanini, PhD
Head of Neutronics Group
European Spallation Source ERIC, Lund

2019

Acknowledgments

First of all, I would like to express my sincere gratitude to my supervisors. Szabina Török has contributed by great deal of support and assistance. Péter Zagyvai has shared his comprehensive knowledge in radiation protection since the first year of my university studies, his reliable guidance and expertise has been invaluable throughout my research. Luca Zanini has supervised my research at ESS with great competence.

I am very grateful to Ferenc Mezei, for his valuable guidance and advices.

I would like to express my gratitude to Alan Takibayev, for his essential collaboration, and for sharing his great knowledge in Monte Carlo simulations.

I am very thankful to Márton Markó, Gábor Náfrádi, and Gábor Patriskov, for their cooperation throughout writing this thesis.

I would like to thank all of my colleagues at Centre for Energy Research, especially Eszter Dian, Dávid Hajdú, János Osán, Felicián Gergely, Ákos Horváth, József Janik, and Endre Börcsök.

I would like to acknowledge all of my colleagues at ESS, especially Douglas Di Julio, Carsten Cooper-Jensen, Phillip Bentley, Konstantin Batkov, Esben Bryndt Klinkby, Riccardo Bevilacqua, Günter Muhrer, and Bengt Jönsson.

The PhD program and scholarship has been provided by The Doctoral School of Environmental Science, additional financial and technical conditions of the research have been provided by the Centre for Energy Research and by the European Spallation Source ERIC.

Finally, I would like to thank my family and friends for their great support throughout my studies, in particular my husband, my sons, my mother, and my grandparents.

"Oh, a szárnyas idő hirtelen elrepűl,
S minden míve tünő szárnya körül lebeg!
Minden csak jelenés; minden az ég alatt,
Mint a kis nefelejcs, enyész."
/Berzsenyi Dániel: A közelítő tél/

"Oh fluttering time flies by so rapidly,
And all of its creatures hover around his passing wing!
All is just a phenomenon, all things under the sky,
Such like the tiny forget-me-not, fade."
/Dániel Berzsenyi: As winter approaches,
translated by Dóra Roberta Garai/

Table of Contents

Abstract

For the sake of the future generations, decommissioning planning and providing the necessary resources to be at hand in time are required for medical, industrial, and research facilities producing radioactive waste[1]. Planning is important to ensure that decommissioning will be carried out in a safe and effective way. Several types of information are required to make a precise decommissioning plan. For proper planning, a good estimation of the radioactive inventory of the facility is needed. The objective of decommissioning with respect to radioactivity is the removal of all hazardous material produced during the operation of a facility and protection of human health and the environment. The compilation of an adequate initial decommissioning plan is obligatory before the construction in order to optimize the design in respect of the decommissioning. The decommissioning plan needs to be reassessed every few years[2].

The European Spallation Source (ESS)[3] is under construction in Lund, Sweden. It will be the world's most intense neutron source suitable for research related to materials science, nanotechnology, energy, health and environment. ESS includes a linear proton accelerator, a target monolith building with a rotating tungsten target, neutron instruments and experimental laboratories. ESS will be the world's first spallation source using long pulses in the ms range, as originally devised by Ferenc Mezei[4]. The 2 GeV protons impinge on the solid, rotating tungsten target wheel and initiate spallation reactions, releasing neutrons from the tungsten nuclei. After moderation, the neutrons are guided to the experimental halls. The tungsten target is planned to be replaced in every five years. The envisaged lifetime of ESS is 40 years.

During the operational time the structural materials will be activated resulting in different categories of radioactive waste at the time of their replacement and/or decommissioning. In order to decrease the amount and the hazard of the produced radioactive waste, preliminary analysis of the activation is required. The material selection and the design can be optimized based on these calculations. In the initial decommissioning plan for ESS[5] we identified the most crucial parts of the facility regarding the radioactive waste.

The aim of this PhD thesis is to present calculation methods developed for predicting the quality and the quantity of the produced radioactive waste at ESS, thus in turn supporting the material selection and design. The results show that in addition to the bulk material composition impurities also have a significant effect on the activation. The developed calculation methods are able to identify the source elements of the most important radionuclides in terms of decay gamma dose rate (for maintenance and refurbishment) and waste index (for processing requirements and for temporary and final disposal). Based on these calculations, the material selection can be optimized for decommissioning. The object of this thesis focused on the most crucial parts of ESS specified in the following; however, these methods can be extended for the whole facility.

The replaceable rotating solid tungsten target will apparently be the most active part. The activation of the neutron guides and inserts is an important topic, because the replacement of the guides is envisaged after about ten years use due to radiation damage, mechanical failure, and progress in guide technology. The beryllium reflector is also problematic as the activated toxic beryllium requires specific treatment. At ESS, metal-based shielding plays an important role in the attenuation of high-energy neutrons. The activation of the materials in experimental caves needs particular consideration in terms of radiation protection of the workers. In this thesis the NMX experimental cave was studied as an example. The activation properties in these selected parts depend strongly on the material choice.

In order to validate the model calculations, aluminium and glass neutron guide substrate samples were irradiated at the Budapest Neutron Centre and the measured activity concentrations were compared with the model predictions.

1. Introduction

1.1. Application of neutron sources

The experimental tools based on different neutron sources play a great role in the development of materials science. The neutron activation analysis is a method for the qualitative and quantitative determination of material composition based on the measurement of characteristic radiation from radionuclides formed by irradiating materials by neutrons.

The neutron scattering provides detailed information about the atomic structure of the materials and magnetic properties. It can analyze physical properties of fundamentally new materials, e.g. heavy-fermion systems, quasicrystals, fullerenes, and high-temperature superconductors. It can determine the atomic properties, the formulation of impurity phases, the lattice and rotational dynamics, the role of phase stability, phase transitions and the nature of magnetism. It can also analyze the structure, domain sizes and dynamics of spin glasses and disordered ferromagnets. It has led to a lot of new discoveries in materials, like structure and dynamics of hydrogen in metals including the quantum-mechanical tunneling of the protons between double-well potentials, the role of the calcification in bone structure, etc. It can promote better understanding of fundamental problems by providing information about fundamental properties of condensed matter systems and low dimensional systems. It can provide detailed information about the magnetic structure on the nanometer scale of artificially structured layered materials which are used in magnetic recording media. It can also analyze the buried interfaces, surfaces and surface effects in magnetism, superconductivity, and liquids[6].

The neutron sources can be used to give information on the dynamics and structure of biological systems such as biological tissues, DNA and proteins on different length and time scales[7].

The neutron sources can be used also for medical application, e.g. fast neutron radiotherapy and boron neutron capture therapy (BNCT)[8]. Neutron-based analytical

methods such as neutron activation analysis are used to study the behavior of trace elements in human body[9].

The neutron sources can be used for transmutation of the most harmful nuclides and have the potential to solve problems posed for the management of radioactive waste by reducing the fraction of long-lived isotopes it contains[10].

The neutron sources provide possibilities for fundamental neutron physics experiments. Accurate measurements of the neutron β-decay confirm the number of particle families predicted in the Standard Model. Ultracold neutrons can be used for measurements of the neutron properties like neutron oscillation time[11].

1.2. Comparison of nuclear fission reactors and spallation sources

The main application of nuclear fission reactors is energy production. The spallation is not an exothermic process; therefore, the main application of spallation sources is neutron production.

In fission, the nucleus typically divides into two major fragments. In spallation, the nuclei that remained after the reaction completed are lighter than the original target. The spallation residuals are distributed closer to the original target material[12] (Figure 1-1).

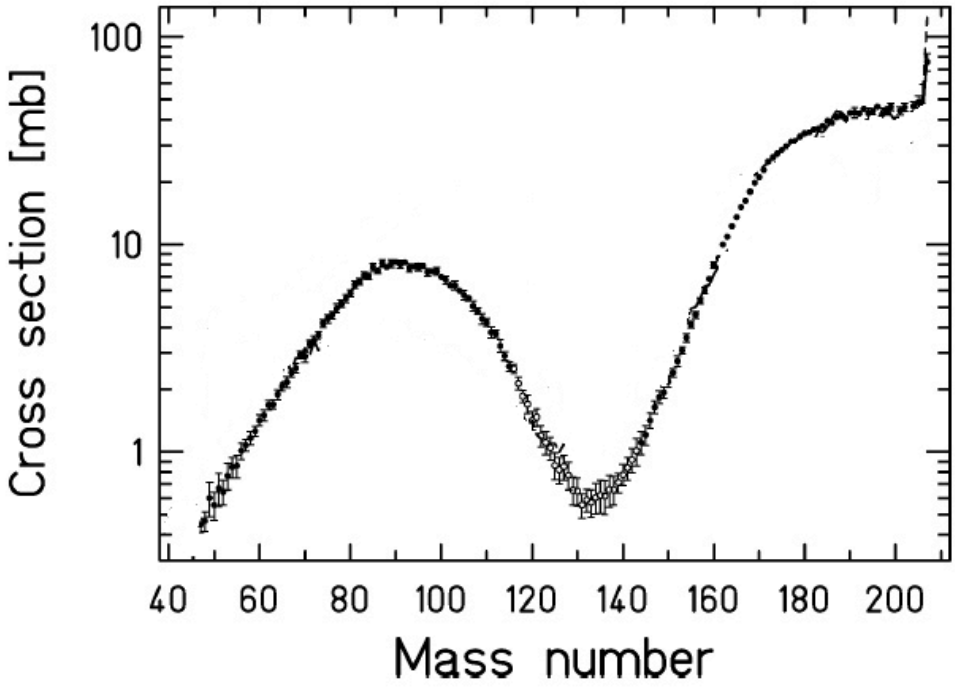

Figure 1-1 Experimentally measured spallation residual mass distributions of 1 GeV p+^{208}Pb reaction[12]

The number of neutrons released per fission event is about 2.5 to 3 – much less than the number of neutrons released per spallation event, about 25 to 30 using heavy target materials bombarded by protons in the GeV range. The amount of energy deposited that belongs to the emitted neutrons in fission is about 200 MeV, while in spallation is about 32 MeV (in tungsten). The heat generated is significantly less in spallation. However, spallation neutrons have higher energies, the high-energy tail of the spallation spectrum is remarkable[13] (Figure 1-2).

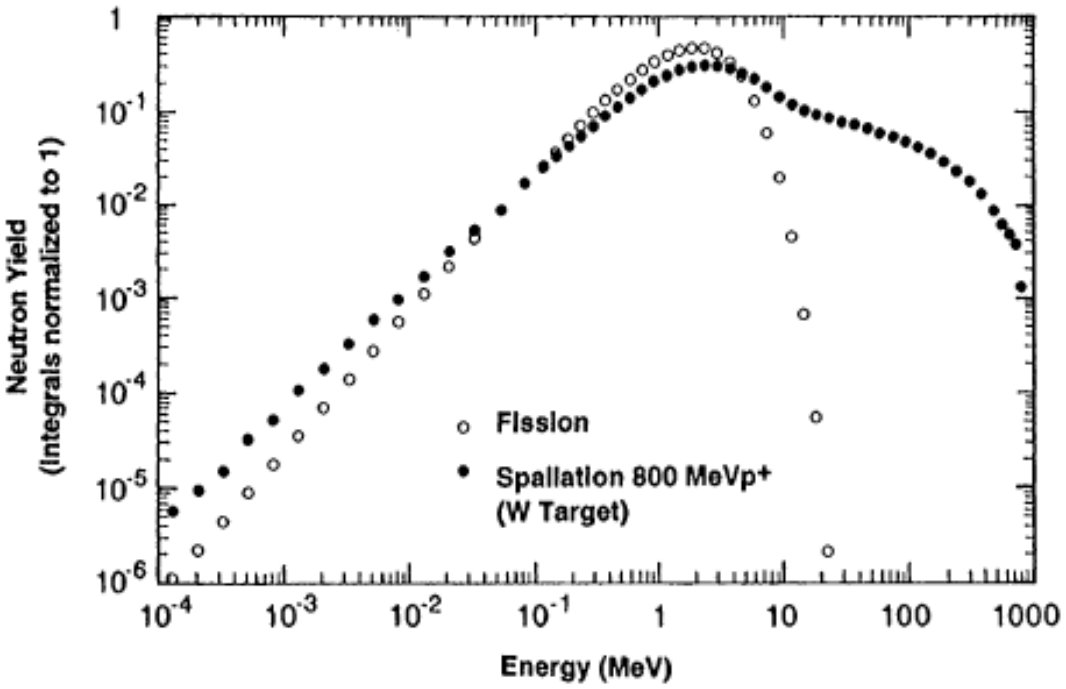

Figure 1-2 Neutron production from fission and spallation[13]

1.3. Description of the spallation process

Spallation can be defined as a high-energy nuclear reaction in which a target nucleus struck by an incident (bombarding) particle of energy greater than about 100-150 MeV ejects numerous lighter particles and becomes a product nucleus correspondingly lighter than the original nucleus[11]. The incident particle can be hadron, photon, or light nucleus. Spallation neutron sources are aimed to get high number of released neutrons from a target nucleus by bombarding it with high-energy particles.

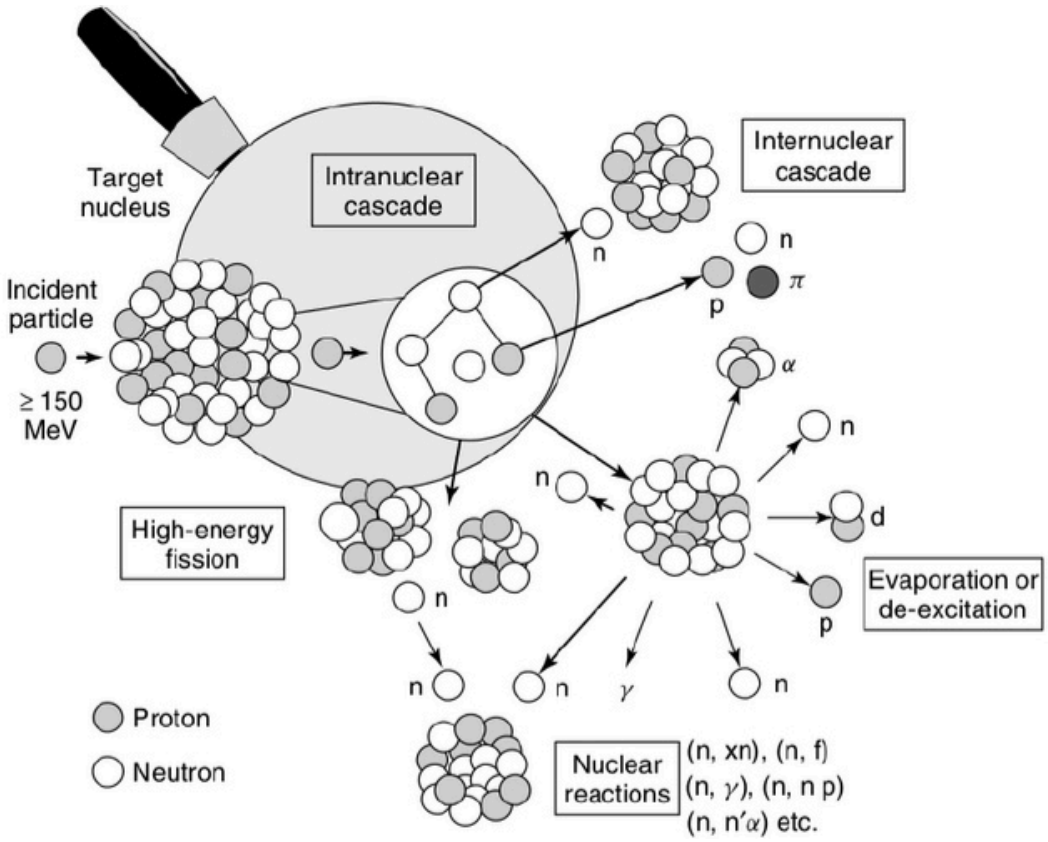

Figure 1-3 The principal scheme of spallation[11]

At energies of about 100-150 MeV the de Broglie wavelength of the bombarding particle becomes shorter or comparable to that of the average internucleon distance within the nucleus (10^{-15} m). With these circumstances, the bombarding particle is able to interact with the individual nucleons inside the nucleus[11]. It leads to a series of direct reactions called intranuclear cascade process[14] (INC), where individual nucleons or small groups of nucleons are ejected from the nucleus. These particles can be in high enough energy range resulting in further fragmentation. The secondary high-energy particles from INC move approximately in the same direction as the incident particle beam and can collide with other nuclei in the target. The nucleus remains in an excited state after the INC reaction.

In the so-called evaporation or de-excitation stage, the excited nucleus emits low-energy (typically less than 20 MeV) neutrons, protons, alpha particles, light heavy ions, etc. – but mostly neutrons. During the evaporation stage, high-energy fissions can also occur

for heavy nuclei, e.g. tungsten. After the evaporation, the resulting nucleus can be radioactive and emits gamma rays. The internuclear cascade or hadronic cascade is a series of a secondary spallation reactions caused by primary and secondary particles in the target[11].

1.4. Description of the different high-energy nuclear models

The INC models

Modeling of the INC process has to be described with considerable accuracy in order to predict the radioactive composition of the material of the target and its surroundings and the resulting radiation field. Suitable high-energy collision and energy transfer models are examined for selecting the proper solution. The common features of Bertini[15], Isabel[16], and INCL[17] models are:

- the nucleons move along straight line after collisions
- the Fermi motion, namely the quantum motion of the nucleons bound inside the target nuclei, is taken into account
- free nucleon-nucleon cross sections are used
- Delta-resonances (consists of three quarks whose intrinsic spins of ½ are lined up in the same direction[18]) and pion productions from elastic nucleon-nucleon collisions are taken into account
- the Pauli's exclusion principle states that two or more fermion cannot occupy the same quantum state within a quantum system at the same time[19]. According to this principle, interactions where the collision products would be in occupied states are prohibited

The INC models differ in the description of the cascade processes. In the Bertini and the Isabel models, the nucleus is a continuum and the places of the collisions are defined by lottery of the free path. After the collision, the collided nucleon starts moving and can collide with other nucleons. In case of the INCL model, every nucleon is moving according to its proper initial Fermi-distribution and they are collided by approaching each other. The nucleons are moving according to relativistic laws[20].

The evaporation models

Evaporation describes the equilibrium decay of an equilibrium nucleus with the excitation energy reached at the end of the pre-equilibrium stage. In any statistical evaporation model, an excited compound nucleus generally decays via fission or by the emission of light particles. All models considered are based on the Weisskopf-Ewing approximation[21], which has the following assumptions:

- The formation and decay of the compound nuclei are independent of each other
- All possible decay channels have the same probability
- Barriers for particular channels are defined by transmission coefficients

The abrasion-ablation[22] (ABLA) model is a dynamical code that describes de-excitation of the compound nucleus through evaporation of light particles and fission. It uses the Fermi-gas theory to describe the nucleus. Its strength is that it considers the dynamical nature of fission using time-dependent fission width. It treats the evolution of the fission degree of freedom as a diffusion process.

In the Dresner model[23], the fission part is simulated by the RAL model. Post-fission parameters depend only on the state of the nucleus at the time of fission, only binary fissions can occur, the mass split is always complete, and fission is allowed only for the nuclei with atomic number above 70.

The CEM model

The cascade-exciton model (CEM)[24] contains both steps of spallation by merging specific features of the cascade model with the exciton version of the pre-equilibrium decay model. It considers the spallation process as a three-stage process: cascade, pre-equilibrium, equilibrium.

In this model the effective local optical absorptive potential ($W_{opt.}$) is defined from the local interaction cross sections of particles, including Pauli blocking effect which occurs when the final transition states are filled[25]. The particle is leaving the cascade when the difference between the calculated and the experimental value of $W_{opt.}$ increases above a

certain empirically chosen value. After the cascade, the final state interactions among cascade particles create high-energy ^{2}H, ^{3}H, ^{3}He, ^{4}He ejectiles in significant amount[26].

The equilibrium evaporation-fission stage is based on the Weisskopf-Ewing approximation and RAL fission model.

In case the residuals have atomic numbers smaller than 12, the residuals can de-excite by a simultaneous statistical breakup into multiparticle exit channels. This process is represented by the Fermi break-up model. A break-up decay can occur if the total kinetic energy is positive for all fragments of a certain channel[11].

1.5. Particle interactions

Nuclear interactions between high-energy particles and matter produce charged secondary particles and uncharged neutrons and photons. Electrons, positrons and photons can undergo further electromagnetic interactions with matter. Seven types of particles participate in spallation reactions:

- Protons and heavier charged particles, e.g. tritons, deuterons, alpha particles
- High-energy neutrons (some tens of MeV to several GeV)
- Low-energy neutrons
- Electrons
- Photons
- Pions and muons
- Antiparticles, e.g. positrons, antiprotons

Summary of cross section definitions

The differential cross section expresses the angular and energy distributions of particles produced in nuclear reactions with matter. The probability of producing a particle of energy in the range $E+dE$ during an interaction into the solid angle region in range $\Omega+d\Omega$ is denoted by $d^2\sigma/dEd\Omega$[11].

The integration of these differential cross sections over space and energy ranges gives the total cross section σ_{tot}[27]:

$$\sigma_{tot} = \sigma_a + \sigma_{elastic} + \sigma_{inelastic} \quad (1.1)$$

where σ_a is the absorption cross section, $\sigma_{elastic}$ is the elastic scattering cross section, and $\sigma_{inelastic}$ is the inelastic cross section.

The macroscopic cross section Σ (unit 1/cm) is given by

$$\Sigma = \sigma \cdot n \quad (1.2)$$

where n is the number of nuclei in the given volume (unit 1/cm^3).

The mean free path or interaction length of a particle in matter is a measure of its probability of undergoing a certain interaction and it is the reciprocal of the macroscopic cross section[28].

Electromagnetic and atomic interactions

Neutral particles interacting with matter can produce charged particles. Charged particles lose their kinetic energy transporting through matter by ionization and excitation of bound electrons. Excitation processes produce low-energy photons[11].

A charged particle is scattered due to Coulomb potential of the nuclei and, to a lesser degree, due to the fields of the electrons of the atom. When hadronic incident particle impinges on large target masses many small-angle scatterings or multiple Coulomb scatterings can occur. If charged particles are decelerated in the Coulomb field, one part of the particle kinetic energy will be emitted as photons called bremsstrahlung. By traversing the Coulomb field of the target nucleus, high-energy particles can produce electron-positron pairs. The charged particles can also lose energy by virtual photon exchange undergoing inelastic collisions[11].

High-energy hadronic cascades and nuclear interactions

The main features of hadron-nucleus collisions are the following:

- Above about 300 MeV the total elastic and inelastic cross sections are approximately linear function of the energy, above 1 GeV they are approximately constant[29]
- The secondary particle direction relative to the incident particle direction is roughly straight ahead
- The number of the created high-energy particles increases with kinetic energy of the incident particle, approximately as ln(E)
- Secondary particle production in nucleon-nucleon interactions exhibits resonances[11].

Hadronic and electromagnetic showers

A shower is a cascade of secondary particles produced by high-energy particle interactions with matter[11].

A high-energy hadron interacting with a nucleus produces numerous lower energy hadrons, it is called hadronic shower. A high-energy electron or photon entering a material produces electromagnetic shower. High-energy photons interact primarily by pair production, while high-energy electrons and positrons primarily emit bremsstrahlung photons. Higher incident energies and smaller material densities result in deeper penetration.

Particle transport, Boltzmann equation

The particle transport in matter is described by Boltzmann equation[11]. The density of particle radiation can change in the following ways:

- Uniform translation changes only the spatial coordinates
- Collisions change only the energy-angle coordinates

- Continuous slowing down of the particle energy, in this process the uniform translation is combined with a continuous energy loss
- Radioactive decay
- External source

The combination of these processes is expressed in Boltzmann equation[11]:

$$\frac{1}{v_i}\cdot\left(\frac{\partial \Phi_i}{\partial t}\right) = -\boldsymbol{\Omega}\,\nabla\Phi_i + \sum_i \Big[\int \sigma_{i,j}(\boldsymbol{r}, E_B \to E, \boldsymbol{\Omega} \to \boldsymbol{\Omega}')d\boldsymbol{\Omega}' dE_B \cdot \Phi_j(\boldsymbol{r}, E_B, \boldsymbol{\Omega}', t) - \int d\boldsymbol{\Omega}' dE_B \cdot \sigma_{i,j}(\boldsymbol{r}, E_B \to E, \boldsymbol{\Omega} \to \boldsymbol{\Omega}') \cdot \Phi_j(\boldsymbol{r}, E_B, \boldsymbol{\Omega}, t)\Big] - \sigma_i(\boldsymbol{r}, E)\cdot\phi_i(\boldsymbol{r}, E, \boldsymbol{\Omega}, t) + \left(\frac{\partial}{\partial E}\right)\big(\phi_i(\boldsymbol{r}, E, \boldsymbol{\Omega}, t)\cdot S(\boldsymbol{r}, E)\big) - \frac{1}{\lambda_i}\cdot\phi_i + Y_i(r, E, \Omega, t) \quad (1.3)$$

Where $\boldsymbol{\Omega}$ is a unit vector in the particle direction of motion given in polar coordinate system, v is the velocity of the particle, $\Phi_i(\boldsymbol{r}, E_B, \boldsymbol{\Omega}', t)$ is the angular flux (the number of particles of a given type in the volume $dxdydz$ about $\boldsymbol{r}$ in the energy element $E+dE$ with the direction of motion $d\boldsymbol{\Omega}$ around $\boldsymbol{\Omega}$, multiplied by the velocity of these particles[30]), $\Phi_i(r)$ is:

$$\Phi_i(\boldsymbol{r}) = \int_E dE \int_{4\pi} d\boldsymbol{\Omega} \int_t \Phi_i(\boldsymbol{r}, E, \boldsymbol{\Omega}, t) \quad (1.4)$$

$\sigma_{i,j}(\boldsymbol{r}, E_B \to E, \boldsymbol{\Omega} \to \boldsymbol{\Omega}')$ represents the cross section, which is the probability of producing an i-type particle with the phase-space coordinates $(\boldsymbol{r}, E, \boldsymbol{\Omega}', t)$ as a result of a collision with a j-type particle with the phase-space coordinates $(\boldsymbol{r}, E_B, \boldsymbol{\Omega}, t)$, S is the stopping power of particles by traversing matter; particles are losing energy continuously at a rate $S(\boldsymbol{r}, E)$ per unit path length, Y_i is an external source, this means the direct emission of particles into the volume of phase space of interest, e.g. a spallation neutron source, a fission source, other radioactive sources as electrons and photons, cosmic rays, etc[11].

Neutron deceleration and thermalization

Neutrons slow down to the thermal region where the neutrons are in thermal equilibrium with their surroundings by a series of elastic scattering.

The energy loss per collision can be described using logarithmic energy decrement or lethargy energy unit[11]:

$$\xi = \ln(E_{int}) - \ln(E_{final}) = \ln\left(\frac{E_{int}}{E_{final}}\right) \quad (1.5)$$

where ξ is the average logarithmic energy decrement, E_{int} is the average initial neutron energy, E_{final} is the average final neutron energy. The average logarithmic energy decrement is a constant for a given material. For hydrogen, ξ=1, for large atomic masses A, $\xi \approx 2/(A+2/3)$.

The total number of collisions N needed to slow down a neutron to a given energy can be described by the average logarithmic energy decrement:

$$N = \frac{\ln\left(\frac{E_{int}}{E_{final}}\right)}{\xi} \quad (1.6)$$

where ξ is the average logarithmic energy decrement, E_{int} is the average initial neutron energy, E_{final} is the average final neutron energy.

An efficient moderator should have large scattering cross section and small absorption cross section in order to produce a large number of thermal neutrons and reduce the number of neutron absorptions.

Activation, Bateman equation

The differential equation (1.7) describing the rate of change in the atomic density $n_m(t)$ of a nuclide m is constructed as the sum of the rates of losses and gains in nuclide densities. The losses are due to the radioactive decay and particle absorption reactions producing daughter and product nuclides, respectively, different from the original nuclide m. Gains

are from the radioactive decay and particle absorption reactions of other nuclides having the nuclide m as a daughter or a reaction product. For many applications, an additional constant production rate, $\overline{Y_m}$, can be included accounting for production beyond the energy and particle domain of the applied nuclear data library[31]. The differential equation can be written as

$$\frac{dn_m(t)}{dt} = -n_m(t)\beta_m + \overline{Y_m} + \sum_{k \neq m} n_k(t)\gamma_{k \to m} \quad (1.7)$$

where $\gamma_{k \to m}$ is the probability of nuclide k decaying or absorbing to nuclide m and β_m is the total decay probability together with absorption probability of nuclide m:

$$\beta_m = \lambda^m + \Phi\sigma_a^m \quad (1.8)$$

where Φ is the energy-integrated neutron flux, σ_a^m is the flux-weighted average cross section for neutron absorption by nuclide m, and λ^m is the total decay constant of nuclide m.

1.6. Decommissioning

The main goal of decommissioning of a nuclear or radiological facility is to remove all hazards resulted by the operation of the given facility in order to release the facility and its site from regulatory control, protecting the workers, the general public and environment during the process. In case of the presence of radioactive hazards, the main phases of decommissioning are the radioactive decontamination and dismantling phase. Strict project management and environmental monitoring is required. The radioactive waste management is a key element of this process. Therefore, the qualitative and quantitative estimation of the radioactive waste is one of the most important part of the decommissioning plan[32].

The decommissioning strategy can be immediate dismantling, deferred dismantling, or entombment. The immediate dismantling is the planned option for ESS[3]. It means that the decommissioning begins in a few years after shutdown and then proceeds continuously without long "dormant" periods. It is the preferred option if the financial funding and

waste management facilities are available. This option allows clearance or unrestricted use of non-hazardous components and employment of the current work force. The disadvantage of this option is that there is no time for significant decay of the radionuclides, thus dose exposures may be high and so detailed radiation protection ordinance is required[32].

1.7. Radioactive waste management

During the operational time, the structural materials of ESS will be activated resulting in different categories of radioactive waste. The activated parts will constitute the vast majority of the waste produced during the operation of ESS. The radioactive waste is defined as a material of no intention of further use which cannot be released to the environment directly because otherwise the dose consequence of the cleared material would be higher than the negligible dose (defined as 10 μSv/year) for a representative person[33].

The main principles of radioactive waste management are[34]:

- Protection of human health
- Protection of environment
- Protection of foreign countries
- Protection of future generation
- Authority control
- Minimization of radioactive waste production
- Adequate treatment of radioactive waste
- Safety of nuclear waste treatment and storage facilities

According to its origin, the following waste streams can be distinguished[34]:

- continuous operational emissions: materials containing radioactivity in liquid or gaseous phase; their quality and quantity are regulated by the public dose constraint (DC) of the appropriate facility

- local residual waste: produced during operation and decommissioning of the facility, stored in local storage and transported for the final disposal
- accidental waste produced by an accidental event

Characterization of waste according to its dose consequences, the waste categories are the following[35]:

- exempt (cleared) waste (CW)
- very short lived waste (VSLW)
- very low level waste (VLLW)
- low level waste (LLW)
- intermediate level waste (ILW)
- high level waste (HLW)

Clearance levels defining the limiting values for waste streams are different for waste quantities below and above 1 t, the decision on release from regulatory control depends on this criterion. (See equation 1.9 below). Publications by Swedish Radiation Safety Authority[36,37] contain rounded values of the clearance levels. In the present practice of radiation protection two data sets are in parallel use for exemption and clearance. As it is clearly described in article 37 of the European Basic Safety Standards[38], exemption levels (ELs) of the former IAEA International Basic Safety Standards[39] (IBSS) are to be applied as clearance levels (CLs) for moderate amounts of radioactive material (practically below 1 t), while the levels presented in RP122[40] are to be applied for bulk amounts from that time on. This distinction is repeated in IAEA GSR Part 3[33] where the two data sets are called "clearance levels for moderate amounts = specific clearance levels" and "clearance levels for bulk amounts = general clearance levels"). It is worth noting that the otherwise obsolete IBSS published ELs for many radionuclides (some of them are of importance in this thesis) which were missing from the general CL data set because they were treated neither in RP122[40], nor in its less frequently referenced and applied IAEA tally SRS 44[41]. It is also not favourable for the safety of decommissioning waste management that an inconsequent rounding rule was applied to the values of the data sets. EL and CL values with mantissa between 1 and 3 are rounded to 1; between 3 and 10 they are rounded to 10.

As the CLs are applied in the denominator (See equation 1.10), an underestimation of the waste index and thus the overall risk associated with the cleared material may easily occur. Therefore – in accordance with the method followed in RP122[40] – we do not round the CLs that we calculate in the procedures described in Chapter 4.

In order to have more precise, but conservative estimation, in this thesis the clearance levels were taken and calculated based on RP122 IAEA publication[40]. The RP122 set up six different scenarios for dose calculations, three external exposure scenarios, two inhalation scenarios, and one skin dose scenario – all of them were characterized by a specific dose consequence (SDC). The clearance level was deduced as the ratio of negligible dose (10 μSv/year) and the maximum specific dose consequence, SDC_{max} [(μSv/year)/(Bq/g)]:

$$CL = \frac{10}{SDC_{max}} \tag{1.9}$$

For numerical waste classification the waste index *WI* of the whole waste stream should be calculated. It directly relates the waste classes to the respective values of clearance level *CL* associated with the negligible dose and thus to the potential maximum dose exposure of the reference person:

$$WI = \sum_{i=1}^{n} \frac{c_i}{CL_i} \tag{1.10}$$

Here, *c* is the activity concentration in units of Bq/g, and *n* is the total number of radioisotopes present and detectable in the waste stream.

Based on the clearance index the following radioactive waste classification was set up by the Hungarian Atomic Energy Agency[42]:

- LLW: $1 \leq WI \leq 10^3$
- ILW: $10^3 \leq WI \leq 10^6$
- HLW: $WI > 10^6$ or heat generation ≥ 2 kW/m^3

In the following chapters the heat generation was calculated only for the tungsten target and the beryllium reflector (Chapter 5 and 8), since these parts are expected to exceed this limit.

The present Swedish radioactive waste ordinance[43,44] is concentrated on the capability of the disposal sites rather than on an "independent" waste classification system. Short- and long-lived low- and intermediate level radioactive wastes are distinguished, but separate classes like those of the Hungarian system, are not defined at the moment.

2. Computer codes for radioactive inventory and dose rate calculations

All events occurring to a particle from the time it leaves the source until it is absorbed or until it leaves the system are called the particle history[11]. Particle histories can be generated by simulating real physical situations. The results of simulations (particle flux spectra and reaction rates) serve as input for an activation code which is capable to solve Bateman equation (equations 1.7-1.8). If the activation code has the capability to output spectral information about the gamma source strength, it can be brought into a format suitable for gamma dose rate calculation[45].

Based on the literature, MCNPX coupled with CINDER/FISPACT, or PHITS code are the most often used codes for activation calculations of spallation sources. For example, gamma- and alpha-emitting isotopes after irradiation and cooling were studied by measurements and MCNPX/CINDER simulations at PSI for solid lead target (SINQ) in continuous operational mode at MW level[46,47,48].

2.1. Monte Carlo particle transport codes

The Monte Carlo method is powerful and widely applied method to treat three dimensional configurations in multiparticle transport problems. It is a numerical stochastic method. In this method, the expected value of a certain random variable is equivalent to the physical quantity to be determined. The expected value is estimated by the average of numerous independent samples of the random variables. The method contains full mathematical description of probability relationships that define the track length of particles between interactions, the choice of interaction types, new energies, new angular directions and the possible production of secondary particles[11].

For the time being, the most advanced Monte Carlo particle transport code systems are MCNPX, PHITS, FLUKA, GEANT4, and MARS. The MCNPX code was selected for the present work, since it can give especially detailed information about reaction rates and particle flux spectra in a given geometry which can be used then for advanced activation calculations. The calculations in this thesis have been performed with MCNPX Version 2.7[49].

2.2. MCNPX

The MCNPX code[49], developed and maintained by Los Alamos National Laboratory, is the internationally recognized code for analyzing the transport of particles of different types in a wide range of energies by the Monte Carlo method. Bertini, Isabel, INCL, ABLA, Dresner and CEM models are available in most versions of MCNPX for high-energy calculations. MCNPX treats geometry problems primarily in terms of regions or volumes bounded by first and second-degree surfaces. Cells are defined by intersections, unions, and complements of the regions, and contain user defined materials. The characteristics of the source (particle type, energy distribution, geometry) are also defined by the user. MCNPX uses estimator methods to calculate particle fluxes and reaction rates. The formalism of estimators is called tallies[49].

The activation and gamma source script

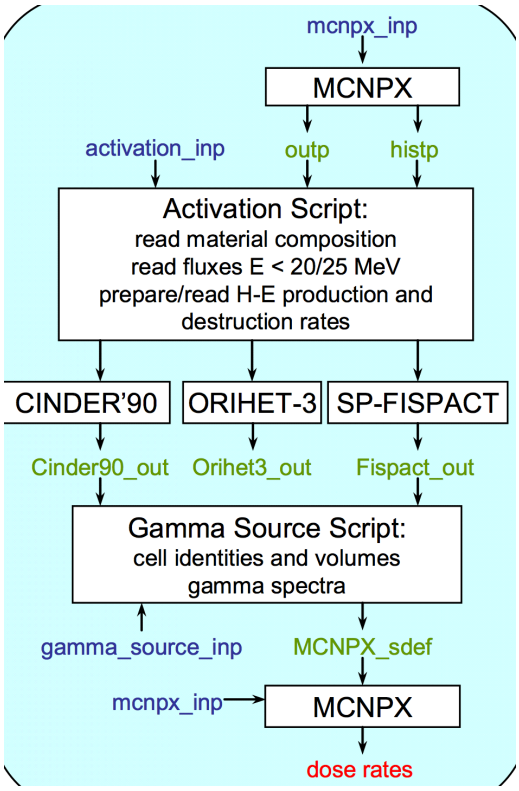

Figure 2-1 The scheme of activation and dose rate calculation[50]

MCNPX calculates energy-integrated reaction rates for all isotopes with cross-section information including (n,gamma), (n,fission), (n,2n), (n,3n), (n,alpha), (n,proton), etc. The activation code must use the MCNPX-calculated neutron spectrum to determine the rest of the interaction rates accumulated in the transmutation process, as well as to determine reaction rate information for the isotopes without cross-section information [50]. The activation script may serve as the driver of such a calculation. Using the gamma source script, the activation code results in a gamma source definition which can be used for subsequent particle transport calculation with MCNPX.

2.3. Nuclear cross-section libraries

There is an ongoing major international effort to provide a complete-as-possible compilation of evaluated cross section data for nuclear calculations. Major evaluation compilations are ENDF (USA), JEFF (Europe), JENDL (Japan), CENDL (China), and BROND (Russia). Since the quality of evaluated data strongly depends on the measurements upon which they are based, there is also an ongoing need for more accurate and precise measurements. After studying the literature and measurement data, the ENDF/B-VII library was selected for most of the calculations. ENDF data can be accessed at the National Nuclear Data Center operated by Brookhaven National Laboratory[51].

2.4. Nuclear inventory codes

Nuclear inventory codes solve Bateman equation (see equations 1.7 and 1.8 above) using analytical formalism. The CINDER'90, ORIHET-3, and SP-FISPACT codes are the most capable codes to be used together with MCNPX. CINDER'90[31] code was selected because the experimental results (comparisons of measured and calculated values) show that this is the most suitable code for high energy activation calculations[52].

2.5. CINDER'90

CINDER'90 uses Markovian chains to determine temporal densities of nuclides in a radiation environment, solving for independent contributions to atomic densities in each of a number of linear nuclide chains. The underlying assumption of Bateman equation is that the total decay probability together with absorbing probabilities β_m and $\gamma_{k\to m}$, and the flux Φ, are constant for the time interval for which the solution is desired. In CINDER'90, any temporal history can be approximated using histograms made of consecutive boxes of constant-flux intervals[31].

The differential equation describing the rate of change in the atom density $n_m(t)$ of a nuclide m is constructed as the sum of the rates of losses and gains in nuclide density. The losses are due to transmutation, the radioactive-decay and particle absorption reactions producing daughter and product nuclides, respectively, different from the

original nuclide m. Gains are from the transmutation of other nuclides having nuclide m as a daughter or a reaction product. For many applications, an additional constant production rate, Y_m can be included:

$$\frac{dn_m(t)}{dt} = -n_m(t)\beta_m + \overline{Y_m} + \sum_{k \neq m} n_k(t)\gamma_{k \to m} \qquad (2.1)$$

where γ_m is the probability of nuclide k transmuting (decaying or absorbing) to nuclide m and β_m is the total transmutation probability of nuclide m.

This set of differential equations describing all nuclides is interconnected, since each equation in general contains the temporal atomic density of other nuclides. This set of coupled differential equations can be reduced to a set of independent, linear differential equations using the Markov method. Based on the literature, it is accurate, but requires more computer capacity[31].

The differential equation for the rate of change of the i-th element, $n_i(t)$, is coupled to the preceding element in the sequence for which all parameters are known and solutions have been obtained[31]:

$$\frac{dn_i(t)}{dt} = +\overline{Y_i} + n_{i-1}(t)\gamma_{i-1} - n_i(t)\beta_i \qquad (2.2)$$

where quantities are indexed by their order in the decay sequence, γ_{i-1} is the decay probability together with absorption probability for forming the i-th element from the i-1-th element in the sequence.

The general solution for a linear sequence of nuclides is derived for use in the CINDER code. CINDER'90 differs from the earlier code versions in that this code does not require a predefined set of sequential nuclides or linear chains. It tests each transmutation step for significance and constructs the sequences to be calculated. The algorithm propagates the initial density and constant production rate of only the first nuclide of the chain in order to limit the length of the chains followed. This set up completely defines the total inventory of all nuclides in the system of chains beginning with the first nuclide[31].

3. The European Spallation Source

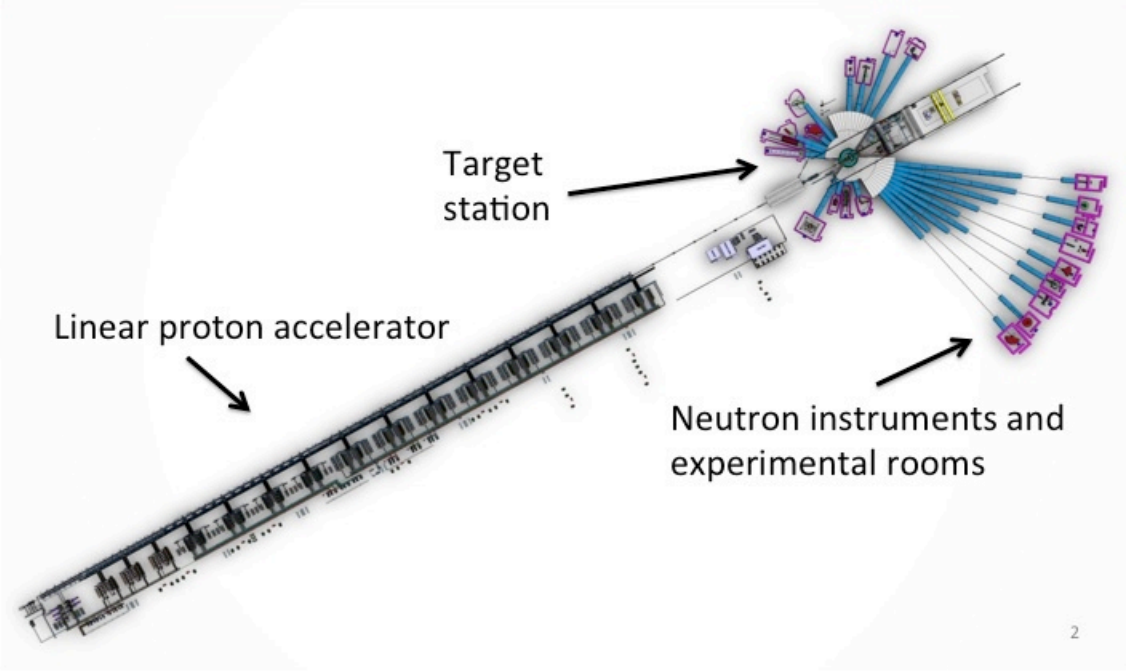

Figure 3-1 The main parts of ESS[3]

The European Spallation Source, ESS, consists of a linear proton accelerator, a target monolith building with a tungsten target, neutron instruments and experimental laboratories[3].

The linear accelerator drives protons onto the target. The proton beam window separates the ultra-high vacuum of the proton beam tube and the helium atmosphere inside the target monolith. The accelerated protons impinge on the rotating target wheel and initiate spallation reactions, releasing neutrons from tungsten nuclei. After slowing-down and moderation, the neutrons are guided to experimental rooms[3].

Groundbreaking of ESS was done in 2014, and the initial operations (first neutrons for science) are scheduled to start in 2023. There will be a gradual ramp up in energy and power, and eventually ESS will reach design parameters of 2 GeV energy and 5 MW power[53].

3.1. Linear accelerator

The superconducting linear accelerator takes protons from the ion source, accelerates them to 2 GeV energy using clystrons and modulators, and drives them onto the target. The time-average current is 2.5 mA, which means 1.56×10^{16} proton/s time-average beam intensity. In this work, the 2 GeV proton beam-on-target was characterized by rectangular footprint spatial profile of about 14 cm width and 3.2 cm height. This footprint is based on pulse-average raster beam to be employed at ESS. The macro-pulse duration is 2.86 ms[53].

3.2. Target station

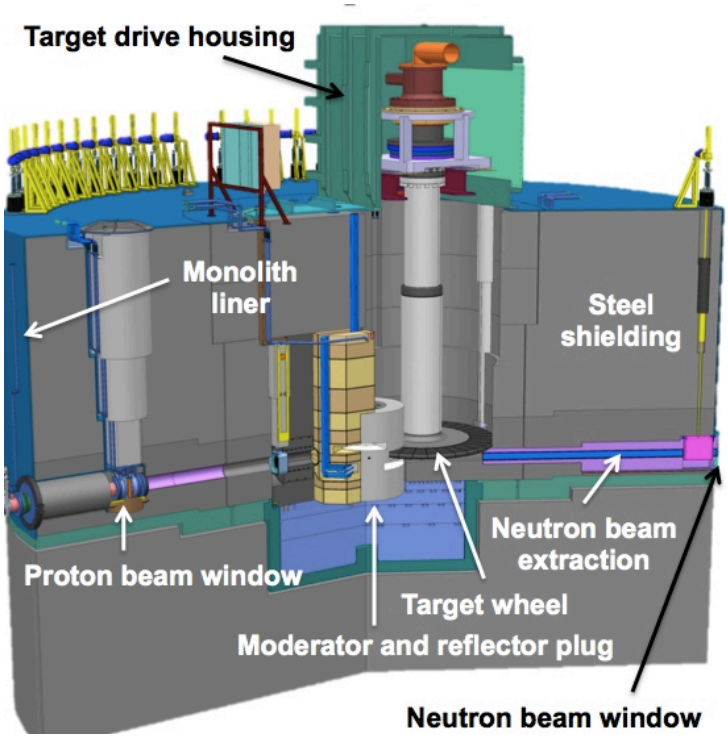

Figure 3-2 The target station monolith[54]

The target station monolith is a cylinder made of 6000 tonnes of steel and reinforced concrete, housing the irradiated components during ESS operation. The target is cooled by helium, the monolith "immerses" into a helium atmosphere as well. The monolith contains the proton beam window, the target assembly with a rotating target wheel, the moderator-reflector system, and 42 neutron beam ports guiding neutrons to the neutron instruments.

The target station also has an active cell facility in order to store irradiated components that will be taken out from the monolith after they will reach the end of their lifetime[54]. New techniques were developed in order to perform remote handling within hot cells[55].

The target wheel

The target wheel is a 4 tonne, 2.5 m diameter stainless steel vessel containing about 7000 tungsten bricks. It will be replaced in every five years. The wheel rotates at the rate of 23.3 RPM. The helium coolant passages, the drive motor, and the support bearings are integrated into the target shaft[54].

The moderator-reflector system

The moderator-reflector system is housed in a replaceable plug. It includes cryogenic hydrogen and water-cooled systems. The moderators slow down and moderate the neutrons to provide intense thermal and cold neutron beams (see Chapter 1.5). Different moderator concepts were considered[56]. The final moderator design is based on an innovative concept of low-dimensional liquid hydrogen moderators, partially surrounded by water premoderators, all placed on top of the spallation target[57]. The thesis calculations were performed for both the TDR-case (ESS technical design report) liquid hydrogen volume moderator, as well as for the finally low-dimensional moderator. The comparison of their time-average neutron brightness can be seen in Figure 3.3.

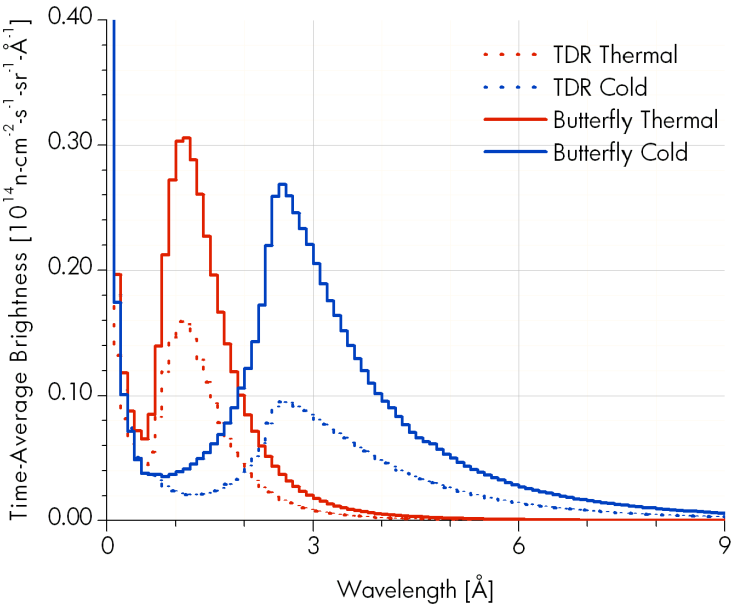

Figure 3-3 Comparison of moderator systems based on time-average brightness[3,57]

The neutrons that otherwise would leak pass into the reflector, and some of them diffuse back into the moderators. The reflector includes water channels and is composed of inner and outer parts. The outer reflector is made of stainless steel with 10% volume fraction of water for cooling. The inner reflector, which extends to a diameter of 0.6 m and a height of 0.3 m, is made from beryllium contained in an aluminium vessel[3].

3.3. The neutron guide system

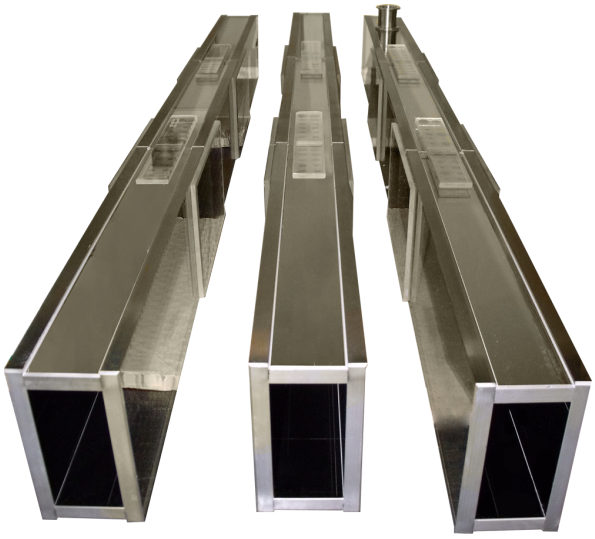

Figure 3-4 Standard free-standing neutron guides[58]

In order to avoid the drop off in neutron intensity as would be the case with a beam expanding openly in vacuum, a neutron guide system is needed to channel the neutron beams from the moderator system to neutron instruments. In the neutron guides the neutrons are passed by series of total or Bragg reflections. Neutron guides consist of many layers of interspersed nickel and titanium, in order to achieve good reflectivity beyond the critical scattering angle [58]. In the past, mainly glass materials were manufactured as a substrate for the layers, the metal substrate is today a new and fast developing solution due to its better mechanical properties.

The activation of the neutron guides is an important topic because the replacement of the guides is envisaged after 10 years use due to radiation damage that includes the generation and increasing interstitial presence of He gas generated mainly by (n,α) reactions, mechanical failure, as well as progress in guide technology.

3.4. The neutron instruments and experimental halls

At the beginning, 15 neutron instruments will be operated at ESS including diffractometers, spectrometers, reflectometers, small-angle neutron scattering, and

radiography instruments. They will cover a wide and important range of experimental material research. During the experiments, the structural materials of the experimental caves will be also activated. In this thesis the Macromolecular Diffractometer (NMX) cave was selected as an example and, therefore, this instrument is briefly described below.

Macromolecular Diffractometer (NMX)

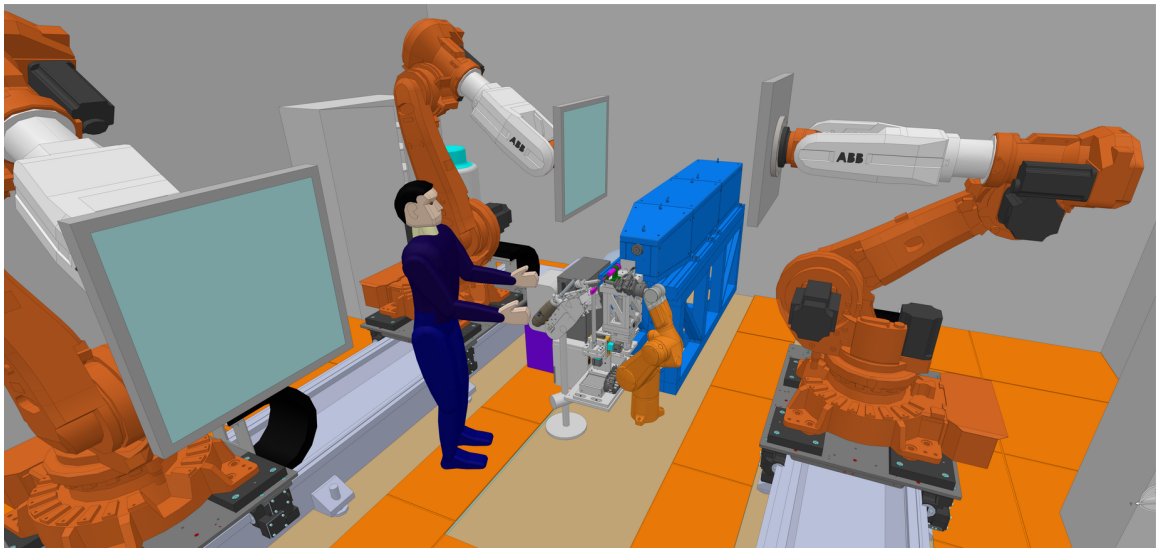

Figure 3-5 NMX experimental cave[59]

The NMX is a time-of-flight (TOF) quasi-Laue Macromolecular Diffractometer optimized for small samples and large unit cells dedicated to the structure determination of biological macromolecules by crystallography. The main scientific driver is to locate the hydrogen atoms relevant for the function of the macromolecule. It contains triple gas electron multiplier (GEM) detector with natural gadolinium as a neutron converter[59]. After the neutron capture, gadolinium releases prompt gammas with energy up to 9 MeV which require thick concrete shielding. The experimental cave containing this instrument is planned together with aluminium floor and concrete walls.

4. Estimation of the missing clearance levels

For numerical waste classification, the waste index *WI* (equation 1.10) of the whole waste stream should be calculated. As most of the recent IAEA publications[41,60] were elaborated primarily for nuclides produced in nuclear reactors (e.g. fission products), they do not contain several clearance levels which are relevant for decommissioning of ESS, as it was discussed in Chapter 1.7 already. This is the case with the pertinent Swedish regulatory document, SSM FS 2011:2 as well[37].

The missing clearance levels were calculated by two different types of methods: external exposure scenarios were used for gamma emitting radionuclides, and internal exposure scenarios were applied for pure beta- and alpha-emitting radionuclides[61].

4.1. External exposure

According to RP122[40], the three external exposure scenarios are the following:

- A landfill worker working with cleared building rubble
- A truck driver transporting cleared waste to a waste dump
- A person living in a house the material of which contains cleared waste, this case generally turned out to be the most conservative external scenario for radionuclides with half-lives in the range 1-100 years, so it was used in our study as the default method. It is quite similar to the most limiting scenario of IAEA SRS 44[41].

In case of gamma emission, the specific dose consequence, *SDC*, is proportional to gamma emission intensities and energy-dependent absorption coefficient of human body. It is also influenced by the absorption in the waste bulk itself.

The gamma dose rate can be calculated by the following formula:

$$\dot{D} = \frac{k_\gamma \cdot A}{r^2} \qquad (4.1)$$

where k_γ is the specific gamma ray dose constant, or gamma factor, which is the gamma dose rate at a specific distance from a unit amount of a photon-emitting radionuclide, A is the activity of the photon-emitting radionuclide, r is the distance from it.

Considering the absorption in human body and attenuation in the bulk of cleared material, the following formula describes the specific gamma ray dose constant, or gamma factor:

$$k_\gamma = \sum_{j=1}^{P} E_{\gamma,j} \cdot f_{\gamma,j} \cdot \mu_s\left(E_{\gamma,j}\right) \cdot B_j \cdot \exp\left(-\mu_c\left(E_{\gamma,j}\right) \cdot x_{eff}\left(E_{\gamma,j}\right)\right) \qquad (4.2)$$

where E_γ is the gamma energy, f_γ is the gamma abundance relative to one decay, μ_s is the energy dependent absorption coefficient of soft human tissue, μ_c is the energy dependent absorption coefficient of concrete, x_{eff} is the effective thickness of the material containing the cleared radionuclide, P is the number of gamma lines of the radionuclide in question, and B_j is the respective build-up factor for the given energy in concrete.

The external dose from the unattenuated gamma and X-ray photons is increased by the scattered portion traversing the shielding materials in the direction of the target. This is regularly expressed as the build-up factor, a quantity which is strongly dependent on the energy of the photon and the atomic number of the scattering material[62].

The effective thickness of the building material containing the cleared radioactive waste is 20 cm, in accordance with RP122[40] and SRS44[41].

It is worth noting that the physical content of absorption coefficients for the two media is necessarily different. As it is clearly explained in the introductory chapter of the NIST database[63], the shielding process is characterized by a coefficient describing the generation of both the particle and radiation kinetic energy released per unit mass (KERMA) (μ_c in equation 4.2), but the expression should include the build-up factor as well. On the other hand, the absorption in the human body (μ_s in equation 4.2) is characterized by the so-called "mass energy-absorption coefficient" that does not include the scattered radiation KERMA. Build-up calculations can either be performed by validated software packages like MICROSHIELD[64] (this was our primary method) or

factors can be inter- or extrapolated from numerical databases like those published in the pertinent Hungarian Standard[65].

The absorption coefficients of human body were estimated by mean absorption coefficients of the different human tissues. Data for the actual gamma energies were interpolated from the NIST database (see Table 4-1).

Table 4-1 Absorption coefficients[63]

Energy (keV)	Soft tissue abs. coeff.	Concrete abs. coeff.
20	5.66E-01	2.81E+00
30	1.62E-01	9.60E-01
40	1.03E-01	5.06E-01
50	4.36E-02	3.41E-01
60	3.26E-02	2.66E-01
80	2.62E-02	2.01E-01
100	2.55E-02	1.74E-01
150	2.75E-02	1.44E-01
200	2.94E-02	1.28E-01
300	3.16E-02	1.10E-01
400	3.25E-02	9.78E-02
500	3.27E-02	8.92E-02
600	3.25E-02	8.24E-02
800	3.18E-02	7.23E-02
1000	3.07E-02	6.50E-02
1250	2.94E-02	5.81E-02
1500	2.81E-02	5.29E-02
2000	2.58E-02	4.56E-02

Finally, this leads us to the estimation of a previously unknown *CL* of radionuclide *x*:

$$CL_x = CL_s \cdot \frac{k_{\gamma,s}}{k_{\gamma,x}} \cdot \frac{DF_s}{DF_x} \tag{4.3}$$

where the index *s* refers to a well-known radioisotope selected as "standard" and *DF* are the appropriate decay factors calculated in the following way:

$$DF = \frac{1-\exp(-\lambda t)}{\lambda t} \quad (4.4)$$

where λ is decay constant taken from Lund/LBNL Nuclear Data Search[66] and t=1 year, in accordance with the scenario described in RP122[40] in more details.

As it was described in Chapter 1.7 above, the basis of the *CL* calculations was supposed to be the annual effective dose of 10 μSv, and the cleared material was supposed to be present in the vicinity of the representative person during the whole year.

Radionuclides with external exposure scenarios which are relevant for the ESS inventory calculations, but are missing from the present *CL* compilations for bulk amounts of waste are the following (Table 4-2):

Table 4-2 Gamma emitters

Nuclide	Standard	Calculated *CL* [Bq/g]
^{101}Rh	^{137}Cs	7.90E-01
^{133}Ba	^{137}Cs	5.90E-01
^{144}Pm	^{149}Pm	2.04E-02
^{146}Pm	^{149}Pm	3.00E-01
^{150}Eu	^{152}Eu	1.70E-01
^{174}Lu	^{177}Lu	6.60E+00

4.2. Incorporation by inhalation and ingestion

The appropriate internal pathway scenarios were used for pure alpha- or beta-emitting radionuclides. There are two different methods for estimating the clearance level for radionuclides that have a higher threat internally. The dose conversion factor (*DCF*, see Appendix, equation A.5) includes the whole internal scenario, therefore, in case the dose conversion factor is known, the previously undefined clearance level can be calculated

from the known clearance level of an appropriately selected "standard" multiplied by the ratio of the two dose conversion factors[33]

$$CL_x = CL_s \cdot \frac{DCF_{p,s}}{DCF_{p,x}} \tag{4.5}$$

where the index *s* refers to a well-known radioisotope selected as "standard"; the index *p* refers to the intake pathway of inhalation or ingestion.

Various examples occurred for this estimation method. Both inhalation and ingestion scenarios were calculated. The ING-B (ingestion) scenario of RP122[40] covers a case where an infant ingests contaminated dust through various ways, e.g. playing on a built surface, eating vegetables and fruits, etc. In most cases the ING-B scenario was definitive. In the case of ^{148}Gd the inhalation scenario gave the most conservative, that is, the lowest *CL* estimation.

On the other hand, if the dose conversion factor is missing from the database[33] (this was the case, e.g. with ^{91}Nb), the clearance level can be estimated by selecting a "standard" radionuclide with a presumably similar chemical behaviour as the radionuclide in question. This estimation is based on the assumed similarity of transfer factors (*f*) that is the proportion of intake transferred to body fluids for ingestion scenarios and the proportion of intake cleared from the lungs and taken mostly to the gastro-intestinal tract for inhalation, respectively. The undefined clearance level can be then estimated by the following formula:

$$CL_x = CL_s \cdot \frac{\sum_{j=1}^{P} \hat{E}_{j,s} \cdot f_{j,s} \cdot w_{R,s}}{\sum_{j=1}^{P} \hat{E}_{j,x} \cdot f_{j,x} \cdot w_{R,x}} \cdot \frac{T_{s,eff}}{T_{x,eff}} \tag{4.6}$$

where summation is over particle radiation type (α and/or β), w_R is the appropriate radiation weight factor (see Appendix, equation A.2) and T_{eff} is the effective half-life of the radionuclides combining the physical half-life of the radioisotope and the biological half-life of the element factor (see Appendix, equation A.6), $\hat{E}$ is the "effective energy" of the respective α or β decay of the radionuclide:

$$\hat{E} = \sum_{i=1}^{n} E_i \cdot f_{R,i} \quad (4.7)$$

where n is the number of respective energy levels (for beta radiation, the average particle energy), $f_{r,i}$ are the values of their relative abundances (yields).

This calculation method makes use of the fact that the majority of these weakly penetrating radiations will not leave the source organ so the dose to the neighbouring organs can be negligible. Radionuclides provided with estimated clearance levels by these methods are the following (Table 4-3):

Table 4-3 Pure alpha or beta (EC) emitters

Nuclide	Standard	Calculated *CL* [Bq/g]
^{39}Ar	^{3}H	2.2E+01
^{49}V	^{48}V	1.2E+04
^{91}Nb	^{94}Nb	5.3E+02
^{113m}Cd	^{109}Cd	1.4E+00
^{137}La	^{140}La	6.2E+03
^{148}Gd	^{153}Gd	2.7E-01
^{157}Tb	^{160}Tb	6.5E+02
^{163}Ho	^{166}Ho	4.5E+02

5. Inventory and waste index assessment of the tungsten target

5.1. Summary of different target concept options potentially considered for ESS

The activation of the target is a crucial part of decommissioning planning because it will be the most active part during the operational phase and after removal. Moreover, the target will be replaced during the operational phase with a frequency of at least 5 years. Several target materials had been studied, the selected material is tungsten[3]. The other options considered in ESS design study were mercury and lead-bismuth (LBE) liquid targets. The eutectic alloy lead-bismuth, tested in the MEGAPIE spallation target at SINQ at the Paul Scherrer Institut (PSI) in Villigen, Switzerland, would give the advantage of lower melting temperatures than lead. The mercury option was rejected because at present there is no feasible technology to solidify and chemically condition radioactive mercury. Ghiglino and coworkers[67] investigated a possible lead target for ESS with neutronic performances assumed to be close to that of the W target. Their water-cooled rotating solid target was considered as an option for the 5 MW ESS project. However, the thermal behaviour of lead for the pulsed source could pose a problem. The possibility of using a Pb-17%Au eutectic (melting point 212°C) target has also been considered (Pb-Au target, LGE), but its applicability was questioned owing to the envisaged corrosion problems in the operational period in addition to its high cost and lack of operational experience.

5.2. Features of the tungsten target

The tungsten target is expected to be the most active part of the facility when the operation is ongoing and terminates. The target will be replaced at least in every 5 years, so the calculations were performed assuming 5 years of operation and 10 years cooling time for 8 targets during 40 years.

The total nuclide inventory does not depend much on the details of the geometry of the target or that of the beam profile as long as the whole proton beam is stopped in the target. In this thesis the tungsten target wheel geometry from the ESS TDR[3] was used. Its diameter is 2.5 m and it consists of 33 sectors (Figure 5-1).

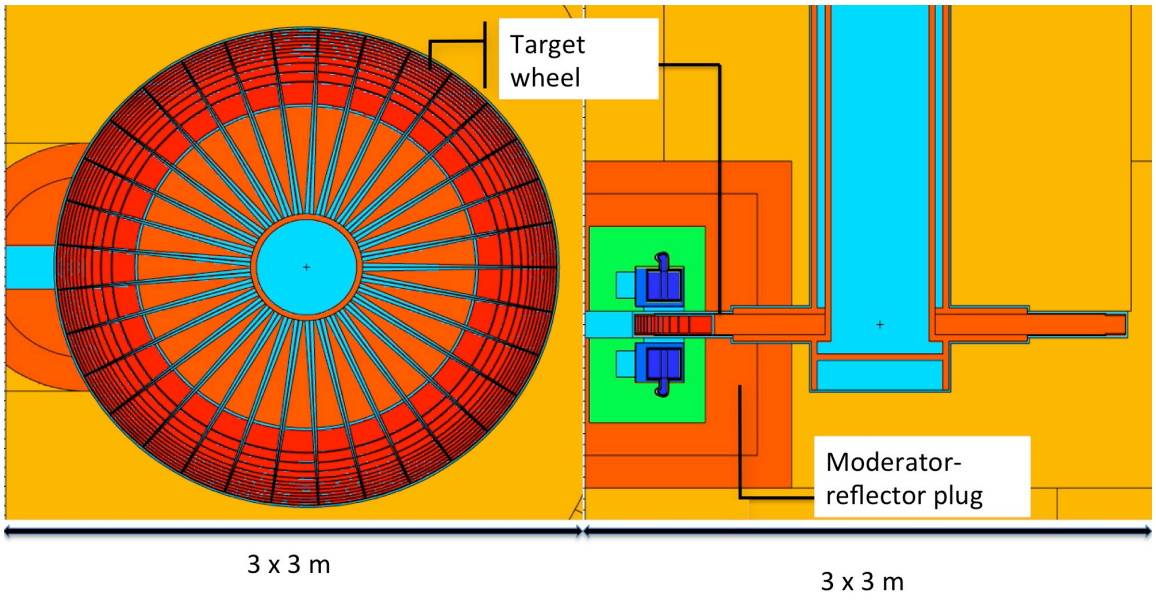

Figure 5-1 TDR-case MCNPX geometry of ESS target monolith[3,68]

The Beijing Tian-Long tungsten[69] material was applied in the calculations which is a homogenous tungsten material containing a few impurities (Table 5-1).

Table 5-1 Initial impurities (weight ppm) of Beijing Tian-Long tungsten(19.3g/cm³)[69]

C	O	Mg	Al	Si	S	K	Ca	Ti	V	Cr	Mn
10	50	10	5	0.56	4	0.13	8	4	4	4	4
Fe	Co	Ni	Cu	As	Mo	Cd	Sn	Sb	Pb	Bi	
10	4	5	1	7	30	1	1	4	1	1	

5.3. Inventory and decay heat calculation method for target

The radionuclide inventory has been calculated with MCNPX2.7[49] using ENDF/B-VII[51] cross-section libraries coupled with CINDER'90[31]. Different spallation models have been used. In order to describe the first step in the reaction mechanism of the spallation process, intranuclear cascade (INC) models the Bertini code[15], Isabel[16] and INCL4.2[17] were applied. For the adequate description of the de-excitation of the nucleus, all three models have been coupled to the code of ABLA[22] and Dresner[23]. CEM02[24] model contains both steps of spallation in one package.

For MCNPX simulations the TDR-like MCNPX monolith model by Alan Takibayev[3,68] was taken (Figure 5-1). The proton beam energy is 2 GeV. The calculations presented below were performed using 1.33 GeV proton energy as well, in order to compare with the results obtained previously with that energy. This energy was proposed for ESS in one of the earlier design studies[70]. The time-average current is 2.5 mA.

ESS is planning with 200 operation days per year, but the exact time schedule will be specified in pre-operational phase. In the calculations, 5 years continuous operation was considered as a conservative estimate. Sensitivity analysis were performed to estimate the uncertainty coming from the irradiation history, it is about 10%.

The activation of the target was calculated using the following moderator concepts: TDR-case pure parahydrogen cylindrical moderator[3] and flat quasi-two-dimensional butterfly moderator[56]. Parahydrogen is treated by scattering kernels that are analogous to the scattering functions of the neutron wave vector and energy transfer, this approach is accurate enough based on the literature[71]. The activation results of the target were the same for both moderator concepts, therefore, the results of the TDR configuration are discussed in this thesis.

5.4. Decay heat results for the irradiated target

After 5 years operation time the total decay heat performance is 40.8 kW ± 10% which means 204 kW/m^3 characterizing the target as a high level radioactive waste (as discussed at the end of Chapter 1.7, this is not defined officially according to the current Swedish regulatory ordinance). It is straightforward that after the removal it needs to be cooled in hot cell. In about two weeks the decay heat goes below 2 kW/m^3 which is widely considered the margin for high level waste, e.g. in the Hungarian radioactive waste regulations[42]. From this point of view the target would not be classified as high level waste further on; however, the target will have to be considered as high level waste (HLW) because of its waste index (see the following chapters) according to our calculations.

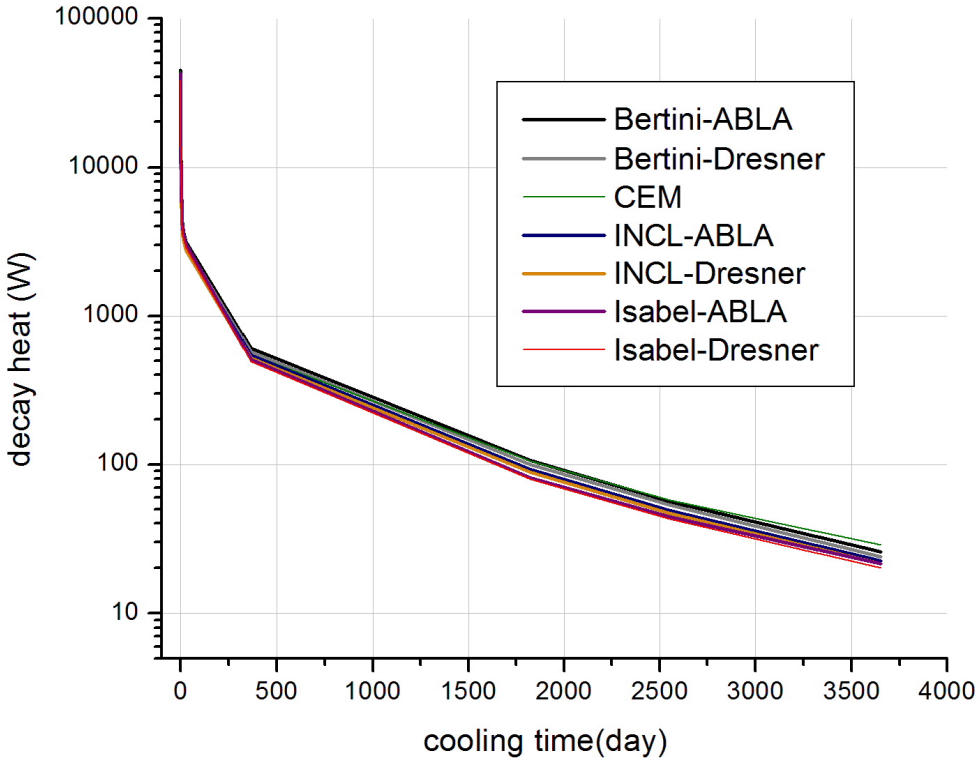

Figure 5-2 Decay heat in tungsten as a function of cooling time, after 5 years of operation using different spallation/evaporation model combinations

5.5. Inventory and waste index results

After 5 years of operation and 10 years of cooling time, the activity concentrations without tritium, obtained with Bertini-ABLA and INCL4.2-ABLA show the maximum values. Comparing the waste index (without tritium) based on these two different calculation methods, the INCL4.2-ABLA results have been accepted as the most conservative estimation.

Table 5-2 Activity concentration of tritium, the sum of activity concentration of all other isotopes in tungsten after 5 years of operation and 10 years of cooling using different models

Model	c_A of ^{3}H (Bq/cm^3)	total c_A without ^{3}H (Bq/cm^3)
Bertini-ABLA	5.81E+07	1.80E+09
Bertini-Dresner	1.26E+10	1.62E+09
CEM	1.44E+10	1.70E+09
INCL4.2-ABLA	2.25E+07	1.78E+09
INCL4.2-Dresner	4.46E+09	1.71E+09
Isabel-ABLA	5.83E+07	1.65E+09
Isabel-Dresner	1.21E+10	1.48E+09

These results show the clearance levels and waste index data comparing two versions of MCNPX as well as two proton beam energies (1.33 GeV and 2 GeV). *CL*s were taken from RP122[40] if they existed there; otherwise they were estimated by the methods described above. Extremely high differences (more than one order of magnitude) occurred in case of ^{22}Na and ^{90}Sr production for the different proton beam energies.

The difference between MCNPX2.5 and MCNPX2.7 is not significant except in case of ^{3}H production. The difference in tritium production is probably significant since cluster emission through a coalescence process has been introduced only in later versions of MCNPX[72]. It should be also noted that the tritium content of the waste stream will strongly depend on the applied waste treatment technologies. Considering its high clearance level, the tritium does not give a significant contribution for the waste index (less than 2.4%) anyway.

Table 5-3 Clearance ratios and waste index of radionuclides for tungsten target

Nuclide	Clearance level [Bq/g] from RP122[40]/ Calculated	Waste index after 10 year of cooling		
		MCNPX2.7 2 GeV	MCNPX2.7 1.33 GeV	MCNPX2.5 1.33 GeV
^{148}Gd	2.70E-01	5.02E+06	3.94E+06	3.92E+06
^{133}Ba	5.90E-01	5.82E+06	1.06E+06	1.17E+06
^{152}Eu	2.10E-01	5.45E+06	2.84E+06	2.74E+06
^{179}Ta	1.10E+01	4.38E+06	3.10E+06	3.12E+06
^{60}Co	9.90E-02	3.75E+06	2.77E+06	3.31E+06
^{154}Eu	1.90E-01	1.72E+06	1.02E+06	1.01E+06
^{150}Eu	1.70E-01	8.86E+05	6.37E+05	8.26E+05
^{3}H (CEM02)	8.60E+02	8.66E+05	4.79E+05	5.29E+02
^{172}Lu	1.00E+01	7.31E+05	5.60E+05	5.81E+05
^{172}Hf	1.00E+01	7.24E+05	5.54E+05	5.76E+05
^{173}Lu	5.10E+00	5.49E+05	4.12E+05	4.17E+05
^{174}Lu	6.60E+00	4.57E+05	3.63E+05	3.61E+05
^{158}Tb	4.30E-01	3.54E+05	2.25E+05	2.02E+05
^{146}Pm	3.00E-01	3.46E+05	2.78E+05	1.01E+05
^{101}Rh	7.90E-01	1.31E+05	4.32E+04	4.65E+04
^{144}Pm	2.04E-02	9.52E+04	4.04E+04	4.04E+04
^{22}Na	1.30E-01	8.31E+04	5.34E+01	4.28E+01
^{90}Sr	1.10E+00	2.74E+04	9.77E-02	2.06E-01
^{145}Pm	5.40E+02	1.81E+04	1.18E+04	1.15E+04

5.6. Uncertainty of the results

The uncertainty of the inventory calculations comes from the inaccuracies in MCNPX geometries and the applied physics models; the statistical variances of the Monte Carlo calculations; the uncertainty of the applied cross-sections; the uncertainty of the material compositions and the approximations in irradiation histories.

The applied MCNPX geometry models were well detailed in the activation calculations; therefore, the uncertainty coming from the geometry is relatively low, 5-10%, based on sensitivity analysis performed by the author.

The applied physics model had a significant effect (see Table 5-2).

The statistical variances of the Monte Carlo calculations were kept under 5% in all calculations by using high statistics.

The uncertainty coming from the applied cross sections was considered within 10% based on the literature[51,73].

The uncertainty coming from the inaccuracies in the irradiation history, such as calculating with continuous proton beam is between 5-10% based on sensitivity analysis performed by the author.

The uncertainty coming from the material composition has the largest contribution for the total uncertainty since the material composition has a significant impact on the inventory. In case an impurity (e.g. cobalt) is not indicated in the nominal composition, but presents in the real composition, production of an important nuclide (e.g. ^{60}Co) can be underestimated by orders of magnitude (see Chapter 9). Therefore, it is advised to validate the material compositions using different experimental techniques. Concerning the total activity, the uncertainty coming from material composition is under 15% based on sensitivity analysis performed by the author.

The uncertainty of the waste index and gamma dose rate values directly inherits the uncertainty of the activity concentration values.

Considering all factors mentioned above, the overall uncertainty of the total activity concentration is within 31%.

In terms of clearance levels, if it was applicable, the clearance level was recalculated using a newly selected standard. The relative difference between the calculated clearance levels using different standards was always lower than 3%. The overall uncertainty of the waste index is within 40%.

The nuclides having the greatest share in the compound waste index are ^{148}Gd, ^{133}Ba, ^{152}Eu, ^{179}Ta, ^{60}Co, and ^{154}Eu. Sensitivity analysis (calculation using cobalt-free material)

performed by the author showed that 99% of ^{60}Co production is due to cobalt impurity, therefore, it is advised to use structural materials with low cobalt content.

The waste index determines the waste category (HLW or ILW) that results in major consequences in the selection of the proper chemical conditioning procedures in waste processing technology and the site of disposal. (This latter argument is all the more important in Sweden where waste classification is closely interconnected[74] with the designation of the disposal facility.) This indicator should be the primary parameter for the cost of target decommissioning. The overall score is represented by the summarized waste index after a 10-year cooling period – it is 1.9E+07 for 1.33 GeV protons. Using 2 GeV proton energy, the result is 3.2E+07. In both cases the target will therefore belong to high level radioactive waste category. The target should be stored in hot cell before conditioning and deep geological repository is advised for final disposal.

5.7. Waste index comparison

Table 5-4 Waste index comparison of different target concepts[61]

	Hg	LBE	LGE	W
Waste index after 10 years cooling	4.5E+07	1.7E+09	5.5E+07	1.9E+07

The heat generation is not an independent indicator from the waste index, but also influences the waste category and the conditioning method. Elevated values might cause e.g. cracks in a cemented or vitrified complex of the conditioned waste. The long-term stability of the engineered and natural barriers depends strongly on the heat load from the waste.

Table 5-5 Heat generation comparison

	Hg	LBE	LGE	W
Heat generated after 10 years cooling [W/m^3]	43	135	53.01	58

Table 5-4 shows that the tungsten target is a better alternative than the other, previously studied options (mercury, LBE, LGE, see Chapter 5.1) in terms of waste characteristics. However, all alternatives have HLW category even after 10 years cooling. Based on heat

generation alone all of the options would be below the HLW limit. Mercury has got the second lowest waste index, but the application of mercury generates additional steps in conditioning process (see Chapter 5.1) considering its highly toxic nature. The third option was the lead-gold eutectic (LGE) target, but its applicability was not considered as a real alternative (see Chapter 5.1). The LBE is the least advantageous alternative based on waste index and heat generation comparison[61].

6. Inventory and dose rate assessment of the neutron guides and inserts using different guide substrates

In addition to the estimation of the activation of the targets defining their waste characteristics, modelling calculations were applied to determine the radioactivity generated in other components of ESS research facility which also have to be considered for the radiation safety of decommissioning operations.

6.1. Features of the neutron guides and inserts

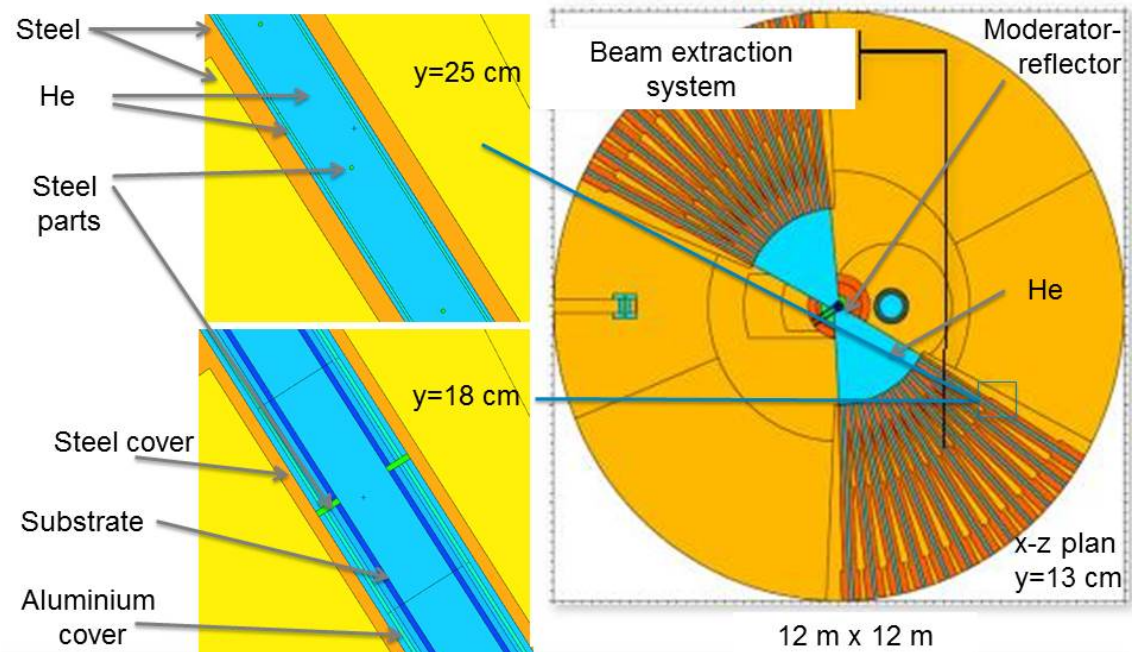

Figure 6-1 TDR-like geometry of neutron inserts inside the monolith[3]

The activation of the neutron guide inserts inside the monolith has an important role in terms of decommissioning, because the replacement of the guides and inserts is planned after every few years. The neutron guides are glass or metal tubes covered by several layers of interspersed nickel and titanium and placed in a steel neutron guide insert. Different neutron guide substrate materials were examined in terms of activation. The material compositions are given in the following (Table 6-1, 6-2, 6-3, and 6-4):

Table 6-1 Material composition of the aluminium substrate and cover (weight%), (2.7 g/cm³)

Al	Mg	Si	Fe	Zn	Ti	Cr
98.725	0.475	0.45	0.2	0.075	0.05	0.025

Table 6-2 Material composition of the zerodur glass substrate (weight%), (2.53 g/cm³)

SiO_2	Al_2O_3	MgO	TiO_2	ZnO	ZrO_2	Li_2O	P_2O_5	As_2O_3	Na_2O
42	34.35	3.82	3.82	3.82	3.82	3.82	3.82	0.38	0.38

Table 6-3 Material composition of the sodium-float glass (float in the following) substrate (weight%), (2.5 g/cm³)

SiO_2	Na_2O	CaO	MgO	Al_2O_3	Fe_2O_3	K_2O	TiO_2
71.86	13.13	9.23	5.64	0.08	0.04	0.02	0.01

Table 6-4 Material composition of the steel cover and insert (weight%), (7.85 g/cm³)

C	Si	P	S	Cr	Mn	Fe	Co	Ni	Mo
0.015	0.4	0.02	0.01	17.002	1.8	65.721	0.03	12.502	2.5

6.2. The method of activation and dose rate calculations

The radionuclide inventories were calculated with MCNPX2.7[49] using ENDF/B-VII nuclear data libraries coupled with CINDER'90[31]. The MCNPX geometry constructed for the neutron guides inside the inserts and monolith is shown in Figure 5.1. For the MCNPX simulations the TDR-like MCNPX monolith model by Alan Takibayev[3,68] was taken and completed by the geometry of the neutron guides and inserts**.** The geometry and material composition of the neutron guides are based on neutron guides produced by MIRROTRON Ltd[58]. In order to get conservative estimation, the calculations were carried out for the most active insert and guide (in the west sector, 30° from the proton beam line, the closest one to the target). A 10 cm wide, 4 m long rectangular guide was

modelled covered by 1 cm thick substrate. In the calculations the neutrons were generated with a proton beam energy of 2 GeV incident on the target. Using the decay gamma source script, the CINDER'90 activation code resulted in a gamma source definition which served as a feedback for another particle transport calculation with MCNPX. The resulted decay gamma dose rate maps show the sum of the gamma dose of all gamma and X-ray emitter nuclide.

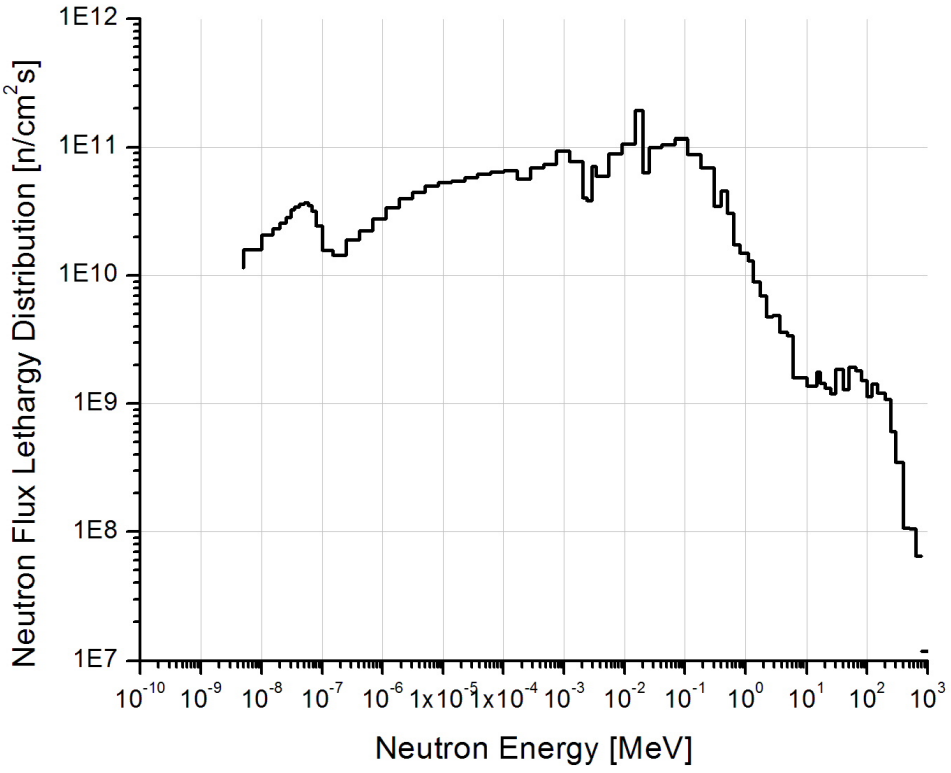

Figure 6-2 Neutron spectrum at the opening of the most active neutron guide inside the monolith calculated by MCNPX

6.3. Results of activation calculations of the neutron guide substrates

It should be noted that the activation of neutron guides shows a significance difference further from the target. Since the amount of fast neutrons is smaller, the number of

radioactive nuclides produced by fast neutrons is also smaller. In case of zerodur, the tritium gives the main contribution for total activity concentration and waste index. As it was mentioned before, the tritium content of the waste stream will depend on the applied waste treatment technologies. It was also shown that calculation of tritium shows significant uncertainty (See Chapter 5.6). Therefore, the total activity and waste index of zerodur was demonstrated without tritium as well. Immediately after shutdown the zerodur substrate is the most active and aluminium is the least active. Without tritium the zerodur would become the least active after ten years of cooling.

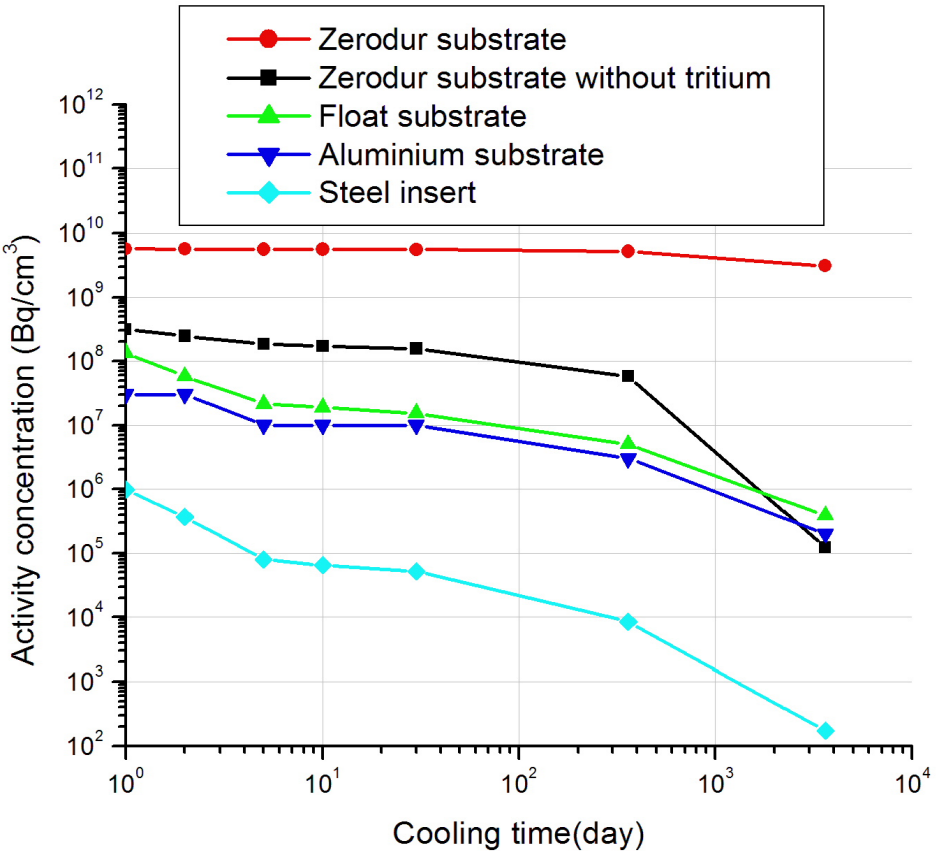

Figure 6-3 Sum of activity concentration after 5 years operation as a function of cooling time in different kind of guide substrates and insert

Using different guide positions resulted approximately in 10% change in results, the uncertainty coming from the inaccuracies in the irradiation history is under 5%, the

statistical standard deviation values were within 3%. Considering all factors described in Chapter 5.6, the overall uncertainty of the total activity concentration of the guide elements is within 26%.

Table 6-4 Inventory of the aluminium substrate after 5 years operation and 1 day cooling

Nuclide	Act. conc. (Bq/cm^3)	Main gamma lines[66] (MeV)	Half-life[66]	Clearance level (Bq/g)[40]
^{65}Zn	1.85E+07	1.11 (50%)	244.3 d	5.20E-01
^{24}Na	5.11E+06	2.75 (100%) 1.37 (100%)	14.96 h	2.10E-01
^{51}Cr	3.71E+06	0.32 (10%)	27.70 d	1.20E+01
^{55}Fe	1.90E+06	-	2.73 y	4.70E+01
^{69}Zn	3.54E+05	-	56.40 m	1.60E+02
^{69m}Zn	3.30E+05	0.44 (95%)	13.76 h	2.70E+00
^{56}Mn	1.20E+05	0.85 (99%) 1.81 (27%) 2.11 (14%)	2.58 h	6.60E-01
^{59}Fe	8.24E+04	1.10 (56.5%) 1.29 (43.2%)	44.5 d	2.60E-01
^{54}Mn	7.14E+04	0.84 (100%)	312.3 d	1.00E-01
^{3}H	5.06E+04	-	12.33 y	8.60E+02

After 1 day cooling time the most active nuclide in aluminium is the ^{65}Zn (1.85E+07 Bq/cm^3), but in aluminium it presents in six time less quantity than in zerodur. ^{65}Zn is produced from ^{64}Zn by thermal neutron capture (σ=0.79 barn)[75]. The quantity of ^{65}Zn decreases by one order of magnitude in 2.2 years. ^{24}Na has the second largest contribution (5.11E+06) which is produced from ^{27}Al in (n,α) reaction[76] by fast neutrons, and with 15 hours half-life its quantity decreases by one order of magnitude in every 2 days.

In activated float ^{24}Na (1.12E+08 Bq/cm^3) is the most active nuclide, which is produced from ^{23}Na by thermal neutron capture (σ=0.517 barn)[75] and its quantity decreases by one order of magnitude in every 2 days. The second most active gamma emitter is ^{22}Na (5.13E+06 Bq/cm^3) which produced from ^{23}Na in (n,2n) reaction[77] by fast neutrons, and its 2.6 years half-life resulting in one order of magnitude decreasing in every 8.6 years.

Since sodium is one of the main component in float glass, its amount and therefore the amount of the main gamma emitters cannot be decreased significantly. The X-ray emitting noble gas ^{37}Ar will probably escape during the waste treatment, therefore, it will not have significant contribution for the waste index and can be neglected.

Table 6-5 Inventory of the float substrate after 5 years operation and 1 day cooling

Nuclide	Act. conc. (Bq/cm^3)	Main gamma lines[66] (MeV)	Half-life[66]	Clearance level (Bq/g)[40]
^{24}Na	1.12E+08	2.75 (100%) 1.37 (100%)	14.96 h	2.10E-01
^{37}Ar	1.35E+07	-	35.04 d	-
^{22}Na	5.13E+06	1.27 (99.9%)	2.60 y	1.30E-01
^{45}Ca	4.02E+06	-	162.6 d	4.00E+01
^{55}Fe	1.88E+05	-	2.73 y	4.70E+01
^{3}H	6.44E+04	-	12.33 y	8.60E+02
^{31}Si	5.52E+04	1.27 (0.07%)	157.3 m	1.20E+02
^{42}K	3.81E+04	1.52 (18%)	12.36 h	4.00E+00
^{47}Sc	1.08E+04	0.16 (68.3%)	3.35 d	5.20E+00
^{47}Ca	9.27E+03	1.3 (71%)	4.54 d	3.20E-01

The pure beta emitter tritium gives most of the activity in zerodur. Tritium is generated by neutron capture and inelastic scattering from lithium nuclides. After 1 day cooling the most active gamma emitter in zerodur is ^{65}Zn (1.16E+08 Bq/cm^3) which is produced from ^{64}Zn by thermal neutron capture (σ=0.79 barn)[75]. The quantity of ^{65}Zn decreases by one order of magnitude in 2.2 years. ^{76}As has the second largest contribution (9.63E+07 Bq/cm^3) but it has only 1.1 day half-life which means it decreases by one order of magnitude in every 3.6 days.

Table 6-6 Inventory of the zerodur substrate after 5 years operation and 1 day cooling

Nuclide	Act. conc. (Bq/cm^3)	Main gamma lines[66] (MeV)	Half-life[66]	Clearance level (Bq/g)[40]
^{3}H	2.33E+09	-	12.33 y	8.60E+02
^{65}Zn	1.16E+08	1.11 (50%)	244.3 d	5.20E-01
^{76}As	9.63E+07	0.56 (45%) 0.57(6.3%)	1.078 d	1.40E+00
^{32}P	7.70E+06	-	14.26 d	9.80E+01
^{69}Zn	4.78E+06	-	56.40 m	1.60E+02
^{69m}Zn	4.46E+06	0.44 (95%)	13.76 h	2.70E+00
^{24}Na	1.84E+06	2.75 (100%) 1.37 (100%)	14.96 h	2.10E-01
^{45}Ca	1.69E+06	-	162.6 d	4.00E+01
^{95}Nb	1.28E+06	0.77 (100%)	34.96 d	4.20E-01
^{95}Zr	1.27E+06	0.72 (44%) 0.76 (54%)	64.02 d	2.90E-01

Table 6-7 Inventory of the steel insert after 5 years operation and 1 day cooling

Nuclide	Act. conc. (Bq/cm^3)	Main gamma lines[66] (MeV)	Half-life[66]
^{24}Na	9.00E+05	2.75 (100%) 1.37 (100%)	14.96 h
^{37}Ar	3.66E+04	-	35.04 d
^{45}Ca	3.33E+04	-	162.6 d
^{55}Fe	1.51E+03	-	2.73 y
^{22}Na	3.11E+02	1.27 (99.9%)	2.60 y
^{42}K	2.32E+02	1.52 (18%)	12.36 h
^{31}Si	1.45E+02	1.27 (0.07%)	157.3 m
^{47}Sc	6.24E+01	0.16 (68.3%)	3.35 d
^{47}Ca	5.34E+01	1.3 (71%)	4.54 d
^{54}Mn	2.34E+01	0.84 (100%)	312.3 d
^{59}Fe	7.12E+00	1.10 (56.5%) 1.29 (43.2%)	44.5 d

In activated steel insert ^{24}Na (9.00E+05) gives the majority of activity. In about 1 week cooling ^{22}Na (3.11E+02) becomes the most active gamma emitter which has 2.6 years half-life resulting one order of magnitude quantity decreasing in every 8.6 years.

6.4. Waste index of neutron guide substrates

Based on our calculations, the neutron guide substrates inside the monolith will have high level waste category immediately after shutdown. It should be noted that neutron guides out of the monolith will be activated much less. After 2.5 years cooling time, the aluminium substrate would belong to intermediate level waste category and it needs 11.5 years cooling time to belong to low level waste category. The float substrate would belong to intermediate level waste category in 10 years. Without tritium, the zerodur needs 8 years to belong to intermediate level waste category and 12 years cooling time to belong to low level waste category.

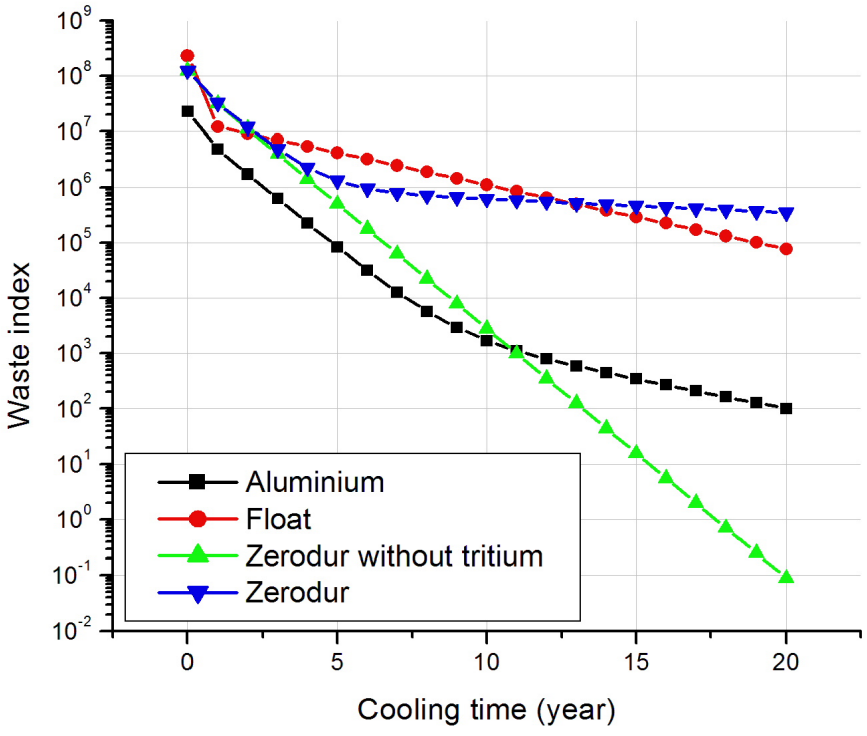

Figure 6-4 Waste index comparison

6.5. Gamma dose rate estimations

The gamma dose rate maps are particularly important because shielding of gamma radiation is more difficult than that of alpha and beta radiation. In the following the dose rate of decay gamma radiation is presented. For the operational period shielding design calculations should be extended for determining the prompt gamma intensities as well originating from nuclear reactions with the actual neutron fluence.

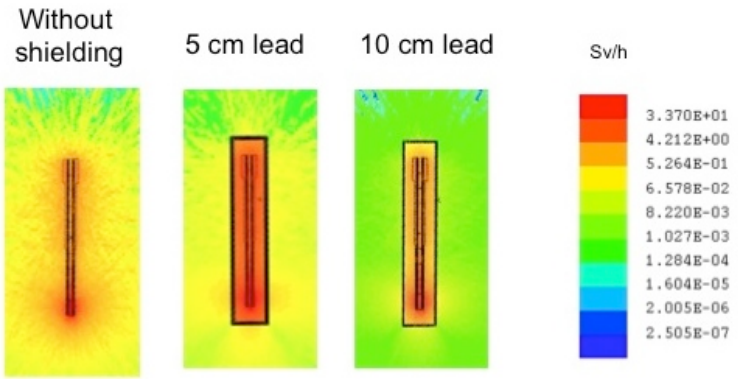

Figure 6-7 Gamma dose rate maps after 5 years operation and one day cooling time surrounding the neutron insert using aluminium substrate

In case of aluminium the high-energy gamma emitter ^{24}Na gives the majority of gamma dose. The decay of ^{24}Na also results in about 50% dose rate decrease in Sv/h surrounding the guide in one week.

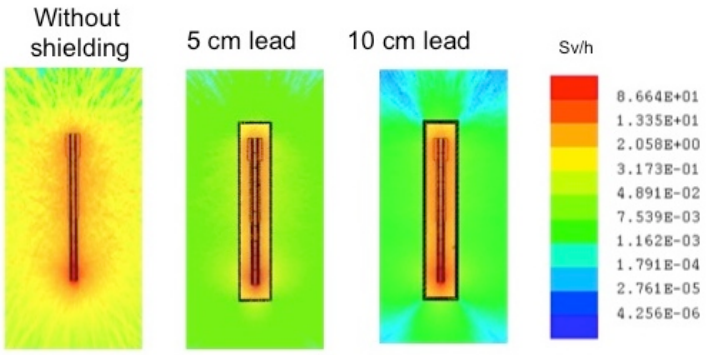

Figure 6-8 Gamma dose rate maps after 5 years operation and 1 day cooling time surrounding the neutron insert using zerodur substrate

In case of zerodur the decay of ^{76}As results in about 30% dose rate decrease in Sv/h surrounding the guide in a few days. It means that it is advised to wait 1 week cooling time before the replacement.

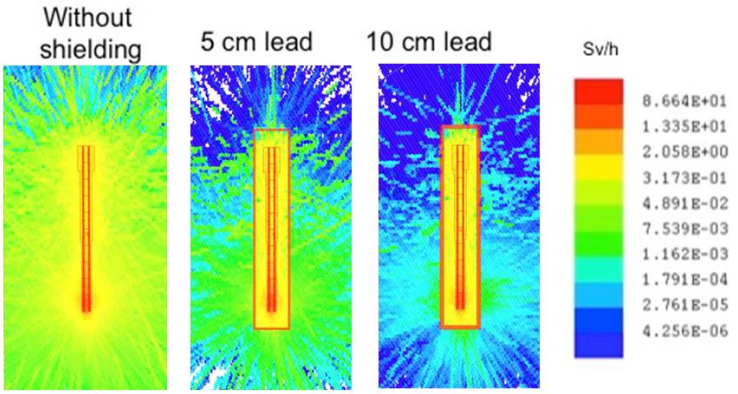

Figure 6-9 Gamma dose rate maps after 5 years operation and 1 day cooling time surrounding the neutron insert using float substrate

In case of float the high-energy gamma emitter ^{24}Na gives the majority of gamma dose. In this case the decay of ^{24}Na results in about one order of magnitude decrease in dose rate in Sv/h surrounding the guide in about 1 week.

In all three cases the gamma dose rates are extremely high surrounding the neutron guide and insert after 5 years operation and 1 day cooling.

After one week the longer-lived nuclides will give the majority of the gamma dose in all three cases. In case of aluminium and zerodur it is ^{65}Zn, in case of float it is ^{22}Na. It is, therefore, advised to decrease the amount of zinc in aluminium and zerodur substrate materials. It also means that several years cooling time would be needed to decrease the dose rate significantly.

After one week cooling the dose rates will be still very high, so probably the replacement will require robotic solutions and the inserts should be handled as highly radioactive materials. They will need strong gamma shielding for storage and transport.

7. Comparison of metal-based shielding materials in terms of activation

7.1. Features of the metal shielding blocks

At reactor-based sources fission produces secondary neutrons up to 20 MeV which requires concrete shielding. At spallation sources like ESS, metal-based shielding plays an important role in terms of radiation protection. Neutron energy can reach up to the primer proton beam energy (GeV) and can induce further secondary neutrons deep in the shielding around the target region. Metal-based shielding is key for attenuation of the high-energy neutrons due to the atomic mass and density, which leads to an increased attenuation at higher energies, compared to standard concrete. The design of the biological shielding around the target consists of several meters of metal shielding (the so-called monolith, see Figure 3.2) and is additionally followed by a concrete layer. In this thesis, copper, steel, and aluminium metal-based shielding blocks were compared in terms of activation. The shielding blocks were modeled as homogenous cubes shot by a rectangular shaped neutron beam. This simple geometry allows us to compare the results with future-planned measurements[78]. The comparison of different materials can be useful for the ESS metal-based shielding blocks in different positions; however, for proper calculations the precise geometry should be used. As explained already in details, our work was focused on radiation from radionuclides produced in the collisions and did not assess the dose rate during ESS operation where a significant part of the dose field is attributed to prompt particle radiation generated only in the nuclear reactions. The activation properties of the metal-based shielding depend firmly on the material choice. The material composition of the shielding options is summarized in Table 7-1, 7-2 and 7-3.

Table 7-1 Material composition of the copper shielding block (weight%)[78]

Cu	Mn	C	S	P
99.95	0.6	0.23	0.05	0.04

Table 7-2 Material composition of the steel shielding block (weight%)[78]

Fe	Mn	C	S	P
99.08	0.6	0.23	0.05	0.04

Table 7-3 Material composition of the aluminium shielding block (weight%)[78]

Al	Si	Mg	Mn	Fe	Cr	Zn	Ti	Cu
95.35	1.3	1.2	1	0.5	0.25	0.2	0.1	0.1

7.2. The method of activation calculations

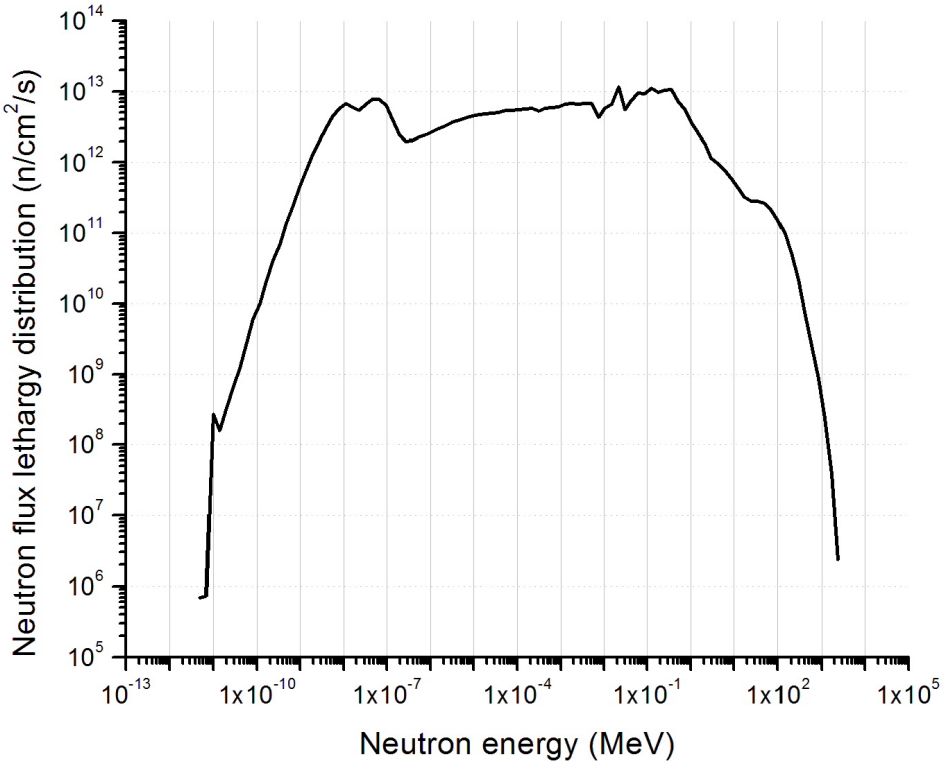

Figure 7-1 Neutron spectrum of the neutron beam reaching the shielding blocks[78]

The radionuclide inventory was calculated using MCNPX 2.7 coupled with CINDER'90. In order to calculate the nuclide inventory due to low-energy neutrons, fluxes for neutrons of less than 20 MeV energy are first obtained. For all other reactions, production rates of the residual nuclides were calculated and collected by MCNPX. The neutron fluxes are folded by CINDER'90 with neutron production cross sections. The shielding

blocks were modeled as homogenous cubes filled with different materials. The shielding blocks were shot by a 1 cm x 1 cm rectangular shaped neutron beam with parallel directions for all neutrons[78].

7.3. Activation results of the metal-based shielding blocks

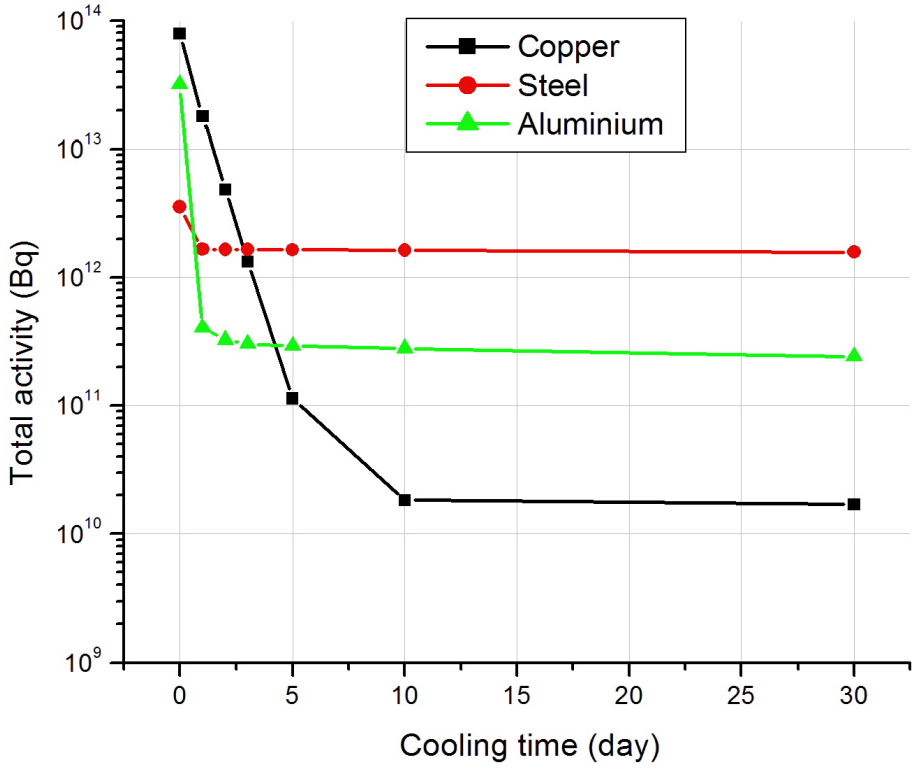

Figure 7-2 Total activity in different shielding materials after 5 years irradiation

Immediately after the final shutdown, the steel shielding block is the least active and copper is the most active, after 1 day cooling aluminium is the least active and still the copper is the most active. After 5 days cooling time the copper shielding block becomes the least active and the steel is the most active. After 10 days cooling time the total activity values decrease very slowly, the steel remains the most active (1.2×10^{12} Bq), followed by aluminium (2×10^{11}Bq), and copper remains the least active (1×10^{10} Bq).

Based on sensitivity analysis the uncertainty coming from the inaccuracies in geometry is under 5%, the uncertainty coming from the inaccuracies in the irradiation history is under 5%, the statistical standard deviation values were within 3%. Considering all factors described in Chapter 2.6, the overall uncertainty of the total activity concentration of the shielding blocks is within 20%.

Table 7-4 Most active nuclides after 5 years irradiation in copper shielding block

Nuclide	Main gamma lines[66] (MeV)	Half-life[66]	Total activity (Bq) in different cooling times		
			At shutdown	1 d cooling	30 d cooling
^{64}Cu	1.3 (0.5%)	12.7 h	5.940E+13	1.603E+13	5.117E-04
^{66}Cu	1.04 (9%)	5.12 m	1.11E+13	0	0
^{60}Co	1.17(100%) 1.32(100%)	5.27 y	4.661E+09	4.661E+09	4.610E+09
^{63}Ni	-	100 y	3.597E+09	3.597E+09	3.597E+09
^{58}Co	0.81 (99%) 0.86 (0.7%) 1.67 (0.5%)	70.9 d	2.178E+09	2.159E+09	1.626E+09
^{57}Co	0.12 (85.6%) 0.14 (10.7%)	272 d	1.702E+09	1.698E+09	1.577E+09
^{55}Fe	-	2.73 y	9.564E+08	9.557E+08	9.367E+08
^{59}Fe	0.84 (100%)	312 d	9.119E+08	9.098E+08	8.531E+08
^{56}Co	1.24(67.6%) 1.77(15.7%)	78.8 d	4.318E+08	4.281E+08	3.317E+08
^{51}Cr	0.32 (10%)	27.7 d	4.318E+08	4.213E+08	2.039E+08
^{49}V	-	338 d	3.049E+08	3.043E+08	2.868E+08
^{3}H	-	12.3 y	2.691E+08	2.691E+08	2.679E+08

After 5 days cooling time the copper shielding block is the least active, because in the activated copper short-lived nuclides ^{64}Cu and ^{66}Cu dominate. ^{64}Cu is produced from ^{63}Cu ($\sigma = 4.5$ barn) and ^{66}Cu is from ^{65}Cu ($\sigma = 2.17$ barn) by thermal neutron capture[75]. After 30 days cooling the long-lived gamma emitter ^{60}Co (4.610×10^{9} Bq) becomes the

most active nuclide which is produced from copper by fast neutrons in $^{63}Cu(n, \alpha)^{60}Co$ reaction[79].

Table 7-5 Most active nuclides after 5 years irradiation in aluminium shielding block

Nuclide	Main gamma lines[66] (MeV)	Half-life[66]	Total activity in different cooling times (Bq)		
			At shutdown	1 d cooling	30 d cooling
^{28}Al	1.78 (100%)	2.23 m	2.07E+13	1.56E+05	1.50E-05
^{65}Zn	1.11 (50%)	244 d	1.73E+11	1.72E+11	1.59E+11
^{51}Cr	0.32 (10%)	27.7 d	7.83E+10	7.64E+10	3.70E+10
^{64}Cu	1.3 (0.5%)	12.7 h	1.91E+11	5.16E+10	1.65E-06
^{55}Fe	-	2.73 y	2.13E+10	2.13E+10	2.08E+10
^{24}Na	2.75 (100%) 1.37 (100%)	15 h	5.12E+10	1.68E+10	1.66E-04
^{56}Mn	0.84 (98.9%) 1.81(27.2%) 2.11(14.3%)	2.58 h	7.60E+12	1.20E+10	6.86E-72
^{69}Zn	-	56.3 m	8.79E+10	7.31E+09	4.34E-06
^{69m}Zn	0.44 (95%)	13.8 h	2.28E+10	6.82E+09	4.05E-06
^{54}Mn	0.84 (100%)	313 d	3.11E+09	3.10E+09	2.91E+09
^{22}Na	1.28(99.9%)	2.6 y	1.66E+09	1.66E+09	1.62E+09
^{59}Fe	1.1(56.5%) 1.29(43.2%)	44.4 d	1.16E+09	1.14E+09	7.25E+08
^{3}H	-	12.3 y	4.09E+08	4.09E+08	4.07E+08

After 1 day cooling aluminium is the least active. In activated aluminium the short-lived ^{28}Al, ^{56}Mn, ^{64}Cu, ^{69}Zn dominate. ^{28}Al is produced from ^{27}Al ($\sigma = 0.231$ barn), ^{56}Mn is produced from ^{55}Mn ($\sigma = 13.3$ barn), ^{64}Cu is produced from ^{63}Cu ($\sigma = 4.5$ barn), ^{69}Zn is produced from ^{68}Zn ($\sigma = 1.07$ barn) by thermal neutron capture[75]. After 30 days cooling time the long-lived gamma emitter ^{65}Zn (1.59×10^{11} Bq) dominates, which requires to decrease the amount of zinc in the material composition in facility parts where aluminium is applied.

Table 7-6 Most active nuclides after 5 years irradiation in steel shielding block

Nuclide	Main gamma lines[66] (MeV)	Half-life[66]	Total activity in different cooling times (Bq)		
			At shutdown	1 d cooling	30 d cooling
^{55}Fe	-	2.73 y	1.22E+12	1.22E+12	1.19E+12
^{59}Fe	1.1(56.5%) 1.29(43.2%)	44.4 d	8.39E+10	8.26E+10	5.26E+10
^{54}Mn	0.84 (100%)	313 d	4.22E+10	4.21E+10	3.94E+10
^{51}Cr	0.32 (10%)	27.7 d	4.06E+09	3.96E+09	1.92E+09
^{32}P	-	14.2 d	3.06E+09	2.92E+09	7.12E+08
^{56}Mn	0.84 (98.9%) 1.81(27.2%) 2.11(14.3%)	2.58 h	1.50E+12	2.37E+09	1.35E-72
^{49}V	-	338 d	1.58E+09	1.58E+09	1.48E+09
^{48}V	0.98(100%) 1.31(97.5%)	16 d	8.45E+08	8.10E+08	2.30E+08
^{52}Mn	0.74(90%) 0.93(94.5%)	5.59 d	4.64E+08	4.11E+08	1.13E+07
^{46}Sc	0.89(100%) 1.12(100%)	83.8 d	3.03E+08	3.01E+08	2.37E+08
^{3}H	-	12.3 y	2.06E+08	2.06E+08	2.05E+08

Immediately after the final shutdown before removal, the steel shielding block is the least active, the most active nuclides are the long-lived ^{55}Fe, ^{59}Fe, ^{54}Mn and the short-lived ^{56}Mn. ^{56}Mn is produced from ^{55}Mn by thermal neutron capture ($\sigma = 13.3$ barn). ^{55}Fe is produced from ^{54}Fe ($\sigma = 2.25$ barn) and ^{59}Fe is produced from ^{58}Fe ($\sigma = 1.32$ barn) by thermal neutron capture[75]. The main gamma emitters are the ^{59}Fe, ^{54}Mn and ^{56}Mn. The decay of ^{56}Mn results in one order of magnitude quantity decrease in every 9 hours. It means that after 1 day cooling ^{59}Fe (5.26×10^{10}) and ^{54}Mn (3.94×10^{10}) become the most active gamma emitters. Therefore, it is advised to decrease the manganese content of the steel without changing its advantageous thermal and physical behavior.

Comparing the shielding block materials, the copper has the best activation properties. After 5 years irradiation and 30 days cooling time, the steel and aluminium blocks contain one order of magnitude larger amount of activity from gamma emitters than the

copper. In case of aluminium the activity can be decreased significantly using less zinc containing aluminium alloy. In case of steel it is advised to decrease the manganese content.

8. Inventory and dose rate assessment of the beryllium reflector

8.1. Features of the beryllium reflector

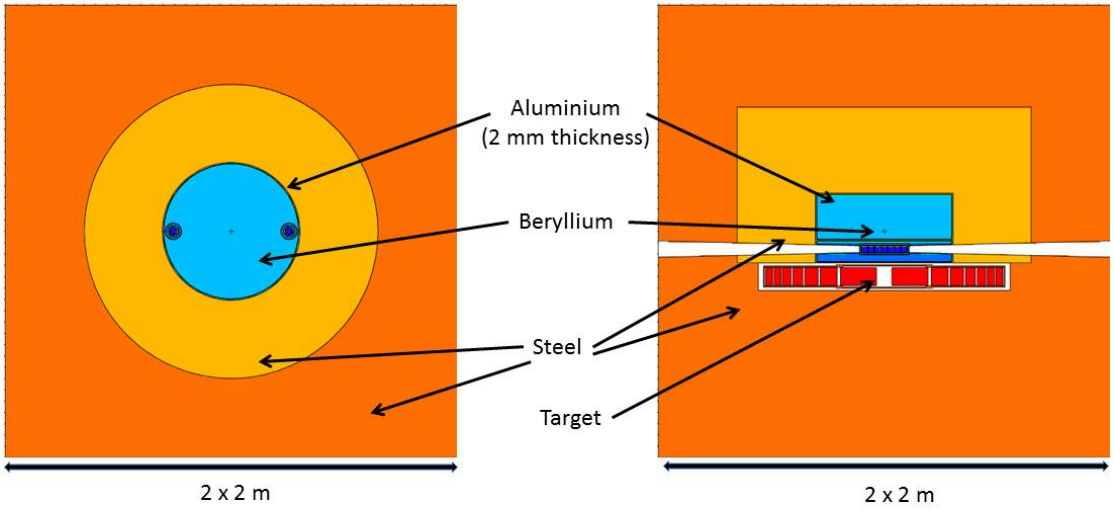

Figure 8-1 Geometry of the reflector system

Table 8-1 Material composition of the beryllium reflector (weight%)[80]

Be	B	C	O	Na	Mg	Al	Si	P	S
0.996	6.0E-7	3.5E-4	5.4E-3	3.5E-7	1.2E-5	3.1E-4	2.1E-4	2.2E-6	1.6E-5
Cl	Ca	Sc	Ti	V	Cr	Mn	Fe	Co	Ni
2.3E-6	7.1E-6	1.7E-6	1.3E-4	3.1E-6	9.0E-5	5.1E-5	9.4E-4	3.7E-6	1.9E-4
Cu	Zn	Ga	Zr	Nb	Mo	Ag	Cd	Sn	Sb
7.6E-5	2.2E-7	8.0E-8	7.3E-6	5.7E-7	7.8E-6	6.8E-7	1.0E-7	4.9E-7	2.7E-7
Pr	Nd	Hf	W	Pb	Th	U			
4.0E-8	2.1E-7	1.5E-6	1.0E-5	1.0E-7	9.7E-8	3.6E-6			

The inner reflector is a cylinder made from beryllium in aluminium container surrounded by steel (Figure 8-1). The appropriate estimation of the activation of the beryllium reflector is a decisive part in decommissioning planning because the activated beryllium requires specific treatment owing to its highly toxic chemical properties. In the handling and processing of any beryllium component, it should be taken into account that after irradiation, beryllium may contain significant quantity of tritium, and the activation of the

impurities present in the beryllium material may involve important levels of other radionuclides. Due to the high toxicity particular attentions should be paid in protecting workers[81].

8.2. The method of activation and dose rate calculations

The radionuclide inventory has been calculated with MCNPX2.7[49] using ENDF/B-VII cross section libraries coupled with CINDER'90[31]. For MCNPX simulations the flat moderated MCNPX monolith model by Alan Takibayev[68] was taken (Figure 8-1). The initial proton beam energy is 2 GeV. Using the gamma source script, the CINDER'90 activation code resulted in a gamma source definition which was used for decay gamma dose rate calculation with MCNPX. In the calculations 1 year of operation time was assumed for the reflector.

8.3. Activation and waste index results of beryllium reflector

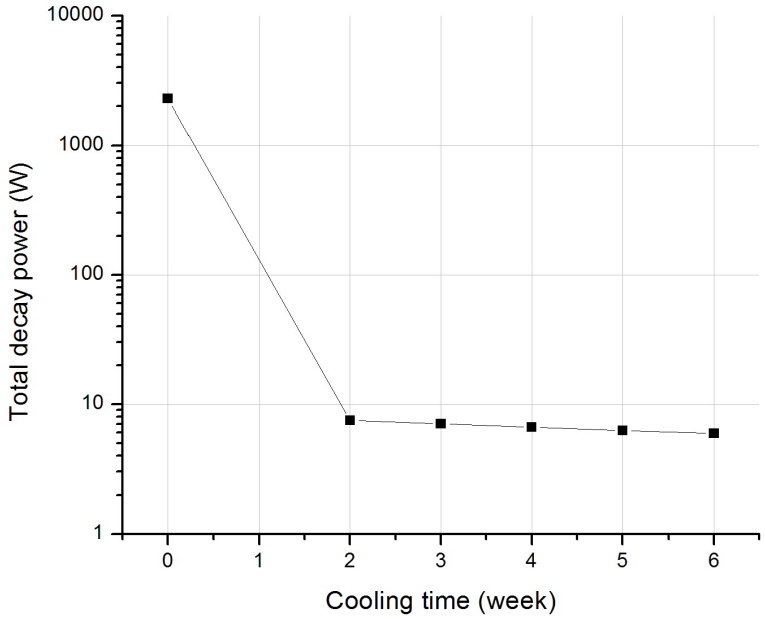

Figure 8-2 Heat generation of the beryllium reflector after 1 year of operation

After 1 year operation time the total decay heat performance is 2.5 kW ± 10% which means 10 kW/m^3 characterizing the beryllium as a high level radioactive waste (as

discussed at the end of Chapter 1.7, this is not defined officially according to the current Swedish regulatory ordinance). After the removal the beryllium needs to be cooled in hot cell. In about five days the decay heat goes below 2 kW/m^3 which is widely considered the margin for high level waste, e.g. in the Hungarian radioactive waste regulations[42]. After 5 days cooling time the beryllium would not be classified as high level waste from this point of view, however, it will have to be considered as high level waste (HLW) because of its waste index according to our calculations.

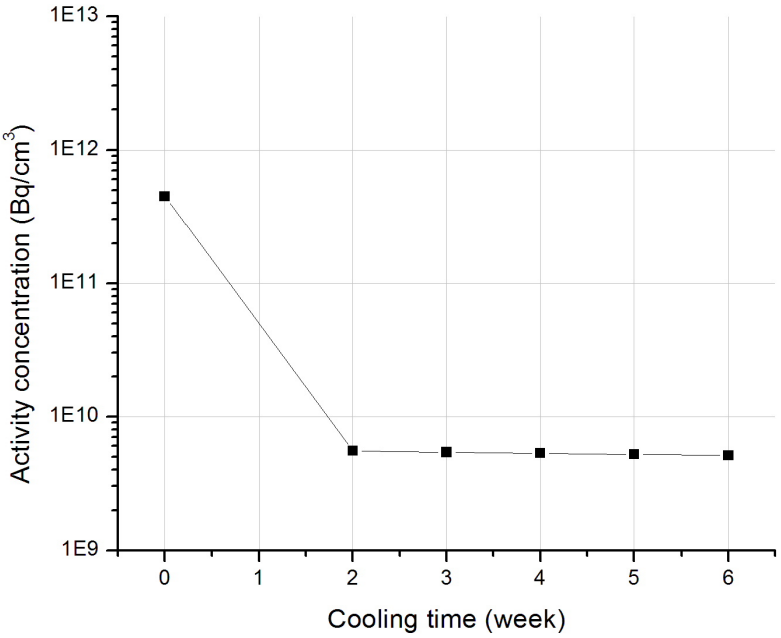

Figure 8-3 Total activity concentration (Bq/cm^3) of the beryllium reflector after 1 year operation as a function of cooling time

Table 8-2 Most active isotopes after 1 year operation in Beryllium reflector

Nuclide	Main gamma lines (MeV) [66]	Half-life[66]	Clearance level (Bq/g)	Activity concentration (Bq/cm^3)		
				Without cooling	2 week cooling	6 week cooling
^{8}Be	-	7E-17 s	-	3.30E+11	0.00E+00	0.00E+00
^{56}Mn	0.85 (99%) 1.81 (27%) 2.11 (14%)	2.58 h	0.66	1.80E+09	0.00E+00	0.00E+00
^{3}H	-	12.3 y	860	4.00E+09	4.00E+09	4.00E+09
^{7}Be	0.478(10%)	53.2 d	6.9	9.60E+08	8.00E+08	5.60E+08
^{35}S	-	88 d	57	1.40E+08	1.30E+08	1.00E+08
^{51}Cr	0.32 (10%)	27.8 d	12	1.70E+08	1.20E+08	6.00E+07
^{46}Sc	0.89(100%) 1.12(100%)	83.3 d	0.15	1.30E+08	1.20E+08	9.40E+07
^{95}Nb	0.77 (100%)	34.7 d	0.42	8.20E+07	8.10E+07	7.20E+07
^{55}Fe	-	2.73 y	47	7.70E+07	7.60E+07	7.40E+07
^{95}Zr	0.72 (44%) 0.76 (54%)	63.7 d	0.29	8.40E+07	7.20E+07	5.30E+07
^{60}Co	1.17(100%) 1.33(100%)	5.39 y	0.099	4.10E+07	4.00E+07	4.00E+07

Immediately after irradiation the most active nuclides are quasi-nuclide ^{8}Be and short-lived ^{56}Mn produced from ^{55}Mn ($\sigma = 13.3$ barn) by neutron capture[75]. ^{8}Be immediately decays into two α-particles (6.8 eV energy).

After 2 weeks cooling time tritium, ^{7}Be, ^{35}S, ^{51}Cr, ^{46}Sc, ^{95}Nb, ^{55}Fe, ^{95}Zr, ^{60}Co, and ^{88}Y are the most active nuclides. Tritium is generated by neutron capture and inelastic scattering from beryllium nuclides and its content in the waste stream will depend on the applied waste treatment technologies. ^{7}Be is produced from beryllium by ^{9}Be(n,3n)^{7}Be reaction[82].

All other nuclides are mostly produced by thermal neutron capture: ^{35}S is from ^{34}S ($\sigma = 0.256$ barn), ^{51}Cr is from ^{50}Cr ($\sigma = 15.4$ barn), ^{46}Sc is from ^{45}Sc ($\sigma = 27.2$ barn), ^{95}Nb is from ^{94}Nb ($\sigma = 14.9$ barn), ^{55}Fe is from ^{54}Fe ($\sigma = 2.25$ barn), ^{95}Zr is from ^{94}Zr ($\sigma = 0.0494$ barn), ^{60}Co is from ^{59}Co ($\sigma = 74.2$ barn) and ^{88}Y is from ^{89}Y ($\sigma = 1.28$ barn) [75].

Based on sensitivity analysis the uncertainty coming from the inaccuracies in geometry is under 5%, the uncertainty coming from the inaccuracies in the irradiation history is under 10%, the statistical standard deviation values were within 5%. Considering all factors described in Chapter 5.6, the overall uncertainty of the total activity concentration of the beryllium is within 22%.

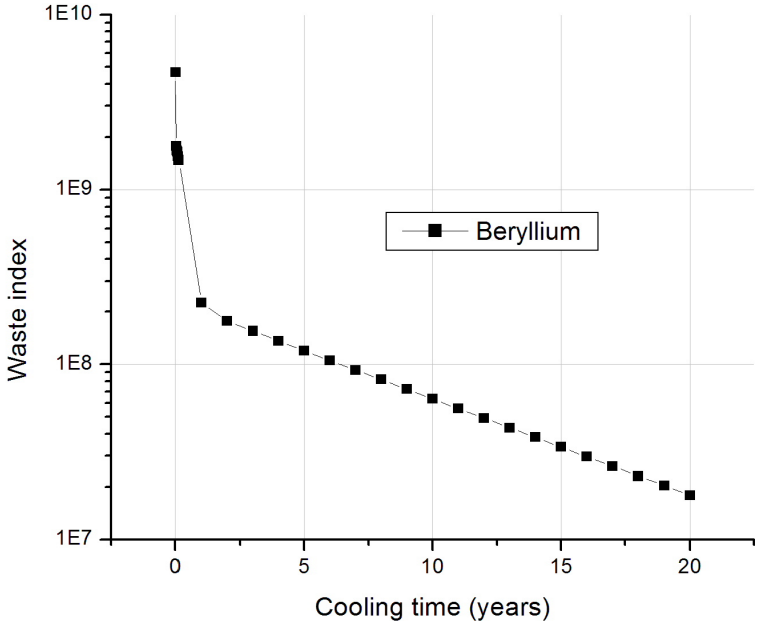

Figure 8-4 Waste index of beryllium reflector

It can be concluded from this analysis that after 1 year of operation the Be reflector will have HLW waste category and has to be disposed of into deep geological repository for long-term.

8.4. Gamma dose rate results

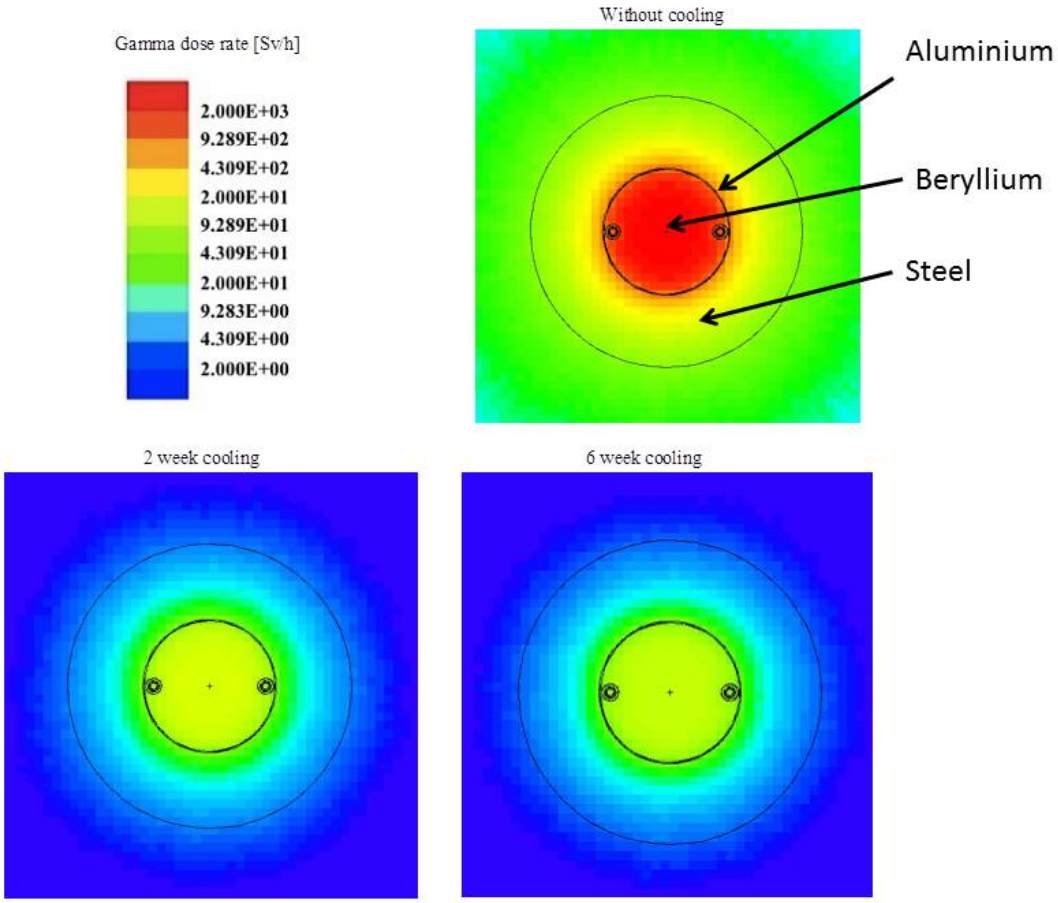

Figure 8-4 Gamma dose rate maps after 1 year operation

Based on these results, there will be extremely high gamma dose field surrounding the activated reflector system. The dose rate decreases by one order of magnitude in two weeks cooling time, but it will be still in Sv/h range.

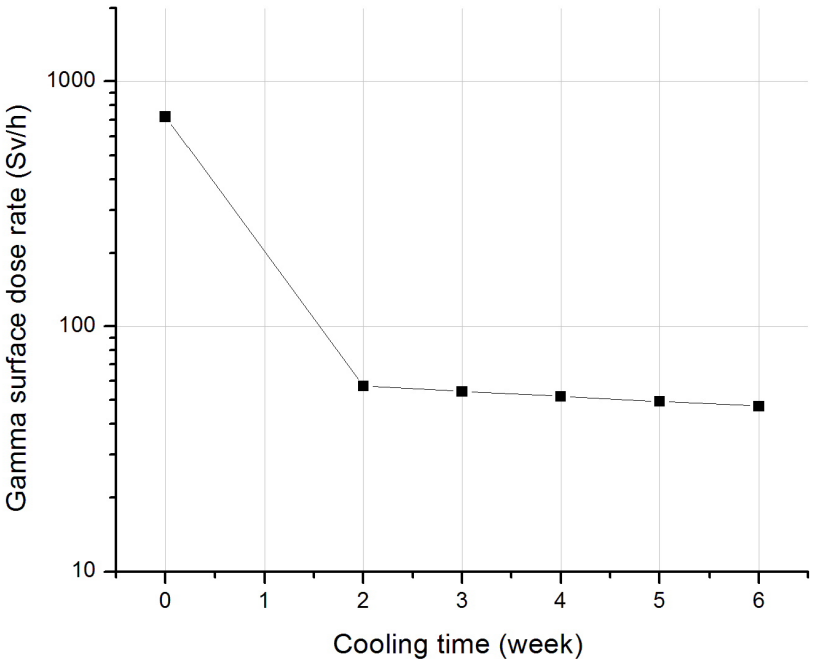

Figure 8-5 Gamma dose rate on the surface of beryllium after 1 year operation

After two weeks cooling time the most active gamma emitters in the activated beryllium are ^{7}Be, ^{51}Cr, ^{46}Sc, ^{95}Nb, ^{95}Zr, ^{60}Co, and ^{88}Y. Most of these nuclides have a few months half-life except ^{60}Co whose half-life is 5.39 years. It is mostly produced from cobalt impurity, therefore, it is advised to use low cobalt material. The other gamma emitters are also produced from impurities except ^{7}Be. It means that beside cobalt, the quantity of other impurities especially the quantity of chromium, scandium, niobium, zirconium and yttrium should be also decreased as much as possible.

It is recommended to wait at least two weeks cooling time before the replacement of the beryllium. The replacement will probably demand robotic techniques. The activated beryllium should be treated as highly toxic and radioactive material, it will need advanced gamma shielding for storage and transport.

9. Inventory assessment of the NMX experimental cave

The NMX cave (see Figure 3-5) will contain the NMX time-of-flight (TOF) quasi-Laue Macromolecular Diffractometer. The activation of the floor and walls needs particular consideration in terms of radiation protection of the workers. The estimates presented here give hint to the personal safety system to assess the radiological risk factors. As it was emphasized in the previous chapters as well, the calculations presented in this thesis considered only the activation products generated in the irradiated structural materials in order to assess the waste generation and the exposure conditions during decommissioning; so, our results are not exhaustive in terms of operational radiation safety. For assessing the total dose exposure of the operating personnel, fragment of primary neutron radiation getting through the shielding and prompt particle (mainly gamma) radiation generated during the application of the neutron beam are also necessary to be considered.

9.1. Features of the NMX experimental cave used in calculations

The NMX experimental cave was originally planned with 10 m x 8 m floor area and 6 m high[83]. It has aluminium floor and concrete walls, the material composition can be found in Table 9-1 and 9-2. The neutrons are lead through 154 m long neutron guide to the cave. It means that the neutron spectrum is highly different from the previously studied cases – it is a cold neutron spectrum (see Figure 9-1 below).

The experimental cave itself contains a labyrinth to avoid direct beam to the door enabling a much thinner necessary shielding of the movable door; this constitutes an important element of the operational radiation protection.

For the aluminium floor Aluminium 3003 alloy and for walls ordinary concrete material composition was selected. These materials are present in NIST database so parameters for calculations could be taken from it.

Table 9-1 Material composition of the concrete walls (weight%)

H	C	O	Na	Mg	Al	Si	K	Ca	Fe
2.21	0.2484	57.493	1.5208	0.1266	1.9953	30.462	1.0045	4.2951	0.6435

Table 9-2 Material composition of the aluminium floor (weight%)

Al	Si	Mn	Fe	Cu	Zn
97.85	0.332	1.25	0.388	0.125	0.055

9.2. The method of activation calculations

As it was already described in the previous chapters, the radionuclide inventory has been calculated with MCNPX2.7[49] using ENDF/B-VII cross-section libraries coupled with CINDER'90[31]. For MCNPX simulations, the NMX MCNPX model by Gábor Náfrádi[83] was taken. The applied MCNPX geometry can be seen in Figure 9-2.

The activation is due to a cold neutron beam scattered on the examined sample and then thermalized by getting energy. In the calculations the full beam was converted into an isotropic point source in order to get conservative estimation.

The initial neutron spectrum was taken from simulations of the NMX neutron guide carried out by Márton Markó[84]. It is shown in Figure 9-1.

For waste index calculations the most active parts of the floor and concrete wall were selected by sensitivity analysis.

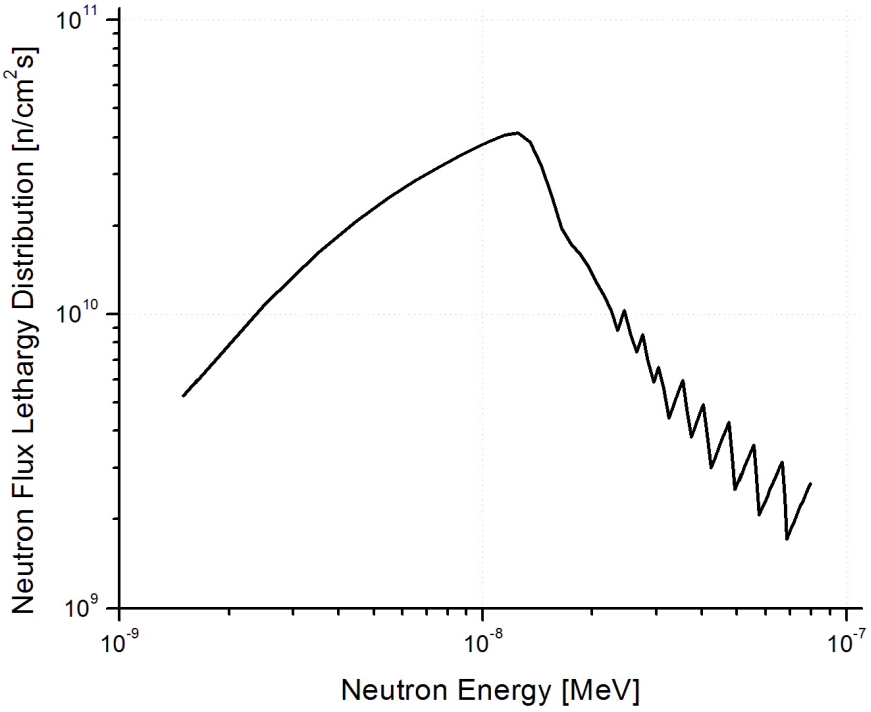

Figure 9-1 Neutron spectrum of NMX beam[84]

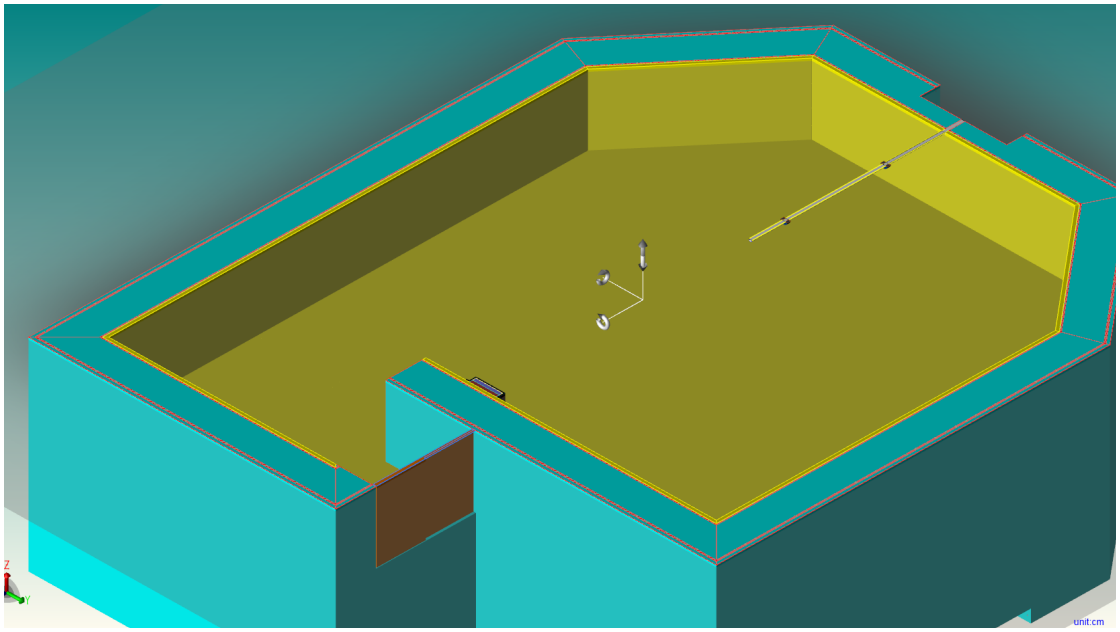

Figure 9-2 MCNPX model of the NMX cave[83]

9.3. Activation and waste index results

For the Personal Safety System optimization and maintenance, the contribution of radionuclides to the dose field for immediate access and different cooling times were estimated.

Table 9-3 Most active nuclides after 40 y of irradiation in the most active part of aluminium floor

Nuclide	Half-life[66]	Main gamma lines[66] (MeV)	Clearance level (Bq/g)	Activity concentration after 40 years operation (Bq/g)		
				Without cooling	1 day cooling	1 year cooling
^{28}Al	2.23 m	1.78 (100%)	-	1.24E+03	0.00E+00	0.00E+00
^{56}Mn	2.58 h	0.85 (99%) 1.81 (27%) 2.11 (14%)	6.60E-01	1.22E+03	1.92E+00	0.00E+00
^{64}Cu	12.7 h	1.3 (0.5%)	6.80E+00	8.99E+00	2.43E+00	0.00E+00
^{66}Cu	5.12 m	1.04 (9%)	-	1.92E+00	0.00E+00	0.00E+00
^{55}Fe	2.73 y	-	4.70E+01	1.34E+00	1.34E+00	1.04E+00
^{65}Zn	244.3 d	1.11 (50%)	5.20E-01	4.60E-01	4.59E-01	1.63E-01
^{69}Zn	56.40 m	-	1.60E+02	2.32E-01	5.21E-03	0.00E+00
^{31}Si	157.3 m	1.27 (0.07%)	1.20E+02	5.83E-02	1.02E-04	0.00E+00

Immediately after shut-down the major contributor for the total activity and gamma dose is the aluminium false floor due to the production of ^{28}Al. ^{28}Al is produced from ^{27}Al by neutron capture[75] ($\sigma = 0.231$ barn). Based on these results it is recommended to omit the use of aluminium as a structural material thereof and use other nuclear grade materials or steel covered by boron containing floor (tiles). However, for the waste index the very short-lived ^{28}Al and ^{66}Cu will not have significant contribution and can be neglected.

Table 9-4 Most active nuclides after 40 y of irradiation in most active part of concrete walls

Nuclide	Half-life[66]	Main gamma lines[66] (MeV)	Clearance level (Bq/g)	Activity concentration after 40 years operation (Bq/g)		
				Without cooling	1 day cooling	1 year cooling
^{24}Na	14.96 h	2.75 (100%) 1.37 (100%)	2.10E-01	2.31E+01	7.60E+00	0.00E+00
^{24m}Na	20 ms	0.47 (100%)	-	1.75E+01	0.00E+00	0.00E+00
^{28}Al	2.23 m	1.78 (100%)	-	1.14E+01	0.00E+00	0.00E+00
^{31}Si	157.3 m	1.27 (0.07%)	1.20E+02	2.43E+00	4.26E-03	0.00E+00
^{42}K	12.36 h	1.52 (18%)	4.00E+00	1.68E+00	4.38E-01	0.00E+00
^{45}Ca	162.6 d	-	4.00E+01	1.31E+00	1.31E+00	2.77E-01
^{55}Fe	2.73 y	-	4.70E+01	1.01E+00	1.01E+00	7.81E-01
^{37}Ar	35.04 d	-	-	2.68E-01	2.62E-01	1.95E-04
^{40}K	$1.28 \cdot 10^9$ y	1.46 (11%)	1.50E+00	2.62E-01	2.62E-01	2.62E-01

The most active nuclides in the concrete walls are the short-lived ^{24m}Na and ^{24}Na produced from ^{23}Na by neutron capture[75] (σ =0.517 barn). Since sodium is an essential component in concrete its quantity cannot be decreased significantly. The quantity of ^{24}Na decreases by one order of magnitude in every 2 days. The very short-lived ^{24m}Na, ^{28}Al, and the noble-gas ^{37}Ar will not have significant contribution for the waste index and can be neglected.

Based on sensitivity analysis the uncertainty coming from the inaccuracies in geometry is under 10%, the uncertainty coming from the inaccuracies in the irradiation history is under 10%, the statistical standard deviation values were within 5%. Considering all factors described in Chapter 5.6, the overall uncertainty of the total activity concentration of the floor and wall elements is within 24%.

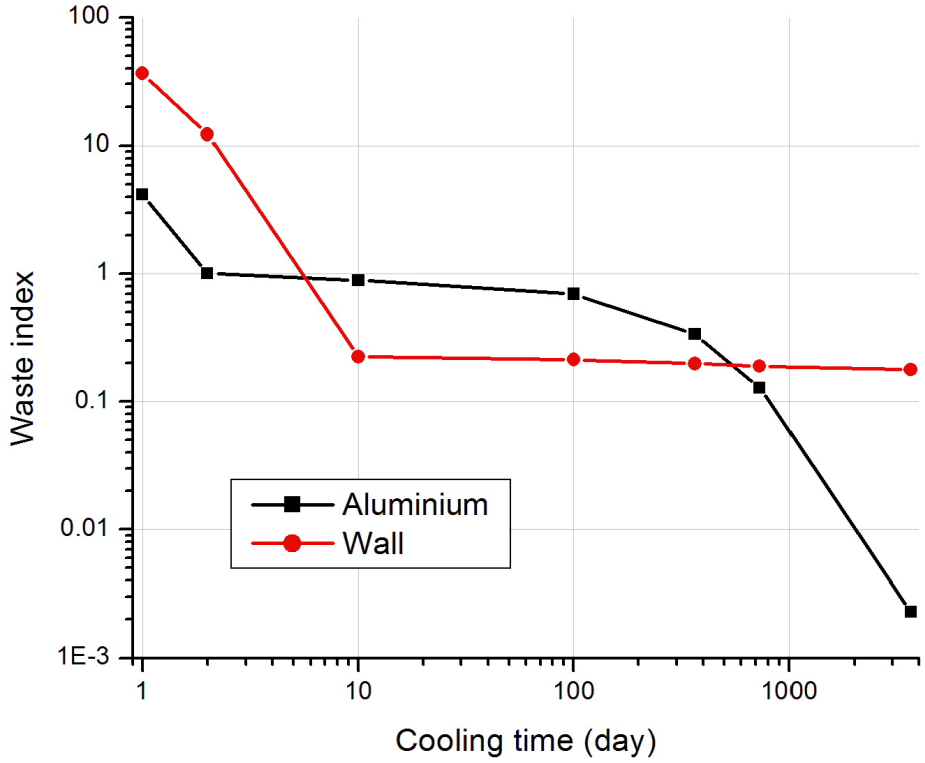

Figure 9-3 Waste index of the most active part of aluminium floor and wall

The aluminium floor concrete wall will be low level waste and probably can be released in a few years. In aluminium floor the long-lived ^{65}Zn gives the major contribution for the waste index which is produced from ^{64}Zn by neutron capture (σ=0.79 barn)[75]. After 10 days cooling time the ^{40}K gives the majority of the waste index. ^{40}K occurs in the wall naturally as well, and below 10 Bq/g activity concentrations it would be usually unnecessary to regulate[85].

10. Irradiation experiments at Budapest Neutron Centre (BNC) and their simulation

In order to validate the method of activation calculations by MCNPX/CINDER'90, irradiation experiments were carried out. Aluminium neutron guide substrate samples from MIRROTRON Ltd. were irradiated in the Budapest Research Reactor of Budapest Neutron Centre (BNC) with power of 10 MW. It should be noted that the material composition of the aluminium substrate is slightly different from the one used in the calculations described in Chapter 6.

10.1. Irradiation experiments

The Budapest Research Reactor is a VVR-class water-cooled, water-moderated tank type reactor with beryllium reflector[86]. The maximum thermal flux is $2.1 \times 10^{14} \frac{n}{cm^2 s}$. The reactor has 160 operational days per year with variable timetable. There are vertical irradiation channels inside and outside of the core.

The 1 cm x 1 cm x 1 cm samples were placed in aluminium sample holder. They were irradiated for 6 hours inside the fast irradiation channel (Channel 426 in Figure 10-2 and BAG-2 in Figure 10-3) where the thermal neutron flux is 6.00×10^{13} n $cm^{-2}s^{-1}$ and the fast neutron flux is 5.42×10^{13} n $cm^{-2}s^{-1}$. The thermal neutron flux variation along the axis of the irradiation capsule is less than 5%[87]. After 1 week cooling time, gamma spectra of the samples were measured by Eszter Dian[87]. Based on the gamma spectra, the activity concentration of the samples was calculated by Dávid Hajdú. Their results were compared to those of my model calculations. Using the nominal composition of the samples, the simulations showed a rather big difference from experimental results. Based on these results, I recommended that the nominal composition of the sample (with special respect to trace elements) should be verified by chemical analysis.

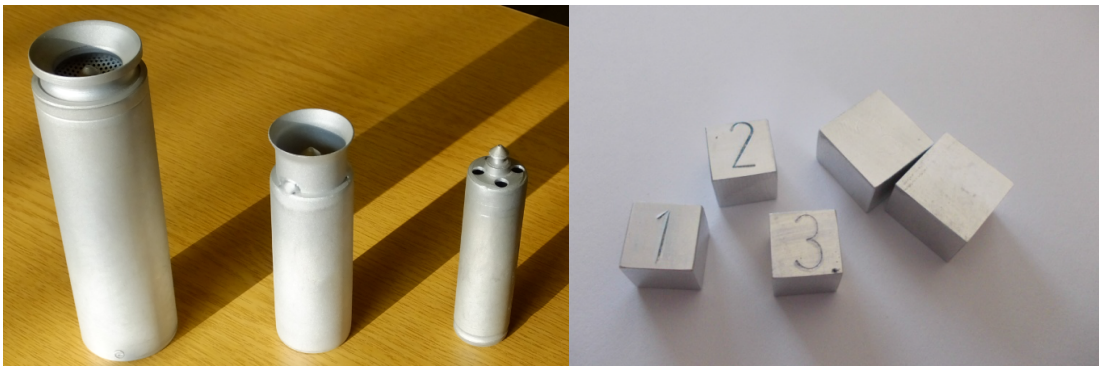

Figure 10-1 Aluminium sample holders and aluminium samples

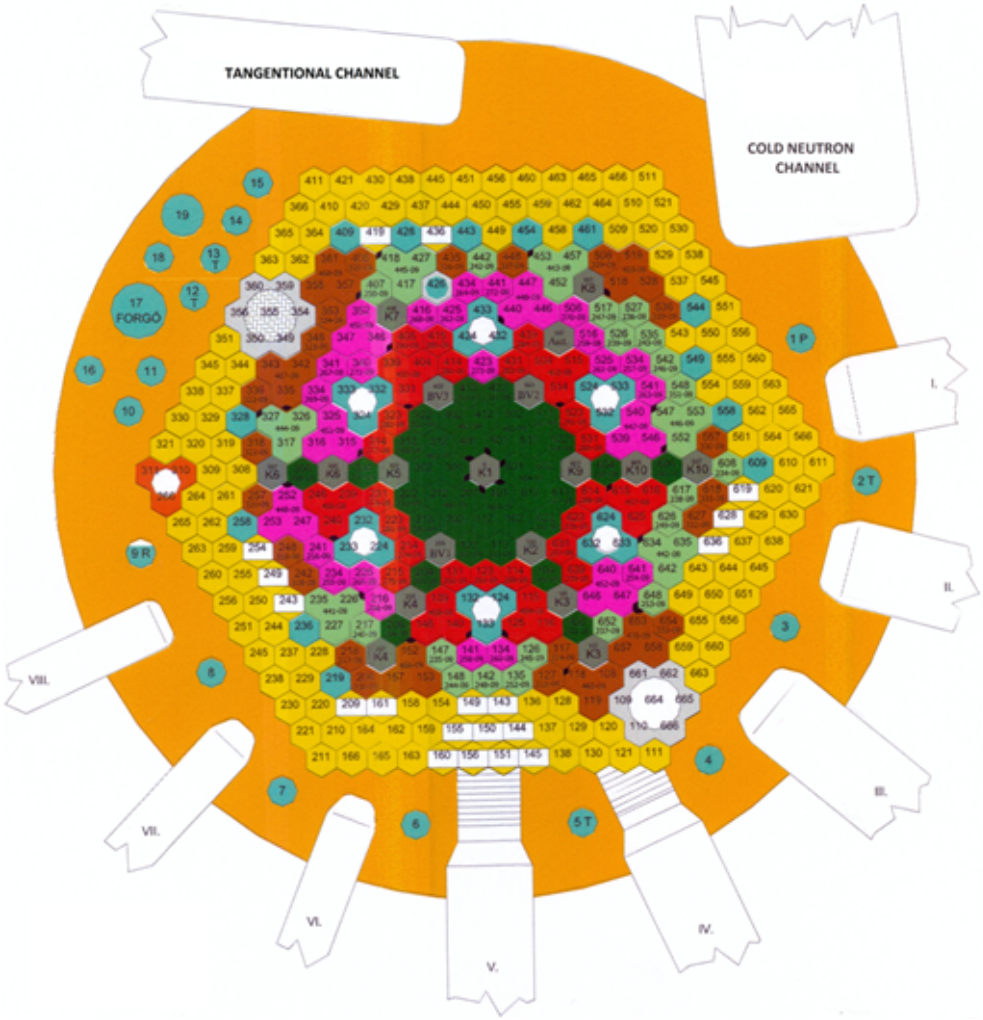

Figure 10-2 The geometry of BNC reactor core[86]

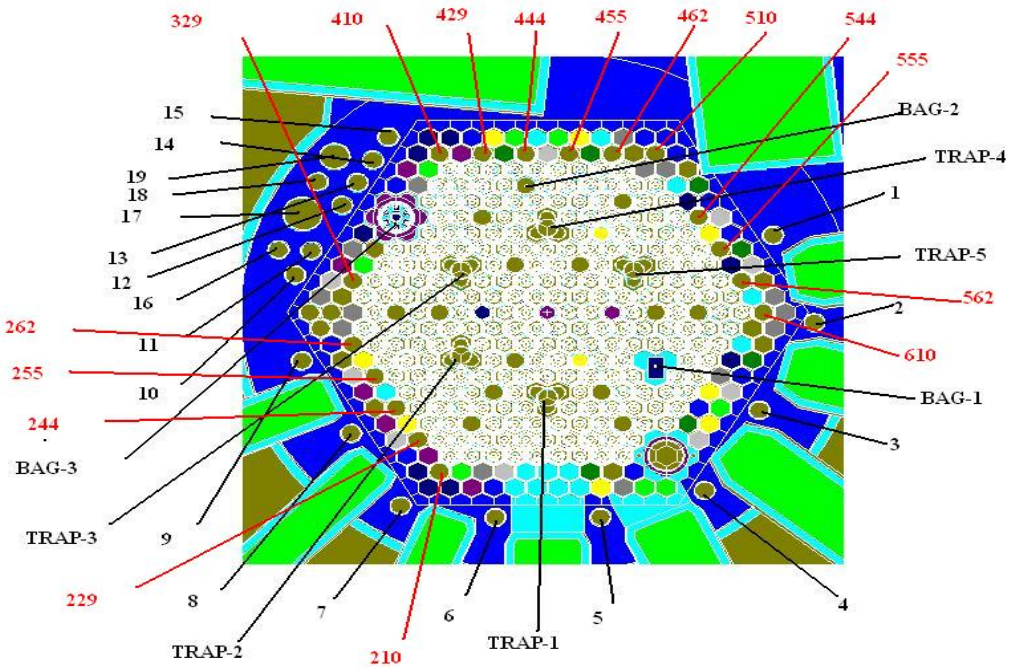

Figure 10-3 MCNPX model of BNC reactor core[88]

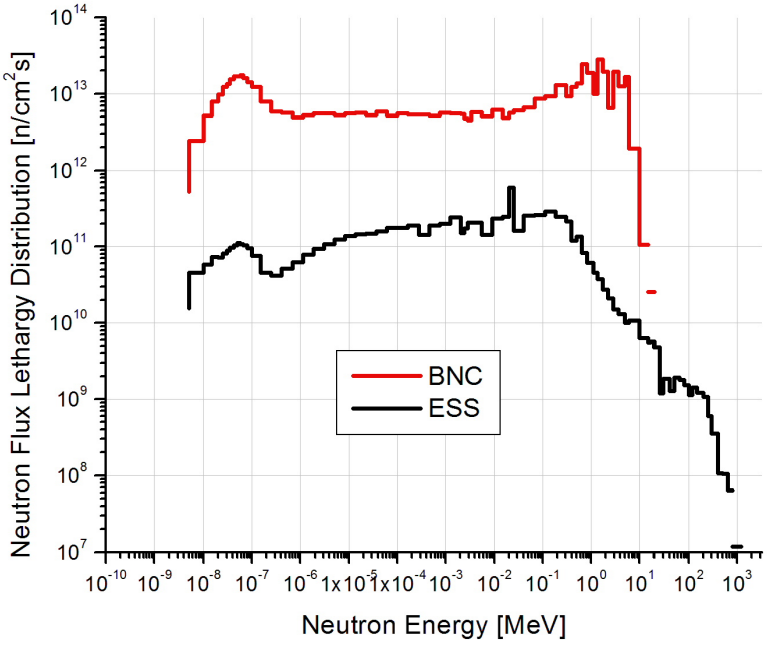

Figure 10-4 Comparison of the neutron spectrum at BNC fast irradiation channel and the most intense ESS neutron guide inside the monolith

10.2. Features of the aluminium substrates

The nominal composition of the substrate materials was verified by X-ray fluorescence spectroscopy (XRF) by Felicián Gergely and János Osán[87]. The difference was significant between the nominal and XRF-measured composition. The uncertainty of the XRF elemental analysis was 10 % on average.

Table 10-1 Nominal and XRF composition of aluminium substrates(weight/weight%)[87]

Sample number	1		2	
	Nominal	XRF	Nominal	XRF
Density [g/cm^3]	2.87		2.72	
Si	n.a.	<20	0.4	<20
Fe	n.a.	0.16	0.4	0.33
Cu	2	2.16	0.1	0.03
Mn	n.a.	0.03	0.4-1	0.63
Mg	2.3	n.d.	4-4.9	n.d.
Cr	n.a.	0.06	0.05-0.25	0.09
Ni	n.a.	<0.001	n.a.	0.01
Zn	6	7.84	0.3	0.02
Ti	n.a.	<0.01	0.15*	<0.01
Zr	n.a.	0.03		n.d.
Ga	n.a.	0.02	n.a.	0.01

n.a. = not available, n.d. = not detectable, * = Ti and Zr together

10.3. Simulation of the irradiation experiments

The radionuclide inventory has been calculated with MCNPX2.7[49] using ENDF/B-VII cross section libraries coupled with CINDER'90[31]. The MCNPX geometry of the irradiation channel containing the sample in aluminium holder was used (Figure 10-5) The neutron spectrum was taken from MCNPX simulation of the reactor carried out by Gábor Patriskov[88]. The XRF-measured material composition was used, for not detectable elements the nominal data were taken. The activity concentration was calculated after 6

hours irradiation time and 1 week cooling time. In order to compare the results with the ESS case, the activation of the most active ESS guide was also calculated with the same material composition and irradiation history (6 hours irradiation and 1 week cooling time).

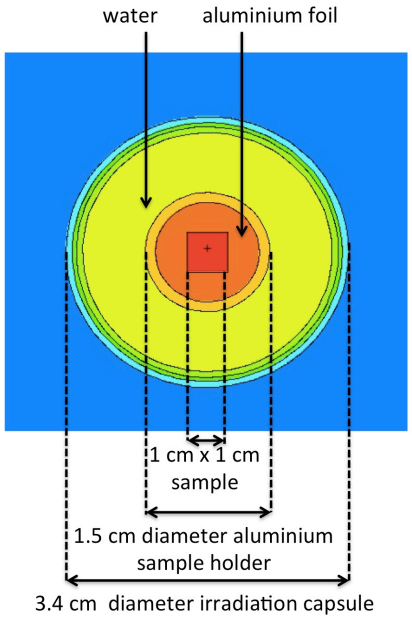

Figure 10-5 MCNPX geometry of the irradiation channel

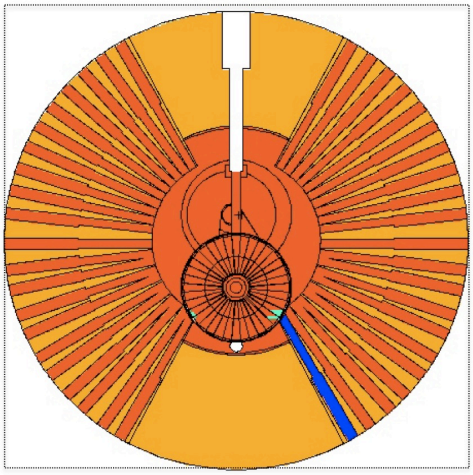

Figure 10-6 MCNPX geometry of the ESS target station

10.4. Gamma spectroscopy

After 6-hour irradiation and 1 week cooling time, the samples were placed in a low-level measuring chamber shielded by 10 cm thick pre-World War II steel and 2 mm thick Cu-lining. The gamma spectra were taken with HPGe detectors[87] and were evaluated by GSANAL software[89,90].

To specify the activity values the following formula was used:

$$\boldsymbol{A = \frac{I}{\eta \cdot f_\gamma}} \tag{10.1}$$

Where A is the total activity in the sample, I is the gamma intensity, f_γ is the gamma yield, and η is the detector efficiency.

The uncertainty of activity can be calculated by the well-known propagation of error rule:

$$\Delta A = \sqrt{\left(\frac{\Delta I}{\eta \cdot f_\gamma}\right)^2 + \left(\frac{\Delta \eta \cdot I}{\eta^2 \cdot f_\gamma}\right)^2 + \left(\frac{\Delta f_\gamma \cdot I}{\eta \cdot {f_\gamma}^2}\right)^2} \tag{10.2}$$

Where ΔA is the uncertainty of the total activity in the sample, ΔI is the uncertainty of the gamma intensity, Δf_γ is the uncertainty of the gamma yield, and $\Delta \eta$ is the uncertainty of the detector efficiency.

The uncertainty of the gamma yields is given in the gamma line library[66], the uncertainty of the respective intensities is calculated by the evaluation software and the average uncertainty of the efficiency function of the applied measurement geometry was 3% as also given by the evaluation software.

10.5. Results

Table 10-2 Activity concentration of the most active nuclides in sample number 1 after 6 hours irradiation and 1 week cooling time, measured and simulated data

Nuclide	Main gamma lines[55] (MeV)	Half-life[55]	Activity concentration (Bq/cm^3)			
			Measured at BNC	MCNPX/ CINDER BNC	Difference between measured and simulated data	MCNPX / CINDER ESS
^{65}Zn	1.11 (50%)	244.30 d	4.74E+07	7.09E+07	49.58%	5.24E+04
^{64}Cu	1.34 (0.5%)	12.7 h	5.10E+06	1.81E+06	-64.51%	1.37E+03
^{51}Cr	0.32 (10%)	27.70 d	6.21E+05	2.39E+06	284.86%	9.18E+02
^{24}Na	2.75 (100%)	14.96 h	5.74E+05	1.75E+05	-69.51%	4.93E+02
^{69m}Zn	0.44 (95%)	13.76 h	1.54E+05	5.15E+05	234.42%	3.79E+02
^{59}Fe	1.10 (57%) 1.29 (43%)	44.50 d	3.72E+04	1.73E+04	-53.49%	1.30E+01
^{72}Ga	0.83 (96%) 2.20 (26%) 2.50(13%)	14.10 h	2.93E+04	3.69E+04	25.94%	6.53E+01
^{60}Co	1.17(100 %) 1.33(100 %)	5.27 y	1.25E+04	8.46E+02	-93.23%	2.68E+01
^{58}Co	0.81 (99%)	70.86 d	1.25E+04	-	-100%	1.40E-01
^{67}Cu	0.18 (49%)	61.83 h	-	9.01E+04	100%	1.16E+02
^{54}Mn	0.84(100 %)	312.3 d	-	6.73E+03	100%	3.58E+00

The most active gamma emitter in number 1 sample is ^{65}Zn which is produced from ^{64}Zn by neutron capture (σ=0.79 barn)[75] The quantity of ^{65}Zn decreases by one order of magnitude in 2.2 years. Most of simulated activity concentration values resulted in same order of magnitude as experimental data. In case of ^{60}Co the measured data was one order

of magnitude bigger than the simulated one. It is probably due to the fact that cobalt content was not detected by XRF and not available in the nominal composition.

Table 10-3 Activity concentration of the most active nuclides in sample number 2 after 6 hours irradiation at BNC and 1 week cooling time, measured[90] and simulated data

Nuclide	Main gamma lines[66] (MeV)	Half-life[66]	Activity concentration (Bq/cm^3)			
			Measured at BNC	MCNPX/ CINDER BNC	Difference between measured and simulated data	MCNPX/ CINDER ESS
^{51}Cr	0.32 (10%)	27.70 d	3.01E+06	3.03E+06	0.66%	1.32E+03
^{24}Na	2.75 (100%)	14.96 h	6.83E+05	1.80E+05	-73.65%	7.93E+02
^{65}Zn	1.11 (50%)	244.30 d	3.34E+04	4.76E+04	42.51%	4.07E+02
^{72}Ga	0.83 (96%) 2.20 (26%) 2.50 (13%)	14.10 h	3.94E+04	1.83E+04	-53.55%	3.05E+01
^{59}Fe	1.10 (57%) 1.29 (43%)	44.50 d	3.80E+04	3.61E+04	-5.00%	2.47E+01
^{58}Co	0.81 (99%)	70.86 d	9.98E+03	1.96E+04	96.39%	3.50E+00
^{54}Mn	0.84(100%)	312.3 d	9.74E+03	1.67E+04	71.46%	3.67+02
^{60}Co	1.17(100%) 1.33(100%)	5.27 y	7.96E+03	1.17E+01	-99.85%	1.73E-02
^{69m}Zn	0.44 (95%)	13.76 h	-	1.67E+02	100.00%	5.18E-01
^{64}Cu	1.34 (0.5%)	12.7 h	-	2.37E+04	100.00%	1.76E+01
^{67}Cu	0.18 (49%)	61.83 h	-	2.35E+02	100.00%	3.05E-01

The most active gamma emitter in number 2 sample is ^{51}Cr produced from ^{50}Cr ($\sigma = 15.4$ barn). The quantity of ^{51}Cr decreases by one order of magnitude in 92 days. In this case, most of simulated activity concentration values also resulted in same order of magnitude as experimental data and again the ^{60}Co was underestimated by simulation. Based on the simulation ^{64}Cu is also produced in significant quantity, however, it was not visible in the gamma spectrum, probably because of its low gamma yield (0.5%).

Using the material composition from XRF analysis, the simulations resulted in same order of magnitude as experimental data. The total activity concentration was estimated conservatively by simulations in both cases. The difference between the measured and simulated activity concentration values comes from the uncertainty of the XRF analysis, the uncertainty of the gamma spectroscopy, the uncertainty of the sample volume, and the uncertainty of the simulations. In both cases the ^{60}Co content was underestimated at least by one order of magnitude by simulations. It suggests that the samples had cobalt content that was neither detected by the XRF analysis, nor given in the nominal composition chart of the supplier. Therefore, it is advised to validate the material compositions using more different experimental techniques beside XRF, e.g. activation analysis.

The overall uncertainty of the activities determined by gamma spectroscopy is combined from the uncertainty of the gamma intensity values, the uncertainty of the gamma frequencies, and the uncertainty of the detector efficiency (see equation 10.2). The uncertainty of the gamma intensity values is under 30% as the acceptance level of full energy peaks was set to this value. The uncertainty of the gamma yields is under 0.02%[66]. It means that the uncertainty of the gamma spectroscopy is not larger than 30% in the worst (that is, most uncertain) case.

Based on mass measurements, the uncertainty of the sample volumes is estimated under 5%.

Based on sensitivity analysis the uncertainty coming from the inaccuracies in geometry is under 10% and the uncertainty coming from the inaccuracies in the irradiation history is under 10%. The statistical standard deviation values were within 3%. Considering all factors described in Chapter 5.6, the overall uncertainty of the total activity concentration is within 27%.

It can be considered that these results validate the activation of ESS guides because the most active nuclides are the same in the case of ESS. It is worth noting that the accuracy of the ESS simulation results depends strongly on the neutron energy distribution of the actual location and this (of course) changes a lot on the way from the target to the end of

an experimental cave. In this chapter it was indirectly confirmed that the simulation for the location with the most intensive neutron field was accurate enough provided that the material composition of the irradiated object was accurately known. This also confirmed the righteousness of the selection of simulation tools and their combination.

After 1 week cooling time the most active isotopes in the different aluminium samples were ^{65}Zn, ^{64}Cu, and ^{51}Cr. These results show that the aluminium substrate should contain the lowest possible Zn, Cu, and Cr concentrations.

11. Conclusions

During the operational time of the European Spallation Source, the structural materials will be activated. The aim of this PhD thesis was to present calculation methods developed for predicting the quality and the quantity of the produced radioactive waste thus supporting the material selection and design. The results show that the material composition including the impurities has a significant effect on the activation. The developed calculation methods were able to identify the source elements of the most important radionuclides in terms of decay gamma dose rate (for maintenance and refurbishment) and waste index (for processing requirements and for temporary and final disposal). Based on these calculations, the material selection can be optimized for decommissioning. The object of this thesis focused on the most crucial parts of ESS, however, these methods can be extended for the whole facility.

Due to the complexity of the geometry and material compositions involved, the calculation of the nuclide inventory was performed with particle and radiation transport codes. The radionuclide inventory and decay gamma dose rate were calculated with MCNPX2.7[49] using ENDF/B-VII cross-section libraries coupled with CINDER'90[31] nuclear inventory code.

For waste classification we defined the waste index (*WI*) for the whole waste stream which directly relates the waste classes to the respective values of clearance level (*CL*) associated with the negligible dose. Two methods for the estimation of the clearance levels not published in IAEA compilations[41,60] were applied for the generation of overall waste indices. In both cases the components of the effective dose rate were compared with that of a well-known standard radionuclide.

The replaceable rotating solid tungsten target will apparently be the most active part. Based on the calculation of radioactive inventory the tungsten target would be classified as high level waste (HLW) after 5 years of irradiation and 10 years of cooling time. The target should be stored in hot cell before conditioning and deep geological repository is advised for final disposal. The nuclides having the greatest share in the compound waste index are ^{148}Gd, ^{133}Ba, ^{152}Eu, ^{179}Ta, ^{60}Co, and ^{154}Eu. Sensitivity analysis showed that 99% of ^{60}Co production is due to cobalt impurity, therefore, it is advised to use structural

materials with low cobalt content. The MCNPX2.7/CINDER'90 runs with the different combinations of high-energy models gave approximately the same total activity concentration for the target without considering the tritium content.

The activation of the neutron guides and inserts is an important topic, because the replacement of the guides is envisaged after a few years use due to radiation damage, mechanical failure, and progress in guide technology. Aluminium, float, and zerodur neutron guide substrate materials inside the monolith were examined in terms of activation. After 5 years of operation the decay gamma dose rates are extremely high surrounding the neutron guide and the insert, and the substrates have high level waste category. After one week cooling time the longer lived nuclides will give the major contribution for the gamma dose and waste index in all three cases. In case of aluminium and zerodur it is ^{65}Zn, in case of float it is ^{22}Na. It is, therefore, advised to decrease the amount of zinc in aluminium and zerodur substrate materials.

At ESS, metal-based shielding plays an important role in the attenuation of high-energy neutrons. Aluminium, copper, and steel shielding blocks were compared in terms of activation. After 10 days of cooling time the steel is the most active, followed by aluminium and copper, respectively. After 30 day cooling, in aluminium the long-lived gamma emitter ^{65}Zn dominates, which requires to decrease the amount of zinc in the material composition in facility parts where aluminium is applied. In copper the long-lived gamma emitter ^{60}Co is the most important nuclide. After 1 day cooling, in steel ^{59}Fe and ^{54}Mn become the most active gamma emitters. Therefore, it is advised to decrease the manganese content of the steel without changing its advantageous thermal and physical behavior.

The beryllium reflector is problematic as the activated toxic beryllium requires specific treatment. It can be concluded, that after 1 year of operation the Be reflector will have HLW waste category, and has to be disposed into deep geological repository for long-term. Based on the results, there will be extremely high gamma dose field surrounding the activated reflector system. The dose rate decreases by one order of magnitude in two weeks of cooling time, but it will be still in Sv/h range. After two weeks of cooling time, the most active gamma emitters in the activated beryllium are ^{7}Be, ^{51}Cr, ^{46}Sc, ^{95}Nb, ^{95}Zr,

^{60}Co, and ^{88}Y. Most of these nuclides have a few months half-life, except ^{60}Co whose half-life is 5.39 years. It is mostly produced from cobalt impurity, therefore, it is advised to use low cobalt material.

The activation of the materials in experimental caves needs particular consideration in terms of radiation protection of the workers. In this thesis the NMX experimental cave was studied as an example. Based on calculations, after 40 years of operation immediately after shut-down the major contributor for the total activity and gamma dose rate is the aluminium false floor due to the production of ^{28}Al. Based on these results it is recommended to omit the use of aluminium as a structural material thereof and use other nuclear grade materials or steel covered by boron containing floor (tiles). The aluminium floor and concrete wall will be low level waste and probably can be released in a few years. In aluminium floor the long-lived ^{65}Zn gives the major contribution for the waste index which is produced from zinc. In concrete wall, after 10 days of cooling time the ^{40}K gives the majority of the waste index.

In order to validate the model calculations, aluminium and glass neutron guide substrate samples were irradiated at the Budapest Neutron Centre and the measured activity concentrations were compared with the model predictions. The nominal composition of the substrate materials was verified by X-ray fluorescence spectroscopy (XRF). The difference was significant between the nominal and XRF-measured composition. In the simulations, the XRF-measured material composition was used, for not detectable elements the nominal data were taken. After 1 week cooling time the most active nuclides in the different aluminium samples were ^{65}Zn, ^{64}Cu, and ^{51}Cr. These results show that the aluminium substrate should contain the lowest possible Zn, Cu, and Cr concentrations. Most of simulated activity concentration values resulted in the same order of magnitude as experimental data. In case of ^{60}Co the measured data was one order of magnitude larger than the simulated one. It is probably due to the fact that cobalt content was not detected by XRF and not available in the nominal composition. Therefore, it is advised to validate the material compositions using more different experimental techniques beside XRF, e.g. activation analysis. It can be considered that these results validate the activation of ESS guides because the most active nuclides are the same in the case of ESS.

Thesis statements

1. As the waste index is obliged to cover all artificial radionuclides present in the material in question I defined the clearance level (*CL*) for those components of the ESS tungsten target inventory which were missing from previous *CL* compilations[40,41,60] by setting up scenarios for estimating *CL*s similarly to the procedures described in the mentioned compilations. [T1].

2. I assessed the radioactive inventory and waste index of the ESS tungsten target in comparison with other previously studied target options.

a. I compiled different compound high energy models combining MCNPX2.7[49] and CINDER'90[31] calculation tools in order to assess the inventory and consequently the waste index of the ESS tungsten target. Spallation events were modelled in two ways: in two separate steps or in a single procedure. The first step of the reaction mechanism of the proton-induced spallation process was described with intranuclear cascade (INC) models: Bertini[15], INCL4.2[17], and Isabel[16] codes were applied. For the adequate description of the de-excitation of the nuclei, that constitutes the second step of the process, these models were coupled to Dresner[23] and ABLA[22] codes, respectively. CEM02[24] model, that was also applied in the calculations, included all steps of spallation process modelling in one package. The runs with the different combinations of these models gave approximately the same total activity concentration for the target without considering the tritium content. The resulting value was 1.7×10^{9} Bq/cm^3(±10%) using the different models; this confirmed their adequacy for our purpose. However, in case of tritium production the differences of the applied models were of 3 orders of magnitude; the CEM02 combined spallation model gave the most conservative estimation of tritium production: 1.4×10^{10} Bq/cm^3. Except for tritium production, the combination of INCL4.2 and ABLA codes resulted in the most conservative estimation of the relevant isotopes contributing significantly to the waste index [T1, T8, T11, T14].

b. Based on the calculation of radioactive inventory I showed that the tungsten target would be classified as high level waste (HLW) after 5-year irradiation and 10-year

cooling time. The inventory was estimated using 2 GeV incident proton energy and activity concentrations were defined after 5 years of irradiation and 10 years of cooling time; this resulted in a waste index of 3.2×10^{7}. I showed that the tungsten target has a more favourable waste index than previously considered lead-bismuth eutectic (LBE) and mercury target, assuming similar operational conditions. The nuclides having the greatest share in the compound waste index are ^{148}Gd, ^{133}Ba, ^{152}Eu, ^{179}Ta, ^{60}Co, and ^{154}Eu. I determined that 99% of ^{60}Co production is due to cobalt impurity. Therefore, I advised to use structural materials with low cobalt content [T1, T8, T12].

3. a. The possible neutron guide substrate materials located the closest to the target were investigated for radiation safety during operation and decommissioning. Coupling MCNPX2.7[49] to CINDER'90[31] code I estimated the radioactive inventory of three different candidate materials as potential ESS neutron guides. In order to assess the radiation hazard of disassembling the device, I showed that after 5 years of operation the aluminium guides (1.9×10^{7} Bq/cm^3) would be less active than the float (1.1×10^{8} Bq/cm^3) and zerodur (1.2×10^{8} Bq/cm^3) guides. However, in case of zerodur, the tritium gives the main contribution. The main gamma-emitting isotopes that define the external dose exposure of the personnel performing the replacement of the device are ^{65}Zn in case of zerodur and aluminium, and ^{24}Na in case of float. Therefore, I advised to decrease the amount of zinc in aluminium and zerodur substrate materials [T6, T7, T10, T12].

b. I studied the effect of material selection on the radionuclide inventory of metal-based shielding blocks by assessing radioactivity generation applying the method of coupling MCNPX2.7[49] to CINDER'90[31] code, thus providing neutron activation conditions in terms of energy flux and energy distribution. Three materials were examined: iron, copper, and aluminium. Immediately after shutdown the steel shielding block will be the least active, the dominant radioisotopes being ^{55}Fe, ^{59}Fe, ^{54}Mn, ^{56}Mn. Therefore, it is advised to decrease the manganese content of the steel without changing its advantageous thermal and physical behaviour. After 5 days of cooling time the copper shielding block becomes the least radioactive, because in the activated copper shielding short-lived copper isotopes ^{64}Cu, ^{66}Cu dominate. In activated aluminium shielding, short-lived ^{28}Al, ^{56}Mn, ^{64}Cu, and long-lived ^{65}Zn will dominate during the maintenance and replacement operations, which

requires to decrease the amount of zinc in the material composition in facility parts where aluminium is applied [T4, T13].

4. I performed activation and dose rate calculations to estimate the dose consequences of the handling of the activated beryllium reflector. In order to assess the radionuclide inventory, simulation was performed with MCNPX2.7[49] using ENDF/B-VII cross section libraries coupled with CINDER'90[31] similarly to the method of statement 3. I showed that at shutdown after 1-year operation the most active gamma-emitting isotopes are ^{56}Mn (1.8×10^{9} Bq/cm^3) and ^{7}Be (9.7×10^{8} Bq/cm^3). The dose rate on the external surface of the beryllium reflector after 1-year irradiation time is 720 Sv/h at the end of operation, decreasing to 60 mSv/h after 2 weeks cooling time. Owing to this dangerous level I recommend to store the beryllium in hot cell before final disposal during the decommissioning process. It is recommended to wait at least two weeks of cooling time before the replacement of the beryllium. After two weeks the most active gamma emitters in the activated beryllium are ^{7}Be, ^{51}Cr, ^{46}Sc, ^{95}Nb, ^{95}Zr, ^{60}Co, and ^{88}Y. It means that the quantity of cobalt, chromium, scandium, niobium, zirconium, and yttrium impurities should be decreased as much as possible [T5, T9].

5. Irradiation experiments were designed and carried out for the purpose of validating the simulation procedure performed with the combination of software tools introduced above. Aluminium neutron guide substrate samples were irradiated for 6 hours at one of the fast neutron channels of the nuclear research reactor at Budapest Neutron Centre. Using the nominal composition of the samples, the simulations showed a rather big difference from experimental results. Based on these results, I recommended that the nominal composition of the sample (with special respect to trace elements) should be verified by chemical analysis. In turn, using the material composition obtained with XRF analysis the simulations resulted in the same order of magnitude as experimental data. After 1 week cooling time the most active isotopes in two different aluminium samples were ^{65}Zn (4.8×10^{4} and 7.1×10^{7} Bq/cm^3), ^{64}Cu (2.4×10^{4} and 1.8×10^{6}Bq/cm^3) and ^{51}Cr (3×10^{6} and 2.39×10^{6} Bq/cm^3). These results show that the aluminium substrate should contain the lowest possible concentrations of Zn, Cu, and Cr. Considering the discrepancies between the nominal and re-determined elemental composition of the samples, the agreement

between the measured and calculated results was sufficient to confirm the suitability of the combined simulation procedure presented in the thesis. This means that the calculations performed with the same software tools for predicting the activation of the examined substrates under the assumed ESS irradiation conditions can also be considered accurate enough. In case of ^{60}Co the measured data were one order of magnitude larger than the simulated one. It is probably due to the fact that cobalt content was not detected by XRF and not available in the nominal composition. Therefore, I advised to validate the material compositions using different experimental techniques beside XRF, e.g. activation analysis [T3].

6. I performed activation calculations for ESS NMX experimental cave considering the walls assumedly made from ordinary concrete and the floor that was scheduled to be manufactured from aluminium. An adjusted version of the previously described combination of MCNPX2.7[49] and CINDER'90[31] was applied, the former code used the ENDF/B-VII cross-section libraries as before. I showed that after 40 years operation the major contributor to the total activity defining the dose field for the operators that would enter the area was the aluminium false floor (2.46 kBq/g) due to the production of ^{28}Al and ^{56}Mn. Therefore, I recommended to ignore aluminium as a structural material and use other, preferably nuclear grade materials, or steel covered boron containing floor. The main component of the concrete wall structure responsible for its contribution to the dose field will be ^{24}Na during operations and interim maintenance and refurbishment procedures [T2].

Related publications

[T1] Zs. Kókai, Sz. Török, P. Zagyvai, D. Kiselev, R. Moormann, E. Börcsök, L. Zanini, A. Takibayev, G. Muhrer, R. Bevilacqua, J. Janik: Comparison of different target material options for the European Spallation Source based on certain aspects related to the final disposal, Nuclear Instruments and Methods in Physics Research Section B: Beam Interactions with Materials and Atoms, Volume 416, 1 February 2018, Pages 1-8 https://www.sciencedirect.com/science/article/pii/S0168583X17309977

[T2] G. Náfrádi, Zs. Kókai, P. Zagyvai: Az NMX mérőhelyének sugárárnyékolása (Shielding of ESS NMX cave), Nukleáris Technikai Szimpózium, 2017

[T3] Zs. Kókai, E. Dian, L. Zanini, F. Mezei, A. Takibayev, E. Klinkby, Sz. Török, P. Zagyvai, G. Patriskov, F. Gergely: Neutron guide activation calculations for the European Spallation Source and validation measurements at Budapest Neutron Centre, International Collaboration on Advanced Neutron Sources (ICANS XXII), 27-31 March 2017, Oxford, UK, http://icansxxii.iopconfs.org

[T4] D. Dijulio, C. P. Cooper-Jensen, H. Björgvinsdóttir, Zs. Kókai, P. M. Bentley: High-energy in-beam neutron measurements of metal-based shielding for accelerator-driven spallation neutron sources, Physical Review Accelerators and Beams, 19, 053501 (2016) https://journals.aps.org/prab/pdf/10.1103/PhysRevAccelBeams.19.053501

[T5] Yongjoong Lee (Ed.): ESS Materials Handbook, Beryllium dose maps in the target area, ESS-0028465, 2015

[T6] Zs. Kókai, L. Zanini, F. Mezei, A. Takibayev, E. Klinkby, P. Zagyvai, Sz. Török: Activation of the neutron guides designed for the European Spallation Source, 6th International Conference "Charged & Neutral Particles Channeling Phenomena - Channeling 2014", Capri, October 5-10, 2014

[T7] Zs. Kókai, L. Zanini, F. Mezei, A. Takibayev, E. Klinkby, P. Zagyvai, Sz. Török: Neutron guide activation and handling for the European Spallation Source, ICANS XXI: International Collaboration on Advanced Neutron Sources, Mito, 29 Sep - 3 Oct 2014

[T8] Kókai Zs., Zagyvai P., Török Sz.: Az Európai Neutronkutató Központ leszerelési terve (Decommissioning plan of ESS), Nukleon VII.évf. 4.szám, 2014, http://nuklearis.hu/nukleon/az-europai-neutronkutato-kozpont-leszerelesi-terve

[T9] P. Zagyvai, Zs. Kókai, D. Ene: Initial decommissioning plan for ESS, SSM2012-131, 2013

[T10] Zs. Kókai, P. Zagyvai. Sz. Török, L. Zanini: Health physics calculations related to the target station radiation project, Accelerator and Integrated Control System Retreat, 2013

[T11] Zagyvai P., Kókai Zs.: A nukleáris energiatermelés radioaktív hulladékai lektorált egyetemi jegyzet (Radioactive waste of nuclear fuel cycle), 2013 https://www.scribd.com/doc/316374945/Nuklearis-Uzemanyagciklus-Radioaktiv-Hulladekai-MTA-EK

[T12] Zagyvai P., Kókai Zs., Török Sz.: Leszerelési tervek európai nagyberendezésekhez (Decommissioning plan of European research facilities), Nukleáris Technikai Szimpózium, Budapest, 2013

[T13] Kókai Zs., Zagyvai P., Bodor K.: Az Európai neutronkutató központ (ESS) előzetes leszerelési tervével kapcsolatos kutatások (Research related to initial decommissioning plan of ESS), XXXVIII. Sugárvédelmi Továbbképző Tanfolyam, Hajdúszoboszló, 2013

[T14] Kókai Zs., Breitner D., Török Sz.: Nagyaktivitású hulladék végleges elhelyezésére vonatkozó nemzetközi elképzelések (Final disposal of high level radioactive waste), Nukleáris Technikai Szimpózium, Paks, 2012

Appendix

A1. Summary of radiation protection definitions

The emission of the ionizing radiation is the most significant environmental effect of the radioactive waste. The alpha, beta, gamma, and X-ray emissions are direct ionizing radiations and produced by radioactive decay of the nuclei. The neutrons are indirectly ionizing radiation.

Radiation effects are usually divided into two categories, depending upon whether the damage arises from external exposure from small and extended sources or from internal exposure due to inhalation, ingestion or immersion. The harms of exposure can be deterministic from high doses or stochastic. The deterministic effect means necrosis of tissues and it occurs above a well-defined threshold (at least 0.3 Gy) The stochastic effect means cell mutation resulting in solid tumour or leukaemia. There is linear no threshold (LNT) relation between effective dose (excess dose above natural level) and associated risk[39].

Dose definitions

The absorbed dose is defined as the statistical average of the energy imparted per unit mass at a point[39]:

$$D = \frac{dE}{dm}\left[\frac{J}{kg} = Gy\right] \quad \text{(A.1)}$$

The equivalent dose derived from the absorbed dose takes into account the biological effectiveness of the radiation, which is dependent on the radiation type and energy[39].

$$H = \mathrm{D} \cdot w_R \quad \text{(A.2)}$$

where w_R is the radiation weight factor, $wR,\alpha = 20$; $wR,\beta = 1$; $wR,\gamma = 1$; $wR,n = 5..20$ depending on the neutron energy The effective dose is the tissue-weighted sum of the equivalent doses in all specified tissues and organs of the human body. The tissue weight factor (w_T) defines the sensitivity of the given tissue[39]:

$$H_E = \sum_T w_T \cdot H_T \left[\frac{J}{kg} = Sv\right] \quad \text{(A.3)}$$

$$\sum_T w_T = 1$$

The committed effective dose is a time-integrated effective dose caused by an internal radioactive source. A time limit (T) of 50 years was set up in case of workers in a radiation hazardous position and of 70 years in case of general habitants[39].

$$H_C = \int_0^T E(t)\dot{dt}\,[Sv] \quad \text{(A.4)}$$

The committed effective dose can be calculated in the following way[39]

$$H_C = DCF \cdot A \quad \text{(A.5)}$$

where *A* is the incorporated activity, *DCF* is the dose conversion factor which gives the relation between the committed effective dose and a unit incorporated activity.

The negligible dose (10 μSv/year) is associated with a risk too low to justify any countermeasures. The risk from negligible dose is under 5E-7[39].

The effective half-life is the period of time required to reduce the activity of an internal organ or the whole body to half of its initial value due to radioactive decay and biological process. It is calculated by combining the physical (radioactive) half-life and biological half-life[39].

$$\frac{1}{T_{eff}} = \frac{1}{T_{phy}} + \frac{1}{T_{bio}} \quad \text{(A.6)}$$

where T_{eff} is the effective half-life, T_{phy} is the physical half-life and T_{bio} is the biological half-life.

Radiation protection regulation

The general goal of nuclear safety is that members and groups of population as well as environmental entities should be safe from harms of radiation. This shall be provided by establishing and maintaining effective safety measures in nuclear installations. The radiation protection goal of nuclear safety is that the dose of both the operating personnel and the general public shall be kept below predefined limits, at a value as low as reasonably achievable (ALARA). This level shall be kept in case of design basis incidents and – as far as reasonably possible – in accident situations as well. The main principles include justification, optimization, and limitation[39].

Most of the radiation protection recommendations are given by the International Atomic Energy Agency (IAEA) and each country use these recommendations to define their own regulations. The dose limit (DL) defines the maximum artificial incorporated effective dose of a reference person. In case of workers in a radiation hazardous position the dose limit is 20 mSv/year, in case of general habitants the dose limit is 1 mSv/year. The dose constraints (DC) define the maximum incorporated effective dose for a reference person caused by the given facility.

Summary

The aim of this PhD thesis is to present calculation methods developed for predicting the quality and the quantity of the produced radioactive waste at ESS, thus supporting the material selection and design. The results show that the material composition including impurities has a significant effect on the activation. The developed calculation methods are able to identify the source elements of the most important radionuclides in terms of decay gamma dose rate (for maintenance and refurbishment) and waste index (for processing requirements and for temporary and final disposal). Based on these calculations, the material selection can be optimized for decommissioning. The object of this thesis focused on the most crucial parts of ESS specified in the following; however, these methods can be extended for the whole facility.

The rotating solid tungsten target will apparently be the most active part. The activation of the neutron guides and inserts is an important issue, because the replacement of the guides is envisaged after a few years use due to radiation damage, mechanical failure, and progress in guide technology. The beryllium reflector is also envisaged to be replaced and the activated beryllium requires specific treatment. At the ESS, metal-based shielding plays an important role in the attenuation of high-energy neutrons in addition to shielding against prompt and decay gammas. The activation of the materials in experimental caves needs particular consideration in terms of radiation protection of the workers. In this thesis the NMX macromolecular diffractometer experimental cave was studied as an example of instrumentation. The activation properties in these selected parts depend strongly on the material choice.

In order to validate the model calculations, aluminium and glass neutron guide substrate samples were irradiated at the Budapest Neutron Centre and the measured activity concentrations were compared with the model predictions.

Magyar nyelvű összefoglalás: Az Európai Neutronkutató Központ leszerelésével kapcsolatos sugárvédelmi számítások

A jövő generációk védelme érdekében a radioaktív hulladékot termelő létesítmények leszerelését meg kell tervezni, és a szükséges erőforrásokat biztosítani kell. Az Európai Neutronkutató Központ a világ legnagyobb intenzitású neutronforrása lesz. Az üzemidő alatt a szerkezeti anyagok felaktiválódnak, radioaktív hulladék keletkezik belőlük. Az aktiváció előzetes elemzése a tervezési szakaszban lehetővé teszi az anyagválasztás és tervezés optimalizálását a keletkezett radioaktív hulladékok veszélyességének csökkentése érdekében.

Jelen kutatómunka célja olyan számítási eljárások kidolgozása, melyek lehetővé teszik az Európai Neutronkutató Központban keletkezett radioaktív hulladékok előzetes mennyiségi és minőségi elemzését. Az eredmények alapján elmondható, hogy az anyagösszetétel jelentős hatással van az aktivációra. A kidolgozott számítási eljárások segítségével előre azonosíthatók a legfontosabb keletkezett radionuklidok és azok forráselemei a gamma dózis (karbantartáshoz és felújítás esetén) és hulladékindex (feldolgozás, ideiglenes és végleges elhelyezés esetén) szempontjából. A számítási eredmények segítségével az anyagösszetétel optimalizálható a részleges és végleges leszerelés szempontjából.

Jelen értekezés az előzetes leszerelési tervben megjelölt kulcsfontosságú részek vizsgálatára fókuszál (target, neutronvezetők, reflektor, fém árnyékolás, kutatólabor), de a számítási eljárások kiterjeszthetők a teljes létesítményre. A számítások validációjára a Budapesti Kutatóreaktorban végzett aktivációs mérések szolgálnak.

References

[1] Decommissioning of medical, industrial and research facilities, IAEA Safety Standards Series no. Ssg-49, Vienna, 2019

[2] Methodologies for assessing the induced activation source term for use in decommissioning applications, Safety Reports Series No. 95, IAEA, Vienna, 2019

[3] S. Peggs (Ed.), ESS Technical Design Report, 2013

[4] F. Mezei, Long pulse spallation sources, In Physica B: Condensed Material, Volumes 234–236, 1997, Pages 1227-1232

[5] P. Zagyvai, Zs. Kókai, D. Ene: Initial decommissioning plan for ESS, SSM2012-131, 2013

[6] D. L. Price: Neutron Sources and Applications, Report of a Review held at Oak Brook, Illinois, 1992

[7] Ashkar, R., Bilheux, H. Z., Bordallo, et al. (2018). Acta Cryst. D74, 1129-1168

[8] Jason K. Rockhill, George E. Laramore, Chapter 20 – Neutron Radiotherapy, Clinical Radiation Oncology (Fourth Edition), Elsevier, 2016, Pages 373-380.e2, ISBN 9780323240987

[9] Hirai S. (1990) A Guideline for Application of Neutron Activation Analysis to Biological and Medical Samples. In: Tomita H. (eds) Trace Elements in Clinical Medicine. Springer, Tokyo, ISBN 978-4-431-68120-5

[10] M. Ripani, Neutron sources and transmutation of nuclear waste, Annals of Nuclear Energy, Volume 62, 2013, Pages 590-595, ISSN 0306-4549

[11] D. Filges and F. Goldenbaum. Handbook of Spallation Research. Wiley, 2010

[12] T. Enqvist, W. Wlazło, P. Armbruster, et al. Isotopic yields and kinetic energies of primary residues in 1 A GeV 208Pb+p reactions, Nuclear Physics A, Volume 686, Issues 1–4, 2001, Pages 481-524

[13] G. J. Russell. Spallation physics – An overview. In Proceedings of ICANS XI, October 22–26, 1990, Tsukuba, Japan

[14] R. Serber: Nuclear Reactions at High Energies, Phys. Rev. 72, 1947

[15] H. W. Bertini, Phys. Rev. 188 (1969) 1711–1730

[16] Y. Yariv, Z. Fraenkel, 1981. Phys. Rev. C. **24**. 488-494

[17] A. Boudard, J. Cugnon, S. Leray, and C. Volant, Phys. Rev. C 66, 044615 (2002)

[18] Dover, Carl, Delta resonance, Department of Physics, Brookhaven National Laboratory, Upton, New York, 2014

[19] E. M. A. Hussein, Radiation Mechanics: Principles and Practice, Elsevier Science; December 5, 2007, ISBN-10: 9780080450537

[20] S. Leray: Nuclear Reaction at High Energy, Workshop on Nuclear Data for Science and Technology: Accelerator Driven Waste Incineration, Trieste, 10 - 21 September 2001, LNS0212005

[21] V. F. Weisskopf and D. H. Ewing, On the yield of nuclear reactions with heavy elements. Phys. Rev., 57:472–485, 1940

[22] A. R. Junghans, M. de Jong, H.-G. Clerc, A. V. Ignatyuk, G. A. Kudyaev, K.-H. Schmidt, Projectile-fragment yields as a probe for the collective enhancement in the nuclear level density, In Nuclear Physics A, Volume 629, Issues 3–4, 1998, Pages 635-655

[23] L. Dresner, 1981. EVAP-A Fortran Program for Calculating the Evaporation of Various Particles from Excited Compound Nuclei, Oak Ridge National Laboratory report ORNL-TM-7882

[24] K. K. Gudima, S. G. Mashnik, V. D. Toneev, Cascade-exciton model of nuclear reactions, Nuclear Physics A, Volume 401, Issue 2, 1983, Pages 329-361

[25] Y. Z. Xing, H. F. Zhang, X. B. Liu, Y. M. Zheng, Pauli-blocking effect in two-body collisions dominates the in-medium effects in heavy-ion reactions near Fermi energy, Nuclear Physics A, Volume 957, 2017, Pages 135-143, ISSN 0375-9474

[26] S. G. Mashnik et al. LAQGSM03.03 upgrade and its validation. Report, LA-UR-07 6198, Los Alamos National Laboratory, USA, 2007

[27] R. K. Bock and A. Vasilescu, The Particle Detector Briefbook, Springer, Berlin, Heidelberg, 1998

[28] Szatmáry Zoltán: Bevezetés a reaktorfizikába, Akadémiai Kiadó, Budapest, 2000

[29] S. Agostinelli et al. GEANT4- A simulation toolkit, Nuclear Instruments and Methods in Physics Research Section A, 506(3):250-303, 2003

[30] K. H. Beckurts and K. Wirtz, Neutron Physics, Springer, Berlin, 1964

[31] W. B. Wilson, S. T. Cowell, T. R. England, A. C. Hayes & P. Moller, A Manual for CINDER'90 Version 07.4 Codes and Data, (2007)

[32] Lecture of Lawrence E. Boing, IAEA Interregional Training Course on Nuclear Facility Decommissioning and Environmental Remediation Skills, 2013

[33] International Basic Safety Standards for Protection against Ionizing Radiation and for the Safety of Radiation Sources, IAEA General Safety Requirements GSR Part 3., Vienna, 2014

[34] International Commission on Radiological Protection Recommendations of the International Commission on Radiological Protection, ICRP#103, 2007

[35] Classification of Radioactive Waste, IAEA General Safety Guide GSG-1, Vienna, 2010

[36] SSMFS 2010:2 Strålsäkerhetsmyndighetens föreskrifter om hantering av radioaktivt avfall och utsläpp från verksamhet med öppna strålkällor

[37] SSMFS 2011:2 Strålsäkerhetsmyndighetens föreskrifter om friklassning av material, lokaler, byggnader och mark vid verksamhet med joniserande strålning

[38] Council Directive 2013/59/Euratom

[39] International Atomic Energy Agency: International Basic Safety Standards, for Protection against Ionizing Radiation and for the Safety of Radiation Sources, Safety Series No. 115., Vienna, 1996

[40] Radiation Protection 122/I Guidance on General Clearance Levels for Practices Recommendations of the Group of Experts (2000)

[41] IAEA Safety Reports Series No. 44 "Derivation of Activity Concentration Values for Exclusion, Exemption and Clearance" Vienna, 2005

[42] Hungarian Standard, MSZ 14344-1/2004 Radioactive wastes – Terminology and categorization, http://www.haea.gov.hu/web/v2/portal.nsf/index_en

[43] https://www.oecd-nea.org/rwm/profiles/Sweden_profile_web.pdf

[44] https://www.oecd-nea.org/rwm/profiles/Sweden_report_web.pdf

[45] F. X. Gallmeier, W. L. Wilson, M. Wohlmuther, B. Micklich, E. B. Iveron, E. Pitcher, W. Lu, H. R. Trellue, Ch. Kelly, G. Muhrer, I. I. Popova, P. Ferguson, 2007. An Environment using Nuclear Inventory Codes in Combination with the Radiation Transport Code MCNPX for Accelerator Activation Problem. Proc. of the 8th Int.

Topical Meeting on Nuclear Applications and Utilization of Accelerators, Pocatello, USA, p. 207

[46] T. Lorenz, Y. Dai, D. Schumann, Analysis of long-lived radionuclides produced by proton irradiation in lead targets – γ-measurements, Radiochim. Acta 101, 661–666 (2013)

[47] T. Lorenz, Y. Dai, D. Schumann, A. Türler, Proton-induced Polonium Production in Lead, In Nuclear Data Sheets, Volume 119, 2014, Pages 284-287, ISSN 0090-3752

[48] D. Kiselev, T. Lorenz, Y. Dai, J.-Ch. David, D. Schumann, M. Wohlmuther (2014), "Po-production in lead: Calculation and measurement on SINQ-samples (PSI)", SATIF-12, Batavia, Illinois, United States, pp. 134 -148

[49] D. Pelowitz. (ed.), 2011. MCNPX User's Manual, Version 2.7.0, LA-CP-11-00438

[50] John S. Hendricks et al., MCNPX 2.6.0 Extensions, LA-UR-08-2216, 2008

[51] www.nndc.bnl.gov

[52] B. J. Micklich, F. X. Gallmeier, M. Wohlmuther, Comparison of Selected Codes for Calculating Induced Radioactivity at Accelerator Facilities, Nuclear Technology Volume 168, Pages 700-705, 2009

[53] https://europeanspallationsource.se/

[54] John Haines: Status of the target program, 2013 www.europeanspallationsource.hu

[55] Emil Boman and Lukas Smisovsky, Remote Handling within the Active Cells Facility at the European Spallation Source, Using Digital Reality Techniques, Master thesis, Department of Design Sciences, Lund University, 2016

[56] K. Batkov, A. Takibayev, L. Zanini and F. Mezei, Unperturbed moderator brightness in pulsed neutron sources, Nuclear Instruments and Methods in Physics Research Section A: Accelerators, Spectrometers, Detectors and Associated Equipment 729 (2013)

[57] F. Mezei, L. Zanini, A. Takibayev, K. Batkov, E. Klinkby, E. Pitcher, and T. Schöfeldt, Low dimensional neutron moderators for enhanced source brightness, Journal of Neutron Research 17 (2014)

[58] www.mirrotron.com

[59] Giuseppe Aprigliano: The NMX Instrument Outline, Phase 2 review22nd June, 2017, www.europeanspallationsource.se

[60] Radiation Protection 157, Comparative Study of EC and IAEA Guidance on Exemption and Clearance Levels Directorate-General for Energy Directorate D — Nuclear Energy Unit D4 — Radiation Protection (2010)

[61] Zs. Kókai, Sz. Török, P. Zagyvai, D. Kiselev, R. Moormann, E. Börcsök, L. Zanini, A. Takibayev, G. Muhrer, R. Bevilacqua, J. Janik: Comparison of different target material options for the European Spallation Source based on certain aspects related to the final disposal, Nuclear Instruments and Methods in Physics Research Section B: Beam Interactions with Materials and Atoms, Volume 416, 1 February 2018, Pages 1-8

[62] Introduction to Radiological Physics and Radiation Dosimetry – F.H. Attix 2004, Wiley, Weinheim

[63] http://www.nist.gov/pml/data/xraycoef/index.cfm

[64] http://radiationsoftware.com/microshield/

[65] Hungarian Standard MSZ 62-2:2017 "Protection against ionizing radiation. Shielding against beta, gamma and X-ray radiation"

[66] S. Y. F. Chu1, L. P. Ekström and R. B. Firestone, The Lund/LBNL Nuclear Data Search Version 2.0, February 1999, http://nucleardata.nuclear.lu.se/toi/

[67] Ghiglino, S. Terrón, K. Thomsen, J. Wolters, M. Magán, F. Martínez, P.J. de Vicente, R. Vivanco, F. Sordo, M. Butzek, J. M. Perlado, F. J. Bermejo, A neutron production target for ESS based upon the Canned-rods concept, Nuclear Instruments and Methods in

Physics Research Section A: Accelerators, Spectrometers, Detectors and Associated Equipment, Volume 756, 21 August 2014, Pages 73-81, ISSN 0168-9002

[68] Personal communication from Alan Takibayev

[69] Certification of Beijing Tian-Long Tungsten from Yong Joong Lee

[70] K. N. Clausen, R. Eccleston, P. Fabi, T. Gutberlet, F. Mezei, and H. Tietze-Jaensch (Eds.), The ESS Project Volume III Update: Technical Report, ISBN3-893336-304-1 (2003)

[71] K. B. Grammer et al., Measurement of the scattering cross section of slow neutrons on liquid parahydrogen from neutron transmission, Phys. Rev. B 91, 180301(R), 2015

[72] S. Leray, A. Boudard, J. Cugnon, J. C. David, A. Kelić-Heil, D. Mancusi, M. V. Ricciardi, Improved modelling of helium and tritium production for spallation targets, Nuclear Instruments and Methods in Physics Research Section B: Beam Interactions with Materials and Atoms, Volume 268, Issue 6, 2010, Pages 581-586

[73] B. Babcsány, Sz. Czifrus, S. Fehér, Methodology and conclusions of activation calculations of WWER-440 type nuclear power plants, Nuclear Engineering and Design 284 (2015) 228-237

[74] SSM 2009:29e Swedish national plan for the management of all radioactive waste

[75] https://www-nds.iaea.org/relnsd/vcharthtml/VChartHTML.html

[76] Saran, Prabhat & Nandy, Maitreyee & Sarkar, Pradip & Goyal, Sneh. (2012). Production of long-lived Al-26 and Na-24 from neutron interaction in Al target. Indian Journal of Pure and Applied Physics. 50. 509-512

[77] L. Adamski, M. Herman, A. Marcinkowski, Cross section measurements of the 23Na(n, 2n)22Na, 58Ni(n, 2n)57Ni and 115In(n,n′)115mIn reactions, Annals of Nuclear Energy, Volume 7, Issue 7, 1980, Pages 397-401

[78] D. Dijulio, C. P. Cooper-Jensen, H. Björgvinsdóttir, Zs. Kókai, P. M. Bentley: High-energy in-beam neutron measurements of metal-based shielding for accelerator-driven spallation neutron sources, Physical Review Accelerators and Beams, 19, 053501, 2016

[79] H. Liskien, A. Paulsen, R. Widera, A check on the consistency of differential 63Cu(n, α)60Co cross sections, Journal of Nuclear Energy, Volume 27, Issue 1, 1973, Pages 39-41

[80] Certificate of Analysis for the beryllium bought from Materion for LANSCE in 2009

[81] Rogante Engineering "Contributions to the decommissioning issue of the ESS project" Cinitanova Marche (2009)

[82] P. Duhamel, W. Galster, J. S. Graulich, P. Jean, P. Leleux, J.-P. Meulders, J. Vanhorenbeeck, G. Vedrenne, P. von Ballmoos, Measurement of cross-sections for the 9Be(n,3n)7Be and 56Fe(n,p)56Mn reactions producing background lines in γ-ray astrophysics, Nuclear Instruments and Methods in Physics Research Section A: Accelerators, Spectrometers, Detectors and Associated Equipment, Volume 404, Issue 1, 1998, Pages 143-148

[83] G. Náfrádi, Zs. Kókai, P. Zagyvai: Az NMX mérőhelyének sugárárnyékolása (Radiation shielding of ESS NMX), Nukleáris Technikai Szimpózium, 2017

[84] Personal communication with Márton Markó

[85] Naturally occurring radioactive materials (NORM IV), IAEA-TECDOC-1472, October 2005

[86] www.bnc.hu

[87] Eszter Dian, Felicián Gergely, Dénes Párkányi, Szabina Török, Péter Zagyvai: Activation experiments on neutron beam guide materials, HAS Centre for Energy Research, 17/03/2015

[88] Zs. Kókai, E. Dian, L. Zanini, F. Mezei, A. Takibayev, E. Klinkby, Sz. Török, P. Zagyvai, G. Patriskov, F. Gergely: Neutron guide activation calculations for the European Spallation Source and validation measurements at Budapest Neutron Centre, International Collaboration on Advanced Neutron Sources (ICANS XXII), 27-31 March 2017, Oxford, UK

[89] http://www.bitt-tehnologije.hr/sites/default/files/AMS02V4_2007.pdf

[90] Personal communication with Dávid Hajdú

ADATLAP

a doktori értekezés nyilvánosságra hozatalához*

I. A doktori értekezés adatai

A szerző neve: Kókai Zsófia

MTMT-azonosító: 10061021

A doktori értekezés címe és alcíme: Radiation protection calculations related to the decommissioning of the European Spallation Source

DOI-azonosító: 10.15476/ELTE.2019.238

A doktori iskola neve: Környezettudományi Doktori Iskola

A doktori iskolán belüli doktori program neve: Környezetfizika

A témavezető neve és tudományos fokozata: Török Szabina (DsC), Zagyvai Péter (PhD)

A témavezető munkahelye: Török Szabina: MTA EK, Zagyvai Péter: MTA EK, BME NTI

II. Nyilatkozatok

1. A doktori értekezés szerzőjeként
a) hozzájárulok, hogy a doktori fokozat megszerzését követően a doktori értekezésem és a tézisek nyilvánosságra kerüljenek az ELTE Digitális Intézményi Tudástárban. Felhatalmazom a Természettudományi kar Dékáni Hivatal Doktori, Habilitációs és Nemzetközi Ügyek Csoportjának ügyintézőjét, hogy az értekezést és a téziseket feltöltse az ELTE Digitális Intézményi Tudástárba, és ennek során kitöltse a feltöltéshez szükséges nyilatkozatokat.

2. A doktori értekezés szerzőjeként kijelentem, hogy
a) az ELTE Digitális Intézményi Tudástárba feltöltendő doktori értekezés és a tézisek saját eredeti, önálló szellemi munkám és legjobb tudomásom szerint nem sértem vele senki szerzői jogait;
b) a doktori értekezés és a tézisek nyomtatott változatai és az elektronikus adathordozón benyújtott tartalmak (szöveg és ábrák) mindenben megegyeznek.

3. A doktori értekezés szerzőjeként hozzájárulok a doktori értekezés és a tézisek szövegének plágiumkereső adatbázisba helyezéséhez és plágiumellenőrző vizsgálatok lefuttatásához.

Kelt: Budapest, 2019. 10. 21.

a doktori értekezés szerzőjének aláírása

**ELTE SZMSZ SZMR 12. sz. Melléklet*